İSTANBUL TECHNICAL UNIVERSITY ★ INSTITUTE OF SCIENCE AND TECHNOLOGY

THREE PHASE FOUR WIRE VOLTAGE SOURCE PWM RECTIFIER WITH LOW INPUT CURRENT HARMONIC

M.Sc. Thesis by

İbrahim GÜNEŞ

Department: Electrical Engineering

Programme: Electrical Engineering

JANUARY 2008

İSTANBUL TECHNICAL UNIVERSITY ★ INSTITUTE OF SCIENCE AND TECHNOLOGY

THREE PHASE FOUR WIRE VOLTAGE SOURCE PWM RECTIFIER WITH LOW INPUT CURRENT HARMONIC

M.Sc. Thesis by

İbrahim GÜNEŞ

(504041065)

Date of submission : 28 December 2007

Date of defence examination: 29 January 2008

Supervisor (Chairman): Asst. Prof. Dr. Deniz YILDIRIM

Members of the Examining Committee: Asst. Prof.Dr. Özgür ÜSTÜN (I.T.U.)

Asst. Prof.Dr. Metin AYDIN (K.U.)

JANUARY 2008

İSTANBUL TEKNİK ÜNİVERSİTESİ ★ FEN BİLİMLERİ ENSTİTÜSÜ

ÜÇ FAZ DÖRT İLETKENLİ DARBE GENİŞLİK MODÜLASYONLU DÜŞÜK AKIM HARMONİKLİ GERİLİM KAYNAĞI TİPİ DOĞRULTUCU

YÜKSEK LİSANS TEZİ

İbrahim GÜNEŞ

(504041065)

Tezin Enstitüye Verildiği Tarih : 28 Aralık 2007
Tezin Savunulduğu Tarih : 29 Ocak 2008

Tez Danışmanı: **Yrd. Doç. Dr. Deniz YILDIRIM**
Diğer Jüri Üyeleri: **Yrd. Doç. Dr. Özgür ÜSTÜN (İ.T.Ü.)**
Yrd. Doç. Dr. Metin AYDIN (K.Ü.)

OCAK 2008

ACKNOWLEDGEMENTS

I would like to express my sincerest thanks to Asst. Prof. Dr. Deniz YILDIRIM for his guidance, support, encouragement and valuable contributions during my graduate studies. His impressive knowledge and technical skills has been a model for me to follow.

I express my deepest gratitude to my family, my wife Kevser, my mother Ümran, my father Ali İhsan, my brother Gökhan, my brother-in-law Fatih for their support throughout. Without their endless love and encouragements, I would not complete this thesis.

Special appreciation goes to Bülent Üstüntepe, Osman Okay and Argun Yüzüşen for sharing their knowledge and valuable times with me during experimental studies. I wish to thank to ENEL Enerji Elektronik A.S. and staff for their help throughout my graduate studies.

İbrahim GÜNEŞ **February 2008**

TABLE OF CONTENTS

LIST OF ABBREVIATIONS

PWM : Pulse Width Modulation
IGBT : Insulated Gate Bipolar Junction Transistor
UPS : Uninterruptible Power Supply
RMS : Root Mean Square
EMC : Electromagnetic Compability
PI : Proportional Integral
THD : Total Harmonic Distortion
PLL : Phase Locked Loop
IPM : Intelligent Power Module
DSP : Digital Signal Processor
ADC : Analog to Digital Conversion
EVA : Event Manager A
EVB : Event Manager B

LIST OF TABLES

LIST OF FIGURES

ÜÇ FAZ DÖRT İLETKENLİ DARBE GENİŞLİK MODÜLASYONLU DÜŞÜK AKIM HARMONİKLİ GERİLİM KAYNAĞI TİPİ DOĞRULTUCU

ÖZET

Yarı iletken eleman teknolojisindeki gelişmeler ile birlikte yüksek güçlü, darbe genişlik modülasyonlu, gerilim kaynağı tipi doğrultucuların kullanımı giderek yaygınlaşmaktadır. Düşük giriş akım harmoniği, ayarlanabilir giriş güç faktörü, ve çift yönlü güç aktarımı özellikleri ile üç fazlı, dört iletkenli, darbe genişlik modülasyonlu, gerilim kaynağı tipi doğrultucular, kesintisiz güç kaynağı ve motor sürücü uygulamalarında yaygın bir şekilde kullanılmaktadır.

Literatürde üç fazlı, dört iletkenli, darbe genişlik modülasyonlu, gerilim kaynağı tipi bir doğrultucunun denetlenmesini sağlayan çeşitli kontrol yöntemleri yer almaktadır. Bu tez çalışmasında, üç fazlı, dört iletkenli, darbe genişlik modülasyonlu, gerilim kaynağı tipi bir doğrultucunun yüksek başarımla denetlenmesini sağlayan kontrol yöntemi geliştirilmiştir. Bu yöntemde, DC bara gerilimini kontrol etmek için gerilim çevriminde, DC kazancı yüksek oransal-integral (PI) denetleyici kullanılmaktadır. Akım çevriminde, her bir fazın akımını kontrol etmek için durağan eksende temel bileşen ve harmonik bileşenlerden oluşan rezonans süzgeç grubu kullanılmaktadır. Rezonans süzgeçlerinin tasarımı ve uygulama kolaylıkları ile ilgili detaylı bilgiler verilmektedir. Akım kontrolünün dinamik başarımını arttırmak amacı ile rezonans süzgeç grubuna paralel bağlı orantısal bir kazanç eklenmiştir. Ayrıca, şebeke gerilimi ileri beslemesi kullanılarak sistemin durağan ve dinamik başarımı iyileştirilmektedir.

Üç fazlı, dört iletkenli, darbe genişlik modülasyonlu, gerilim kaynağı tipi doğrultucunun durağan ve dinamik başarımı farklı çalışma koşulları için ayrıntılı olarak incelenmiştir. Denetim yönteminin başarımı teori, bilgisayarla benzetim ve deneysel çalışmalarla doğrulanmıştır.

THREE PHASE FOUR WIRE VOLTAGE SOURCE PWM RECTIFIER WITH LOW INPUT CURRENT HARMONIC

SUMMARY

As a result of tremendous developments in the semiconductor industry, voltage source PWM rectifiers are becoming cheaper and available at increased power levels. Due to its several advantages such as low input current harmonic, adjustable input power factor, and four quadrant operation, PWM rectifiers are widely used in variable-speed drives and uninterruptible power supplies.

There exist several control methods for three-phase four-wire voltage-source PWM rectifiers in the literature. In this study, a new control method is proposed for high performance operation of three-phase four-wire voltage-source PWM rectifiers. In this method, a PI type controller with high dc gain is used for regulating the DC bus voltage. For controlling the input currents of each phase resonant banks are used. Resonant banks are composed of parallel connected resonant filters for fundamental and harmonic components. Detailed informations for designing optimum resonant filters are given in the thesis. In order to improve the dynamic and steady-state performance of the current controller, a proportional gain is connected parallel to the resonant filter bank. Also, input voltage feedforward is used for improving the dynamic and steady-state performance of the rectifier.

The steady-state and dynamic performance of the three-phase four-wire voltage-source PWM rectifier is tested under different utility conditions. The proposed control method is proven by means of theory, simulations, and experiments.

1. INTRODUCTION

1.1. Rectifiers and Electric Power Quality

In this thesis, three-phase four-wire voltage-source PWM rectifiers are investigated. As a result of tremendous developments in the semiconductor industry, PWM rectifiers are becoming cheaper and available at increased power levels. Today, PWM rectifiers are widely used in industrial applications, such as variable-speed drives and uninterruptible power supplies (UPSs). This is advantageous because using power electronic equipments result in high efficient and high performance operation. However, using the power electronics starts a new dilemma. Since all power electronic circuits behave as nonlinear loads, harmonic currents are injected into the grid.

Most of the power electronic equipments are a source of current harmonics, which results in increase in reactive power and power losses in transmission lines. The harmonics also cause electromagnetic interference and, sometimes dangerous resonances. They have negative influence on the control and automatic equipment, protection systems, and other electrical loads, resulting in reduced reliability and availability. Moreover, nonlinear loads and nonsinusoidal currents produce nonsinusoidal voltage drops across the network impedances, so that nonsinusoidal voltages appear at several points of the mains. It results in overheating of transmission line, transformers and generators due to the increased copper losses.

1.2. Harmonic Reduction Methods

Reduction of harmonic content in line current to a few percent allows avoiding most of the mentioned problems above. Restrictions on current and voltage harmonics maintained in many countries through IEEE 519-1992 and IEC 61000-3-2/IEC 61000-3-4 standards, are associated with the popular idea of clean power.

Today, several techniques are used for reducing the line side harmonics. The most popular techniques used for reducing harmonics are;

- Adding Passive Filters
- Using Multipulse Rectifiers
- Using Active Filters
- Using PWM Rectifiers

The traditional method of current harmonic reduction involves adding passive LC filters. These filters are connected parallel to the grid. Filters are usually constructed as series-connected legs of capacitors and inductors. The number of legs depends on number of filtered harmonics (5^{th}, 7^{th}, 11^{th}, and 13th). The main advantages of passive filters are their simplicity and low cost. On the other hand, it has many disadvantages. These filters are designed for a particular application, and the filter elements are heavy and bulky. There exists a risk of resonance problem at the grid. Beside, these filters consume reactive power which results in extra cost for the user.

Multipulse rectifiers are also used for reducing harmonics. Although it is easy to implement, it possesses several disadvantages such as, bulky and heavy transformer, increased voltage drop, and increased harmonic currents at non-symmetrical load or line voltages.

Active filters, Figure 1.1, are used as a better alternative of the passive filters. They have better dynamics responses and they can control the harmonic and fundamental currents.

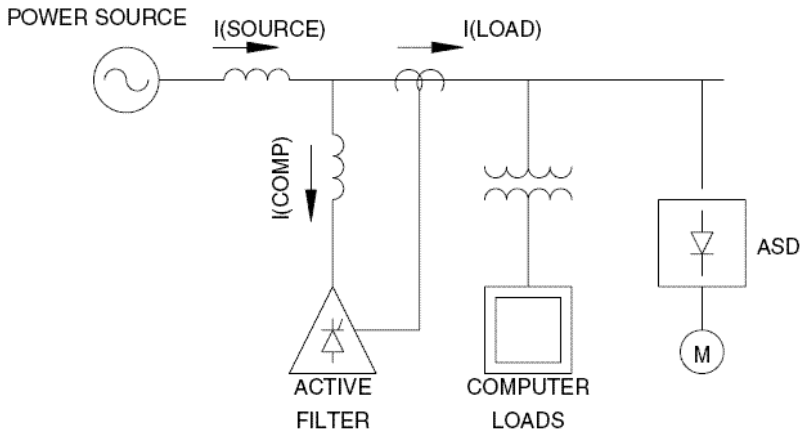

Figure 1.1: Active Filter

Active filters provide compensation of fundamental reactive components of load current, load symmetrization, from grid point of view, and harmonic compensation

much better than passive filters. In spite of its advantages, active filters possess certain disadvantages such as, complex control, switching losses and EMC problems.

PWM rectifiers are the most effective way of reducing line side harmonics. As a result of tremendous developments in the semiconductor industry, they are becoming cheaper and available at increased power levels.

Table 1.1 Advantages and disadvantages of harmonic reduction methods

	Advantages	Disadvantages
Passive Filters	• Simplicity • Low cost	• Bulky filter elements • Resonance problem • Poor performance
Multipulse Rectifiers	• Simplicity	• Expensive transformer • Poor performance
Active Filters	• High Performance	• Complex control • Switching losses • EMC problems
PWM Rectifiers	• High Performance • Low cost	• Switching losses

1.3. General Introduction to Three Phase PWM Rectifiers

During the past twenty years, the interest in rectifying units has been rapidly growing mainly due to the increasing concern of the electric utilities and end users about the harmonic pollution in the power system. As a result, PWM rectifiers have been of particular interest and they have become attractive especially in industrial variable speed drive and UPS applications in the power range from a couple of kilowatts up to several megawatts.

1.3.1. Basic topologies and characteristics

PWM rectifiers are built with semiconductors with gate-turn-off capability. The gate-turn-off capability allows full control of the rectifier, because switches can be switched ON and OFF whenever it is required. This allows the commutation of the switches hundreds of times in one period, which is not possible with line commutated rectifiers, where thyristors are switched ON and OFF only once a cycle. This feature has the following advantages;

- the current or voltage can be modulated (Pulse Width Modulation or PWM), generating less harmonic contents
- power factor can be controlled, and even it can be made leading
- they can be built as voltage-source or current-source rectifiers
- the reversal of power in thyristor rectifiers is by reversal of voltage at the dc bus, on the other hand, PWM rectifiers can be implemented for both, reversal of voltage or reversal of current.

There are two ways to implement three-phase PWM rectifiers;

- as a current-source rectifier, where power reversal is obtained by DC voltage reversal
- as a voltage-source rectifier, where power reversal is obtained by current reversal at the dc bus

Figure 1.2 and Figure 1.3 shows the basic circuits for these two topologies.

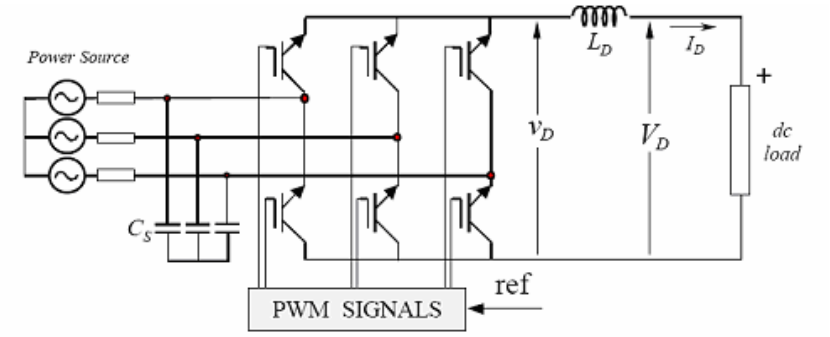

Figure 1.2: Three-Phase Current-Source PWM Rectifier

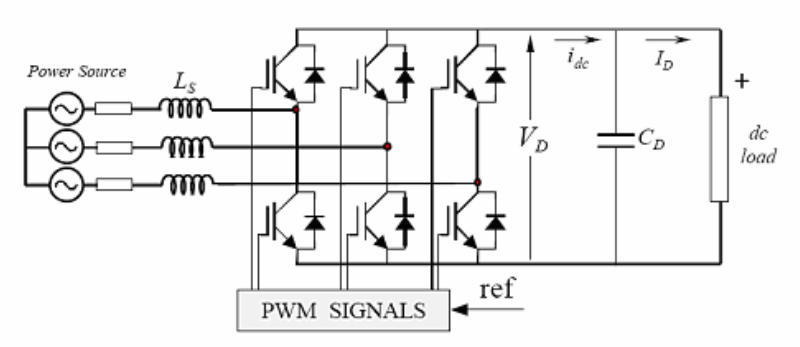

Figure 1.3: Three-Phase Voltage-Source PWM Rectifier

1.3.2. Operation of the Voltage Source PWM rectifier

The voltage-source rectifier is by far, the most widely used type of PWM rectifiers. The basic operation principle of the voltage-source rectifier consists on keeping the DC bus voltage at a desired reference value, using a feedback control loop as shown in Figure 1.4. To accomplish this task, the DC bus voltage is measured and compared with a DC voltage reference V_{REF}.

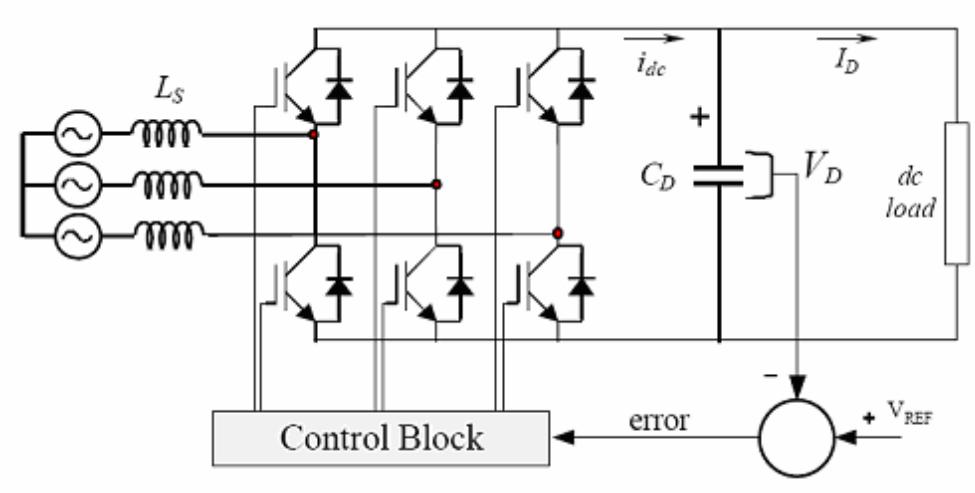

Figure 1.4: Operation Principle of the Three-Phase Voltage-Source PWM Rectifier

When the current I_D is positive, PWM rectifier is in rectifier operation. In this mode of operation the dc bus capacitor C_D is discharged due to the positive I_D, and the error signal ask the Control Block for more power from the AC supply. Inversely, when I_D becomes negative (inverter operation), the capacitor C_D is overcharged, and the error signal ask the control to discharge the capacitor and return power to the AC supply.

The Pulse Width Modulation consists on switching the switches ON and OFF, following a preestablished template. Particularly, this template could be a sinusoidal waveform of voltage or current. The PWM pattern has a fundamental signal V_{MOD}, with the same frequency of the power source, so the rectifier works properly. Changing the amplitude of this fundamental, and its phase shift with respect to the mains, the rectifier can be controlled to operate in the four quadrants. For example, the modulation of one phase could be as the one shown in Figure 1.5. The amplitude of the V_{MOD} in Figure 1.5 is proportional to the amplitude of the template.

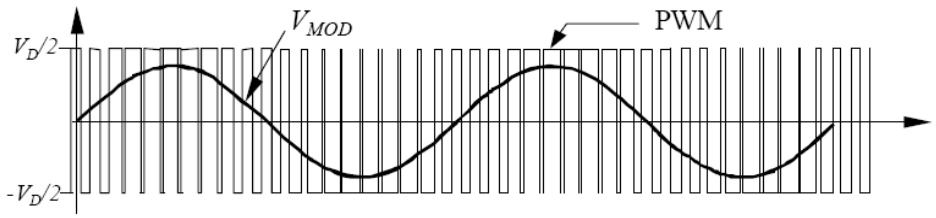

Figure 1.5: PWM pattern

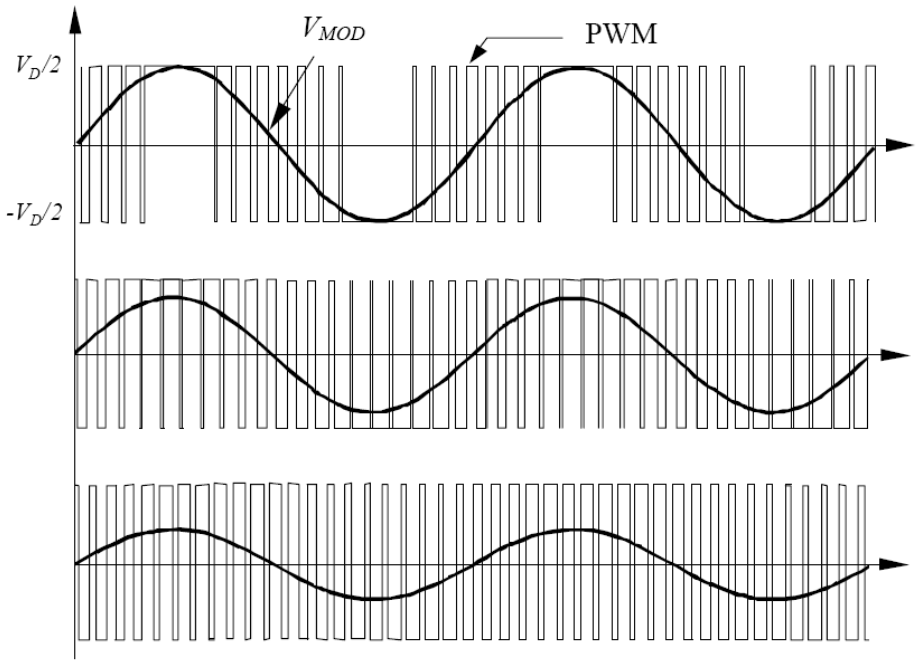

Figure 1.6: Changing V_{MOD} through the PWM pattern

The interaction between V_{MOD} and V (source voltage) can be seen through a phasor diagram. This interaction permits to understand the four-quadrant capability of this rectifier. In the Figure 1.7, the four-quadrant operation is clearly explained. I_S in Figure 1.7 flows through the semiconductors in the way shown in Figure 1.8. During the positive half cycle, the transistor T_N, connected at the negative side of the DC bus is switched ON, and the current i_s begins to flow through T_N (i_{Tn}). The current returns to the mains and comes back to the switches, closing a loop with another phase, and passing through a diode connected at the same negative terminal of the DC bus. The current can also go to the DC load (inversion) and return through another transistor located at the positive terminal of the dc bus.

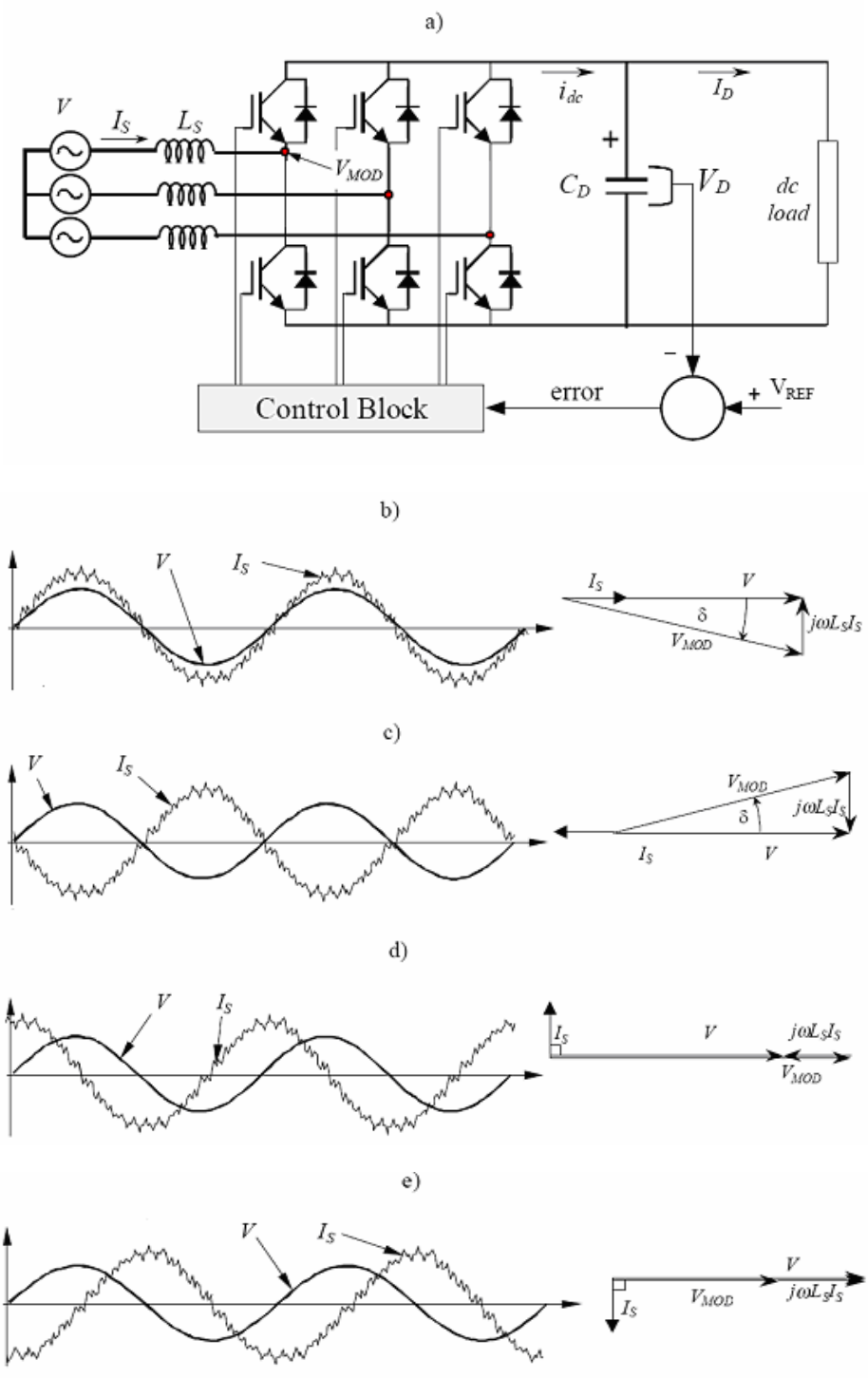

Figure 1.7: Four-quadrant operation of the voltage-source PWM rectifier
a) voltage-source PWM rectifier
b) rectifier operation at unity power factor
c) inverter operation at unity power factor
d) capacitor operation at zero power factor
e) inductor operation at zero power factor

When the transistor T_N is switched OFF, the current path is interrupted, and the current begins to flow through the diode D_P, connected at the positive terminal of the DC bus. This current, called i_{Dp} in Figure 1.8, goes directly to the DC bus, helping in the generation of the current i_{dc}. The current i_{dc} charges the capacitor C_D and permits the rectifier to produce DC power. The inductances L_S are very important in this process, because they generate an induced voltage which allows the conduction of the diode D_P. Similar operation occurs during the negative half cycle, but with T_P and D_N, Figure 1.8.

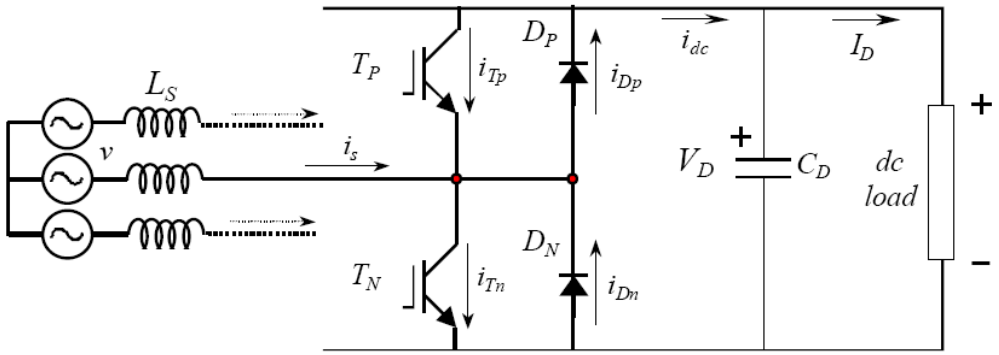

Figure 1.8: Current waveforms through the mains, the IGBTs, and the DC bus

To have full control of the operation of the rectifier, six antiparallel connected diodes must be polarized negatively at all values of instantaneous AC voltage supply. Otherwise diodes will conduct, and the PWM rectifier will behave like a common diode rectifier bridge. The way to keep the diodes blocked is by ensuring a DC bus voltage higher than the peak DC voltage generated by the diodes alone, as shown in Figure 1.9. In this way, the diodes remain polarized negatively, and they only will conduct when at least one transistor is switched ON, and favorable instantaneous AC voltage conditions are given. In the Figure 1.9 V_D represents the capacitor DC voltage, which is kept higher than the normal diode bridge rectification value V_{BRIDGE}.

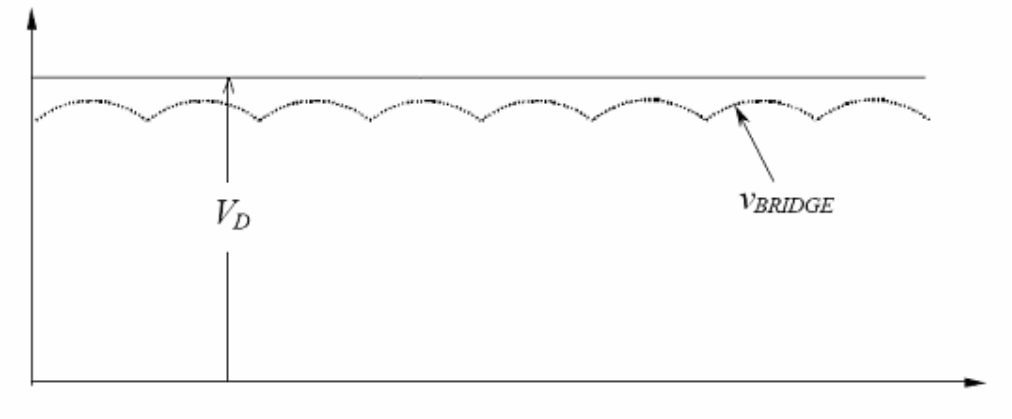

Figure 1.9: DC bus voltage of the Voltage-source PWM rectifier

1.3.3. Control Methods

Voltage-source PWM rectifiers allow a full control over both active and reactive power exchanges between the AC mains and DC source. Different control techniques have been discussed to shape the input current waveforms of the voltage-source PWM rectifiers.

1.3.3.1. Linear Current Control

The conventional version of the linear current controller performs a sine, triangle PWM voltage modulation technique. Linear current control technique provides an unsatisfactory performance level as far as PWM rectifier applications are concerned. This is mainly due to the limitation of the achievable regulator bandwidth which is implied by the necessity of sufficiently filtering the ripple in the modulating signal. This necessity compels one to keep the loop gain crossover frequency well below the modulation frequency. This reflects in a poor rejection of the disturbances injected into the current control loop, mainly due to the AC line voltage at the fundamental frequency. To overcome this limitation, recent versions of the linear current controllers employ reference frame transformations [1-3]. Control variables are transformed into the rotating frame according to the scheme represented in Figure 1.10. The main advantage of such a solution is that the fundamental harmonic components of voltage and current signals appear constant to the current regulator. As a consequence, the rejection of this disturbance is much more effective. On the other hand, the bandwidth limitation of the PI regulators, which remains unchanged,

still implies significant errors in the tracking of the high order harmonic components of the current reference.

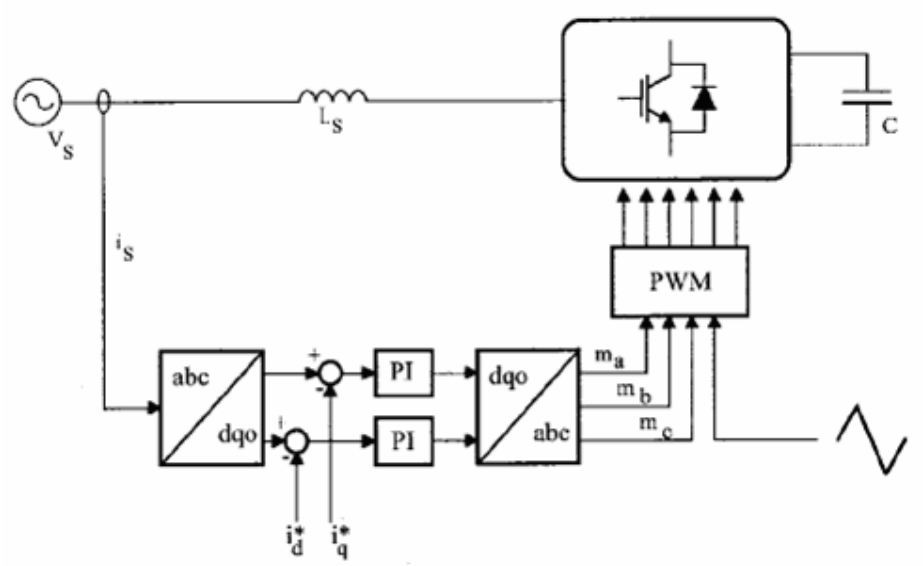

Figure 1.10: Basic scheme of a linear rotating frame current regulator [3]

1.3.3.2. Deadbeat Control

The deadbeat control method can only be implemented on a digitally controlled system. In order to apply the deadbeat control, the mathematical model of the system must be known. Using the reference and feedback signals, and employing the system model, the control signal that forces the input current error to zero in finite number of sampling cycles is calculated and applied to the modulator. When the system model is exactly known, the error due to changes in the state variables is driven to zero in ideally one step, but in practical case it takes two steps. So, the deadbeat controller has a very fast response and high control bandwith. However, the deadbeat control method, which is dynamically very stable for a well defined system, is highly affected by the system parameters. Even a small change in the parameters can make the system unstable. Beside of this, computational and measurement delays effects the control performance greatly. Some techniques are given in the literature for compensating the computational delays [4-6]. The basic scheme of a deadbeat current regulator can be seen in Figure 1.11.

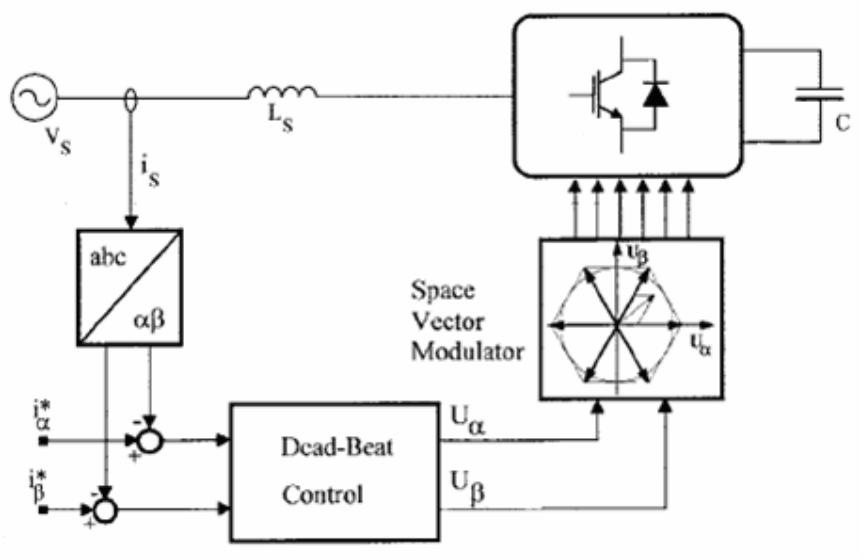

Figure 1.11: Basic scheme of a digital deadbeat current regulator [4]

1.3.3.3. Hysteresis Control

The main goal of the hysteresis control is keeping the current error in a specified hyteresis band. In spite of its simplicity, good accuracy and high robustness, this control technique exhibits several unsatisfactory features [7]. The main one is that it produces a varying modulation frequency for the power converter. Many improvements to the original control structure have been suggested by industrial applications [8-9]. First of all, phase current decoupling techniques have been devised [10]. Secondly, fixed modulation frequency has been achieved by a variable width of the hysteresis band as function of the instantaneous input current [11]. Figure 1.12 shows the simplified scheme of the implementation of such a controller. As can be seen, the controller modifies the hysteresis band by summing two different signals. The first is the filtered output of a PLL phase comparator β_1, and the second is the filtered output of a band estimation circuit β_2. The band estimator implements a feedforward action that helps the phase locked loop, PLL, based circuit to keep the switching frequency constant, in this way, the output of the PLL circuit only provides the small amount of the modulation of the hysteresis band which is needed to guarantee the phase lock of the switching pulses with respect to an external clock signal. This also ensures the control of the mutual phase of the modulation pulses. All of these provisions have allowed a substantial improvement in the performance of the hysteresis current controller, as is discussed in [12].

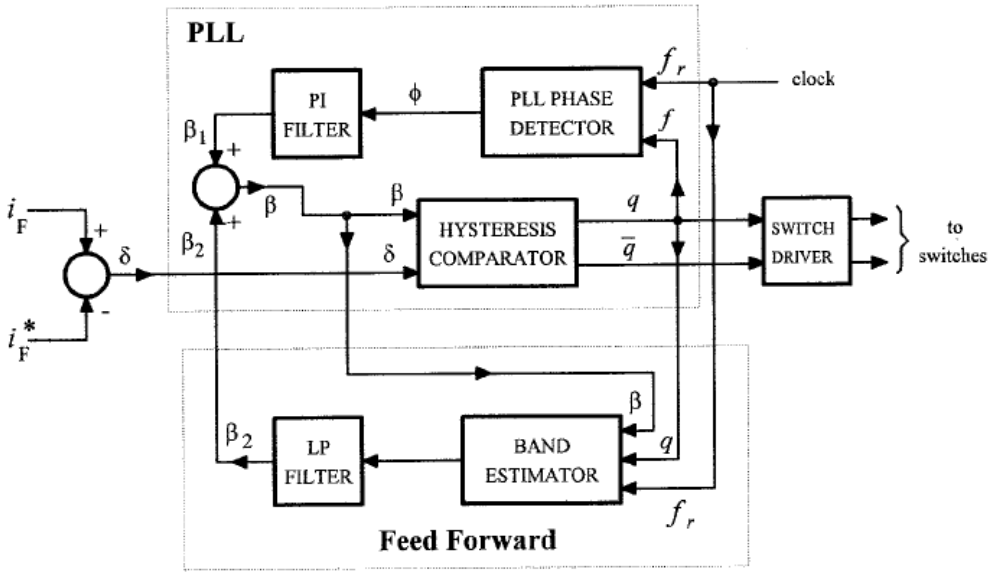

Figure 1.12: Basic scheme of a hysteresis current regulator [12]

1.3.3.4. Resonant Filter Bank Controller

Resonant filters have recently reemerged as a focus in the literature with the recognition that many rotating frame controllers can be transformed to an equivalent stationary frame system. This removes the need for rotating frame transformations and sine tables, [13], and has led to reduced complexity for applications such as current regulators, [13-14], active filters, [15-16], and UPS systems [17].

The method is based on compensator assignment for each frequency of interest. Thus, the controller has a parallel structure. Although various compensator types are possible, the type shown in the following equation is most widely utilized [18-21].

$$G_C(s) = \frac{2K_{im} \cdot s}{s^2 + (m\omega_e)^2} \qquad \textbf{(1.1)}$$

In the resonant filter compensator of Eq. 1.1, K_{im} is the integral gain, and $m\omega_e$ is the frequency of interest where infinite gain is demanded. If the resonant filter controller is tuned at the fundamental frequency (m=1), due to infinite gain and zero phase at the fundamental frequency, the steady state error will be zero at fundamental frequency. As the controller has zero gain at all other frequencies, the controller does not influence other frequency components. Thus, for each frequency of interest a resonant filter at that frequency should be utilized.

Because of its simplicity, perfect accuracy and high robustness, in this thesis, resonant filter banks are used for input current regulation of Three-Phase Four-Wire Voltage-Source PWM Rectifier. As the method does not require positive, negative, zero sequence separation and it is easy to implement, it has been found favorable over other methods briefly discussed above.

Table 1.1: Advantages and disadvantages of control methods

	Advantages	Disadvantages
Linear Current Control	• Simplicity	• Poor performance • Low control bandwith
Deadbeat Control	• High control bandwith • Fast response	• Low robustness • High complexity
Hysteresis Control	• High robustness • High performance	• Variable switching frequency
Resonant Filter Control	• High control bandwith • High performance • High robustness	• Complexity

1.4. Outline of the Thesis

In this thesis, the Three-Phase Four-Wire Voltage-source PWM Rectifier system is investigated in detail. In this topology, neutral line of the supply is directly connected to the centre point of the DC bus using centre tapped capacitors. With this property, this topology can be easily used in a three-phase transformerless UPS system. The neutral connection in the topology decouples the three phases and allows individual control of each phase.With the implementation of the resonant type filters in the current controller, the current tracking performance of the voltage-source PWM rectifier becomes perfect. Designing the resonant filter bank with proper resonant filter components such as the fundamental component, 3^{rd}, 5^{th}, 7^{th}, 9^{th}, 11^{th}, etc. the input current composed of mainly with the desired fundamental component, and less harmonic component, even if the input voltage is highly distorted. All these control algorithms have been implemented on a 15 kVA sytem using a digital signal processor, and the theory has been verified experimentally.

The organization of the thesis is given as follows;

In the second chapter, the input current control of the four-wire voltage-source PWM rectifier is explained clearly. The important points in designing the optimum resonant

filter form that can achieve high performance are clarified. Later on, the implementation of these resonant filters in a fixed point digital signal processor is explained.

In the third chapter, the detailed modelling and computer simulation of a 15 kVA, 50 Hz, four-wire PWM rectifier is provided. Following the establishment of the simulation model, the controller tuning procedure is described. Then the rectifier control performance is investigated for steady state and dynamic operating conditions. The superior steady state and dynamic performance of the proposed control method is illustrated by means of computer simulations involving steady state and dynamic loading conditions.

The fourth chapter of the thesis explains the hardware setup and the experimental studies of the 15 kVA system. In this chapter the experimental system hardware and software are discussed in detail. The steady state performance under various load conditions and dynamic performance under loading transient conditions are shown via laboratory experiments. Correlation with the computer simulation and experimental results are provided.

The fifth chapter summarizes the research results, and concludes the thesis. Finally, recommendations for future work on the study subject of this thesis are given.

2. RESONANT FILTER BASED INPUT CURRENT CONTROL OF THE THREE PHASE FOUR WIRE VOLTAGE SOURCE PWM RECTIFIER

2.1. Introduction

Three-phase AC-DC-AC converters have been used for many years in UPSs and induction motor drives. Three-phase induction motors may be driven from a three wire source and assuming galvanic isolation is not required, a transformerless three wire AC-DC-AC converter is commonly used. On the other hand, a double conversion UPS can operate with a three wire input rectifier, but must have a four-wire output. A three-phase transformer is needed on the front or back end of the converter even when galvanic isolation is not required. The load neutral connection of the UPS is directly connected to the star point of the supply thus preventing the load neutral from floating and providing a path for fault currents to flow via the earth connection. The presence of the three-phase transformer increases the cost, size and the weight of the UPS.

Removal of the transformer in a three-phase UPS would lead to compact converters with significant savings in weight and cost. However, removal of the transformer would lead to harmonics flowing in the supply neutral, mainly third harmonic of the supply frequency. If a four-wire PWM rectifier is used, the transformer can be removed while allowing sinusoidal currents to be drawn from the mains at unity power factor.

This chapter focuses on the input current control of the four-wire PWM rectifier. The current controller of each phase is composed of parallely connected resonant filters, one for fundamental, and the others for harmonic components. In the voltage controller, a PI type controller is used. With this controller structure the four-wire PWM rectifier exhibits superior steady state and dynamic performance under all practical operating conditions.

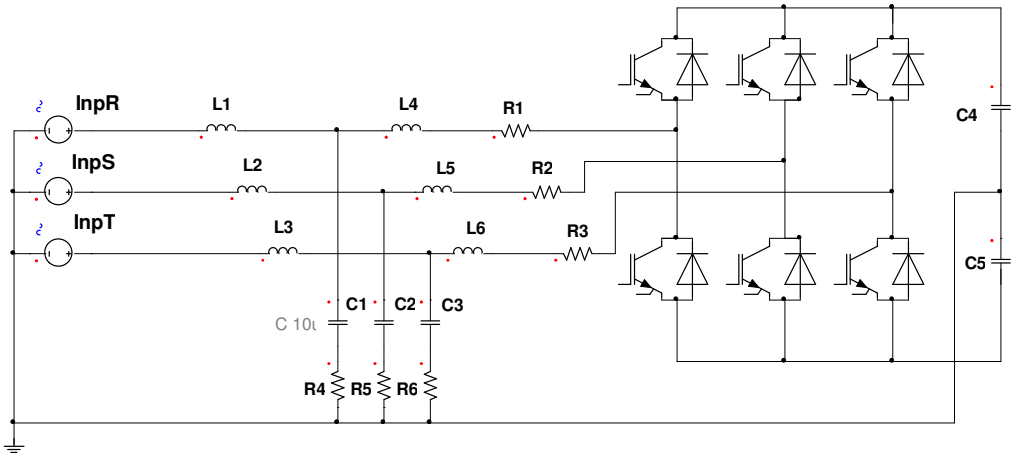

Figure 2.1: Transformerless four-wire voltage-source PWM rectifier [20]

2.2. Resonant Filter Forms

A resonant filter consists of a transfer function which has very large gain and zero phase delay at the desired frequency. The desired frequency is called as the resonant frequency. Frequencies other than the resonant frequency, the gain of the transfer function becomes very small and the phase angle becomes negligible.

The simple linear proportional integral, PI, type controllers are prone to known drawbacks including the presence of steady state error in the stationary frame and the need to decouple phase dependency in three-phase systems altough they are relatively easy to implement [22]. Exploring the simplicity of PI controllers and to improve their overall performance, many variations have been proposed in the literature including the addition of a grid voltage feedforward path, multiple state feedbacks and so on. Generally, these variations can expand the PI controller bandwith, but unfortunately they also push the system towards their stability limits.

Alternatively for three-phase systems, synchronous frame PI control with voltage feedforward can be used, but it usually requires multiple frame transformations. Overcoming the computational burden and still achieving virtually similar frequency response characteristics as a synchronous frame PI controller, resonant controllers are employed for reference tracking in the stationary frame [14, 21]. Resonant controllers are conceptually similar to an integrator whose infinite DC gain forces the DC steady state error to zero.

2.2.1. Ideal Resonant Filter

In the three-phase four-wire voltage-source PWM rectifier application, the resonant filters are employed in the current controller. It is constructed in the stationary frame (without coordinate transformations) and has a superior performance similar to the linear PI regulator in synchronous frame [14]. The ideal resonant filter has a transfer function as given in Eq. 2.1.

$$G_C(s) = \frac{2K_{im} \cdot s}{s^2 + (m\omega_e)^2} \tag{2.1}$$

In Eq. 2.1, K_{im} is the integral gain, and $m\omega_e$ is the frequency of interest where infinite gain is demanded. If the resonant filter controller is tuned at the fundamental frequency (m=1), due to infinite gain and zero phase at the fundamental frequency, the steady state error will be zero at fundamental frequency. It can be mathematically derived by transforming a synchronous frame PI controller to the stationary frame without consideration of the redundant cross coupling terms, and has an infinite gain at the controller's resonant frequency ω_e, which is chosen to be the line fundamental frequency ($2\pi \cdot 50$ rad/s).

Transforming PI controllers in both positive and negative sequence synchronous frames of a three-phase system to the stationary frame, using either frequency domain or time domain technique, the final stationary controller of Eq. 2.1 can be obtained, and the cross coupling terms generated from positive and negative sequence synchronous frames would cancel each other if the same PI parameters are employed in both synchronous frames. Therefore, the resonant filter would achieve zero steady state error for both positive and negative sequence component regulations in principle with infinite gains at fundamental frequency.

The ideal resonant filter has an infinite gain and zero phase at the resonant frequency ($m\omega_e$). A typical bode plot for the ideal resonant filter is shown in Figure 2.2.

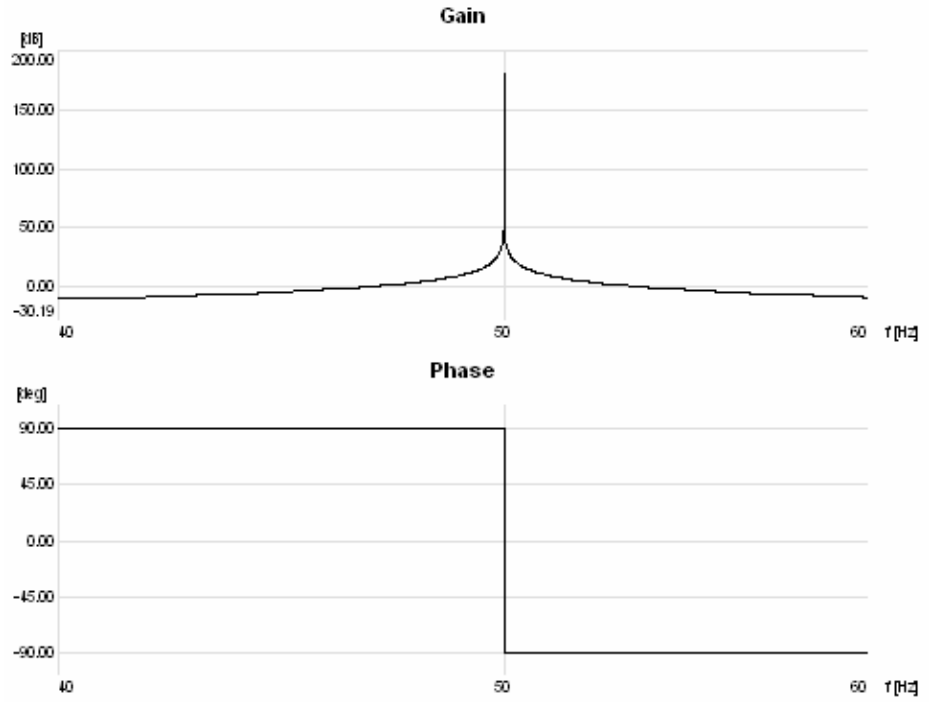

Figure 2.2: Bode plot of the ideal resonant filter for m=1, K_{im}=20, ω_e=2π·50 rad/sec

The phase relation is such that below the resonant frequency the resonant filter provides 90^o leading compensation while above the resonant frequency the filter provides 90^o lagging compensation. The resonant frequency is selected to be the frequency of the AC signal to be controlled. The gain is optimized by considering the system dynamic and steady state performance requirements. For instance, if a resonant filter is used at the fundamental frequency for controlling the input current of a three-phase rectifier, the resonant filter controller precisely controls the fundamental component of the current at the desired phase and magnitude. However, the controller can not compensate the harmonic current components other than the fundamental frequency, because the controller provides nearly zero gain for these components. This problem can be solved by using resonant filters for each dominant harmonic frequency. Thus, depending on the existing harmonic components, the resonant frequency multiplier m is selected. Resonant filter banks are formed by connecting resonant filters at the required frequency in parallel.

In the three-phase four-wire voltage-source PWM rectifier application, due to the occurrance of the fourth wire, neutral wire, each phase can be controlled independently. The outer control loop consists of a PI type DC bus voltage

controller. The output of the voltage controller is multiplied with the sine references for obtaining the current references of each phase. For each phase, one identical resonant filter bank is utilized. Thus, the fundamental component is controlled without involving positive-negative-zero sequence decomposition and complex controllers which is the conventional approach [23]. The resonant filter controller provides an easy design and implementation task with respect to the synchronous frame based controller or other complex control algorithms.

2.2.2. Phase Delay Compensated Resonant Filter

Although theoretically, the ideal resonant filter would achieve zero steady state error at the resonant frequency, there could be practical problems during its implementation as it is sensitive to system delays and frequency variations. The practical implementation of the resonant filters involves more detailed structure than the ideal structure given in Eq. 2.1. If the system delay, which is the total delay originating from the individual delays of the rectifier system stages, is ignored, the controller performance decreases especially at high frequencies. Practically, the measurement, signal processing, and the PWM units introduce delays that can have significant influence on the controller performance. The measurement delay (τ_{mea}) occurs at the stage of the measurement and signal conditioning of the voltage and current feedback signals. The sampling delay (τ_{samp}) is mainly due to the A/D conversion time. The PWM delay (τ_{PWM}) is due to the discrete nature of the rectifier. The sum of all these delays is called as the total delay τ_T.

$$\tau_T = \tau_{mea} + \tau_{samp} + \tau_{PWM} \quad \textbf{(2.2)}$$

This total delay results in a phase shift, ϕ_m which varies with the frequency. It can be obtained as a function of the total system delay and the resonant frequency ($m\omega_e$) of the controller, as given in Eq. 2.3. Since the phase shift is directly proportional to the frequency, it is much more important at high frequencies. The ideal transfer function of the resonant filter, given in Eq. 2.1 should be modified such that the effect of delay is compensated, the control signals should be phase advanced by ϕ_m. Since Eq. 2.1 is the Laplace transform of cos ($m\omega_e t$), the phase shift should be considered as a process of adding a phase advance angle to the resonant term, implying the cosine function angle should be advanced. Thus the delay compensated time domain

equivalent of the resonant filter is cos ($m\omega_e t + \phi_m$) and the Laplace transform of the phase advanced cosine term shown in Eq. 2.4 gives the modified resonant filter as in Eq. 2.5. In this manner, the transfer function of the phase shifted resonant filter controller is obtained.

$$\phi_m = \tau_T \cdot m\omega_e \tag{2.3}$$

$$L\left\{2K_{im} \cdot \cos\left(m\omega_e t + \phi_m\right)\right\} = 2K_{im} \cdot \left(\frac{s \cdot \cos(\phi_m) - m\omega_e \cdot \sin(\phi_m)}{s^2 + (m\omega_e)^2}\right) \tag{2.4}$$

$$G_C(s) = 2K_{im} \cdot \left(\frac{s \cdot \cos(\phi_m) - m\omega_e \cdot \sin(\phi_m)}{s^2 + (m\omega_e)^2}\right) \tag{2.5}$$

2.2.3. Damped Resonant Filter

The modified transfer function of the resonant filter given in Eq. 2.5 can fix the problems due to the delays in the total system, but it still involves difficulties both from performance and implementation point of view. Since the above form is a lossless resonant filter, the gain of the filter at the resonant frequency is very high and the sidebands are very small. This implies that the controller is highly selective and can only track a reference exactly at the designed value of $m\omega_e$. However, in certain applications the frequency of the reference signal is not constant. In such a case, the gain and the phase of the resonant filter changes very rapidly, which results in instabilities in the controller performance. For the four-wire PWM rectifier application, the input voltage frequency can change in a wide range. Typically for a three-phase rectifier, the input voltage frequency variation limit is ±2.5 Hz for 50 Hz utility grid. So the fundamental frequency of the control signal applied to the resonant filter can change a lot. Therefore, the bandwidth of the resonant filter should be widened for improved tracking over a specified frequency range.

Beside of the mentioned practical problems above, implementation of a resonant filter with a fixed point processor is another big problem. The coefficients of a lossless discrete time resonant controller may become extreme values, some of the coefficients approaches to zero and some others approaches to one. Since a number can be represented with a finite word length in a fixed point processor, the coefficients of the discrete time implemented filter become an issue as loss of significance occurs in implementing the resonant controller. In a fixed point

processor some small numbers are lost. As a result, the gain and the magnitude of the resonant controller become significantly different than the evaluated values.

The resonant filter forms in Eq. 2.1 or Eq. 2.5 can not be used because of the above mentioned problems. The original resonant filter form is modified to solve these problems. The damping of the resonant filter is increased. The new form of the damped resonant filter is given in Eq. 2.6. In this equation τ_m is the damping constant and $m\omega_e$ is the resonant frequency of the damped resonant filter.

$$G_C(s) = \frac{2K_{im} \cdot \tau_m \cdot \omega_e \cdot s}{s^2 + 2 \cdot \tau_m \cdot \omega_e \cdot s + (m\omega_e)^2} \tag{2.6}$$

Selectivity function, Eq. 2.7, is defined in [24] for describing the damping. In this equation the resonant frequency is $m\omega_e$ and the corner frequency where the gain drops to 70.7 % is $m\omega_e \pm 0.5\Delta\omega$ as shown in Figure 2.3 which is drawn by utilizing Eq. 2.7. The gain curve of the resonant filter is practically symmetric with respect to the resonant frequency $m\omega_e$ and the gain at $m\omega_e$ - $0.5\Delta\omega$ and $m\omega_e$ + $0.5\Delta\omega$ is practically the same.

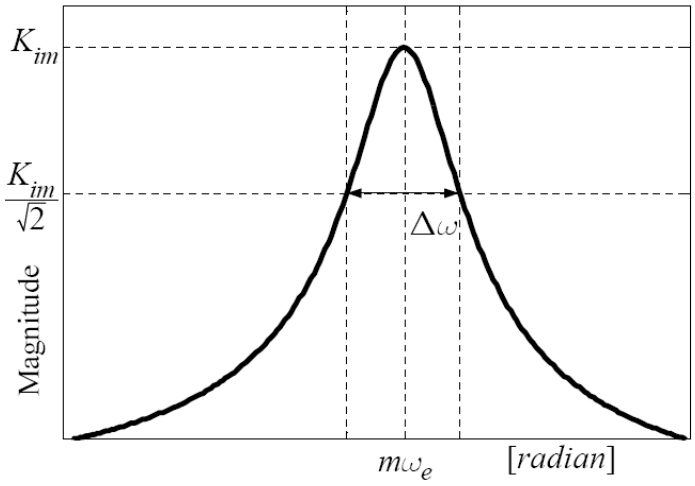

Figure 2.3: The gain characteristic of a damped resonant filter

$$S = \frac{resonant\_frequency}{bandwidth} = \frac{m\omega_e}{\Delta\omega} \tag{2.7}$$

The resonant filter damping τ_m is related to the resonant filter corner frequency.

$$\Delta\omega = 2 \cdot \tau_m \cdot m\omega_e \tag{2.8}$$

The selectivity can be expressed in terms of the filter damping by subtituting Eq. 2.8 in Eq. 2.7.

$$S = \frac{1}{2 \cdot \tau_m} \tag{2.9}$$

Comparing the ideal resonant filter of Figure Eq. 2.1 with a resonant filter with the damping value of $5 \cdot 10^{-3}$ of which the gain characteristic is shown in Figure 2.4, it can be seen that both the gain and selectivity decrease significantly. However, the filter becomes more effective over a wider operating frequency range. In order to compensate for the gain loss at the resonant frequency, the integral gain should be increased to a sufficient value.

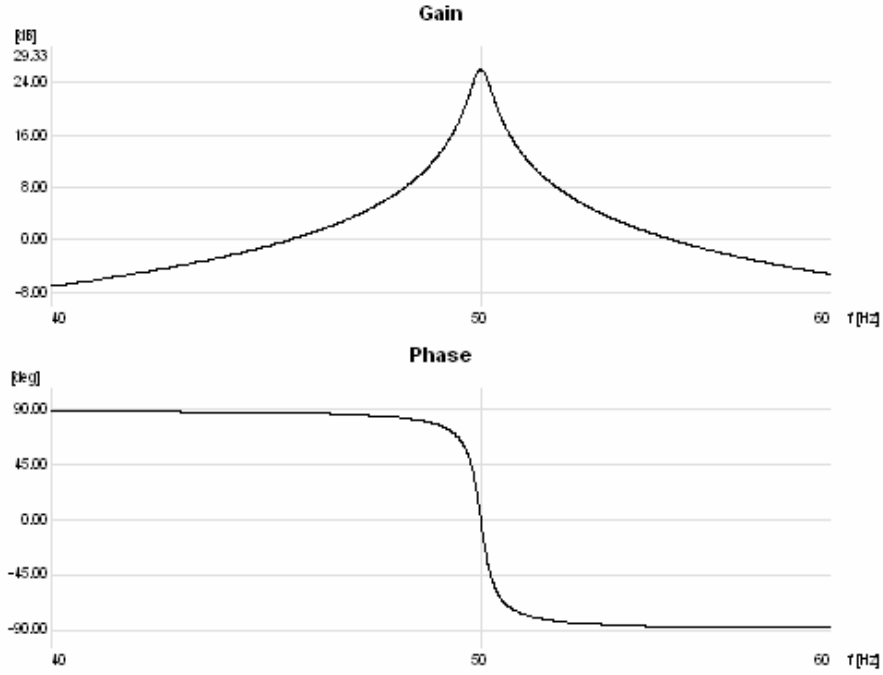

Figure 2.4: The gain and phase characteristics of the damped resonant filter for m=1, K_{im}=20, ω_e=2π·50 rad/s, τ_m=$5 \cdot 10^{-3}$

2.3. Resonant Filter Bank Forms

2.3.1. Damped Resonant Filter Banks

In the three-phase four-wire PWM rectifier application, current controller contains a fundamental frequency resonant filter and a specific number of harmonic frequency

resonant filters in each phase. These resonant filters are parallel connected to each other and they formed the resonant filter bank. The outputs of these resonant filter banks produce pwm signal for each phase. The damping coefficients of the resonant filters in the resonant filter bank may be equal or different than each other. Figure 2.5 shows the damped resonant filter bank gain and phase characteristics for the case that the damping coefficient remains the same for all the frequencies. This implies that for increasing frequencies the frequency sideband remains the same. For this case, the higher frequency resonant filters become highly selective and in practice if the measured harmonics are not exactly at the selected resonant frequency, the filter performance becomes unsatisfactory. On the contrary, for the case where the damping coefficients increases with the increasing filter frequency, the filter performance does not affected by the frequency. Figure 2.6 shows the resonant filter bank with the damping coefficient equals to ($m \cdot \tau$).

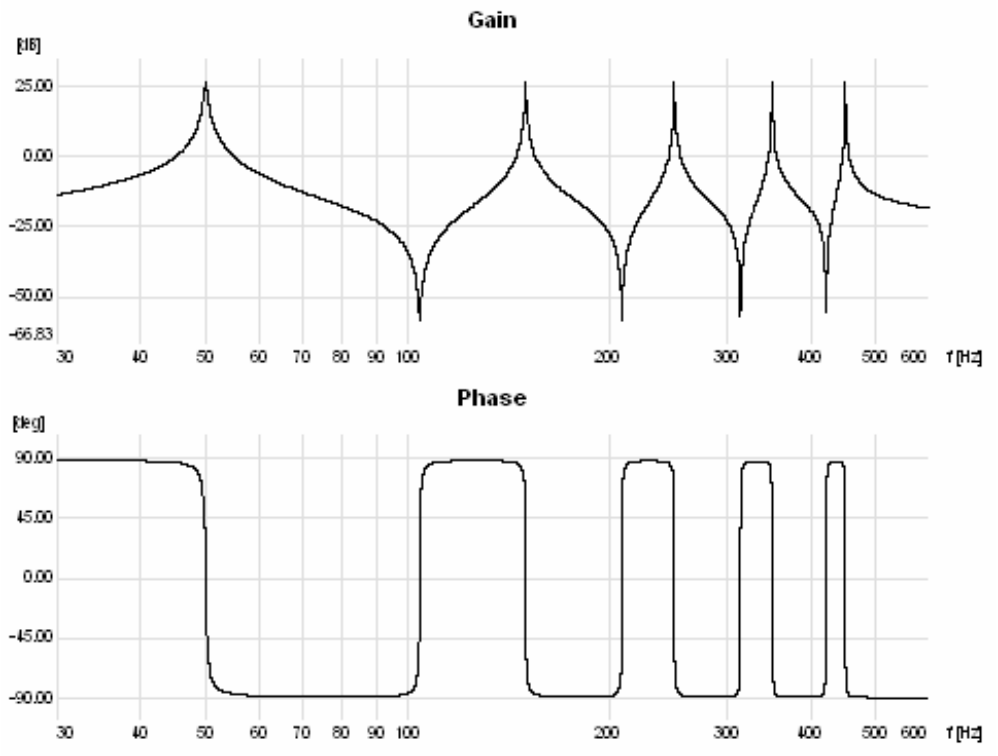

Figure 2.5: The gain and phase characteristics of the constant damped resonant filter bank for $m=\{1, 3, 5, 7, 9\}$, $K_{im}=20$, $\omega_e=2\pi \cdot 50$ rad/s, $\tau_m=5 \cdot 10^{-3}$

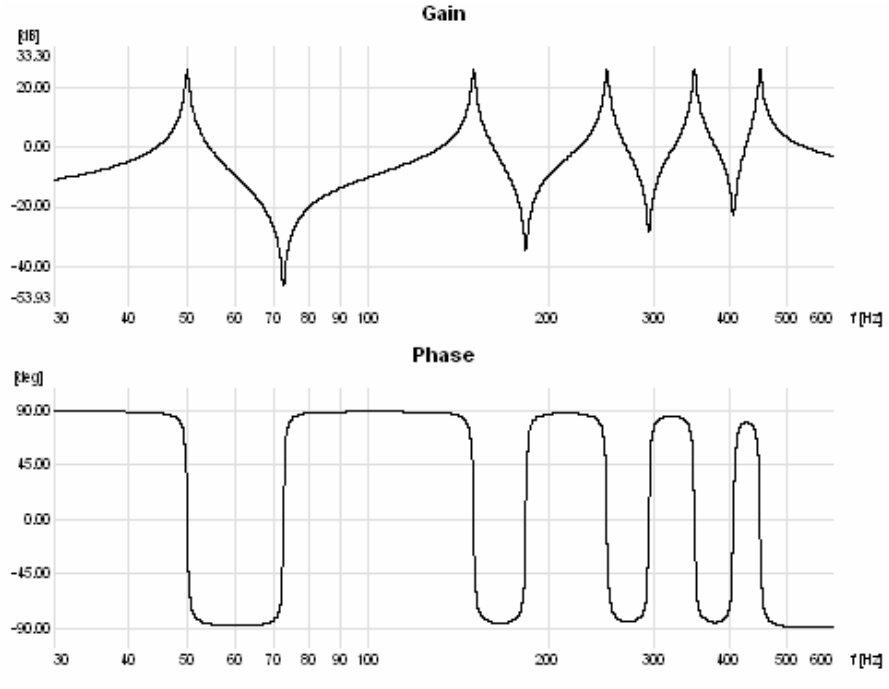

Figure 2.6: The gain and phase characteristics of the variable damped resonant filter bank for m={1, 3, 5, 7, 9}, K_{im}=20, ω_e=2π·50 rad/s, τ_m=m·5·10^{-3}

2.3.2. Phase Delay Compensated and Damped Resonant Filter Banks

The final transfer function of the resonant filter can be obtained by considering the phase delay compensation and the damping in a single filter form. In practical applications τ_m is small and typically τ_m <<1. With this assumption, if the equations Eq. 2.5 and Eq. 2.6 are modified, the final transfer function of the resonant filter is obtained, Eq. 2.10.

$$G_C(s) = \frac{2K_{im} \cdot \tau_m \cdot \omega_e \cdot \left(s \cdot \cos(\phi_m) - m\omega_e \cdot \sin(\phi_m)\right)}{s^2 + 2 \cdot \tau_m \cdot \omega_e \cdot s + (m\omega_e)^2} \qquad \textbf{(2.10)}$$

The transfer function in Eq. 2.10 is the practically necessary form of a resonant filter. The phase compensation angle of the filter ϕ_m must be equal to the phase delay of the system and the damping constant τ_m is chosen by considering the system requirements. These parameters, ϕ_m and τ_m, are the main parameters of the resonant filter that makes it practically applicable. Eq. 2.10 is a basic practical resonant filter structure and its five parameters K_{im}, m, ω_e, τ_m, and ϕ_m are the variables to be utilized in shaping the filter characteristics in the input current controller design procedure of the four-wire PWM rectifier. Figure 2.7 shows the resonant filter bank gain and

phase characteristics for the constant damped and phase compensated case. Whereas, Figure 2.8 shows the variable damped and phase compensated case. Eq. 2.10 is the final form of the resonant filter structure which will be utilized in this thesis for the purpose of controlling the input current of the three-phase four-wire PWM rectifier. The controller will be implemented with a digital signal processor, DSP. Thus, the filter structure must be converted to the discrete time form which involves the discrete domain rather than continuous domain.

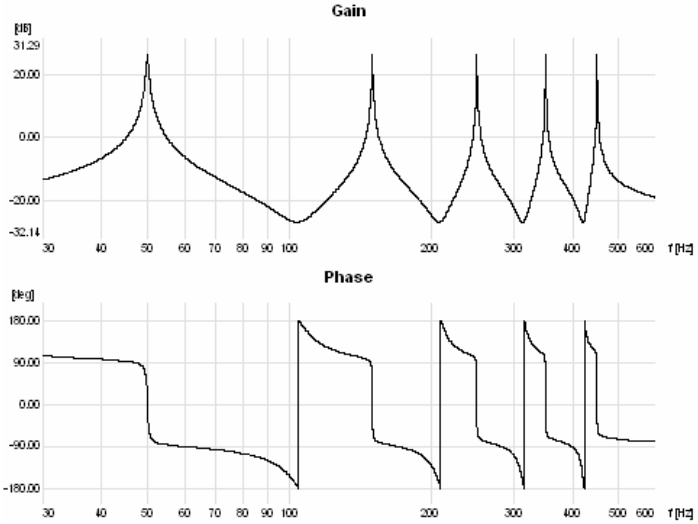

Figure 2.7: The gain and phase characteristics of the constant damped and phase compensated resonant filter bank for m= {1, 3, 5, 7, 9}, K_{im}=20, ω_e=2π·50 rad/sec, $\tau_m = 5 \cdot 10^{-3}$, $\phi_m = 2 \cdot T_s \cdot m\omega_e$

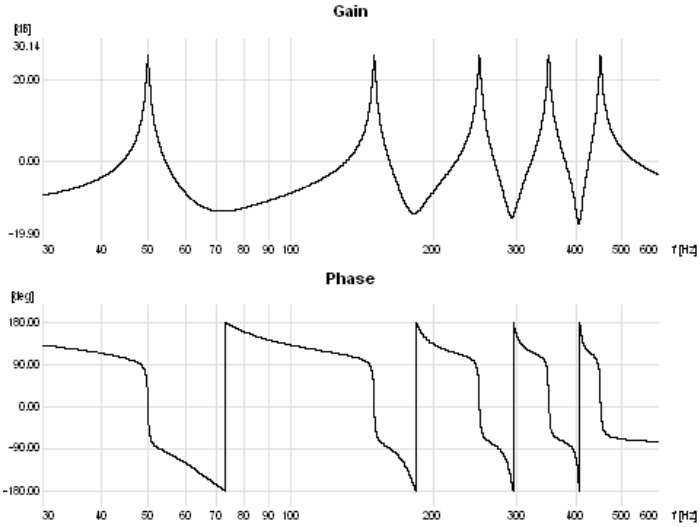

Figure 2.8: The gain and phase characteristics of the variable damped and phase compensated resonant filter bank for m= {1, 3, 5, 7, 9}, K_{im}=20, ω_e=2π·50 rad/sec, $\tau_m = m \cdot 5 \cdot 10^{-3}$, $\phi_m = 2 \cdot T_s \cdot m\omega_e$

2.4. Discrete Time Implementation of Resonant Filter Banks

Usually controllers are designed in the continuous domain for the continuous time systems. Therefore, it is common to design the resonant filter in the continuous domain. However, in order to adapt the controller to a digital signal processor, the controller structure should be expressed in the discrete domain where the discrete time model easily leads to discrete time equations to be utilized in the real time implementation of the controller. There are several methods to provide transformation between continuous domain and discrete domain. Due to its easiness and high accuracy, the Tustin transformation method, Eq. 2.11, will be used in the transformations. In the transformation, the effect of warping is compensated for via the prewarping coefficient A_m which is defined in Eq. 2.12. The prewarping coefficient improves the accuracy of the transformation. By utilizing the Tustin transformation, Eq. 2.10 is transformed to Eq. 2.13 where *X(z)* is the input of the resonant filter and *Y(z)* is the output of the resonant filter. The coefficients of Eq. 2.13 are given in Eq. 2.14 through Eq. 2.18.

$$s = \left(\frac{z-1}{z+1}\right) \cdot A_m \tag{2.11}$$

$$A_m = \frac{m\omega_e}{\tan\left(m\omega_e \cdot \frac{T_S}{2}\right)} \tag{2.12}$$

$$G_C(z) = \frac{Y(z)}{X(z)} = \frac{a_{0m} + a_{1m} \cdot z^{-1} + a_{2m} \cdot z^{-2}}{1 + b_{1m} \cdot z^{-1} + b_{2m} \cdot z^{-2}} \tag{2.13}$$

$$a_{0m} = K_{im} \cdot \frac{2 \cdot \tau_m \cdot m\omega_e \cdot \left(A_m \cdot \cos(\phi_m) - m\omega_e \cdot \sin(\phi_m)\right)}{A_m{}^2 + 2 \cdot \tau_m \cdot m\omega_e \cdot A_m + (m\omega_e)^2} \tag{2.14}$$

$$a_{1m} = K_{im} \cdot \frac{-4 \cdot \tau_m \cdot m\omega_e \cdot m\omega_e \cdot \sin(\phi_m)}{A_m{}^2 + 2 \cdot \tau_m \cdot m\omega_e \cdot A_m + (m\omega_e)^2} \tag{2.15}$$

$$a_{2m} = K_{im} \cdot \frac{-2 \cdot \tau_m \cdot m\omega_e \cdot \left(A_m \cdot \cos(\phi_m) + m\omega_e \cdot \sin(\phi_m)\right)}{A_m{}^2 + 2 \cdot \tau_m \cdot m\omega_e \cdot A_m + (m\omega_e)^2} \tag{2.16}$$

$$b_{1m} = \frac{-2 \cdot \left(A_m{}^2 - (m\omega_e)^2\right)}{A_m{}^2 + 2 \cdot \tau_m \cdot m\omega_e \cdot A_m + (m\omega_e)^2} \tag{2.17}$$

$$b_{2m} = \frac{A_m{}^2 - 2 \cdot \tau_m \cdot m\omega_e \cdot A_m + (m\omega_e)^2}{A_m{}^2 + 2 \cdot \tau_m \cdot m\omega_e \cdot A_m + (m\omega_e)^2} \quad \textbf{(2.18)}$$

If the discrete domain transfer function of the resonant filter given in Eq. 2.11 is transformed to discrete time equations, the discrete response of the filter as shown in Eq. 2.19 is obtained. In Eq. 2.19, x[k] represents the output voltage error at the kT_s interval, and y_m[k+1] represents the m_{th} resonant controller output to be applied to the PWM unit at the $(k+1)T_s$ interval.

$$y_m[k+1] = a_{0m} \cdot x[k] + a_{1m} \cdot x[k-1] + a_{2m} \cdot x[k-2] - b_{1m} \cdot y_m[k] - b_{2m} \cdot y_m[k-1] \quad \textbf{(2.19)}$$

2.5. P+Resonant Controller

In order to improve the rectifier current control loop bandwidth and dynamic performance, a proportional feedback control loop can be added to the system. The proportional controller is connected in parallel with the resonant filter bank. The total feedback control structure becomes one shown in Figure 2.9. The current error signal, which is the difference between the current reference produced by the DC bus voltage controller and the measured current, is multiplied with a proportional gain (K_p) and added to the rectifier reference signal as shown in Figure 2.9. The added proportional gain mainly improves the rectifier performance during loading transients where the current error is large. Additionally, it enhances the current controller bandwidth. By using the proportional term, current controller can compensates for the current harmonic components higher than the largest frequency component of the resonant filter bank. As a result, the performance of the rectifier improves and the input current THD reduces.

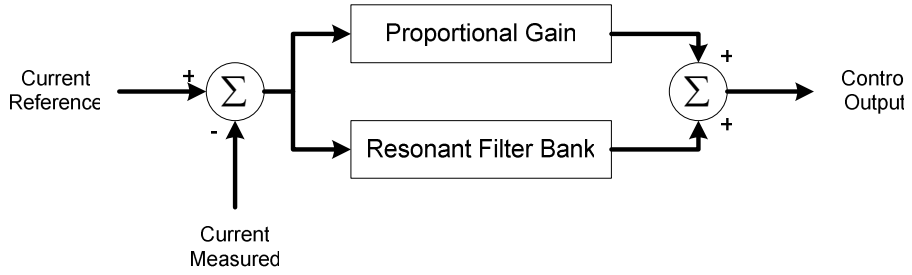

Figure 2.9: Single phase current control block diagram of the four-wire PWM rectifier

Since the proportional control element is in parallel with the resonant filter bank, the gain and phase characteristics of the resonant filter provided in the previous section are modified. The gain and phase characteristic of the ideal P+Resonant controller is given in Figure 2.10. The gain characteristics of both the resonant filter and the P+Resonant filter are the same, but the phase characteristics are different. Figure 2.11 shows the gain and phase characteristics of the damped resonant filter with proportional gain. Similar to the ideal resonant filter case, in the damped resonant filter case, the proportional gain improves the phase characteristic of the controller. The proportional gain also improves the resonant controller gain (K_{im}+K_p).

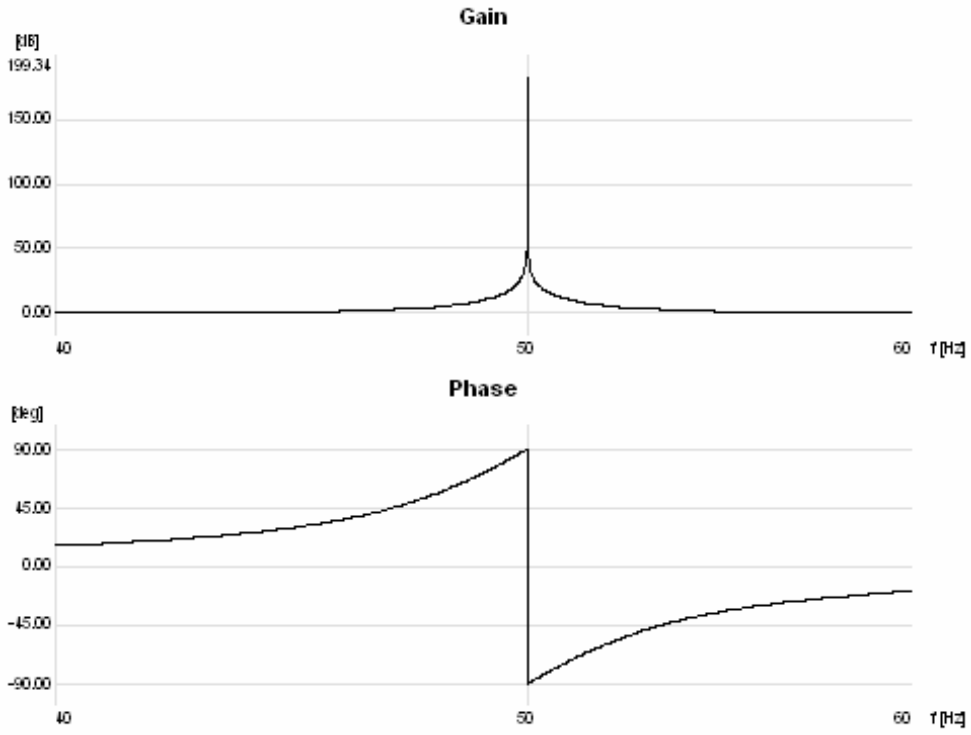

Figure 2.10: The gain and phase characteristics of the ideal P+resonant filter controller for K_p=1, m=1, K_{im}=20, ω_e=2π·50 rad/sec

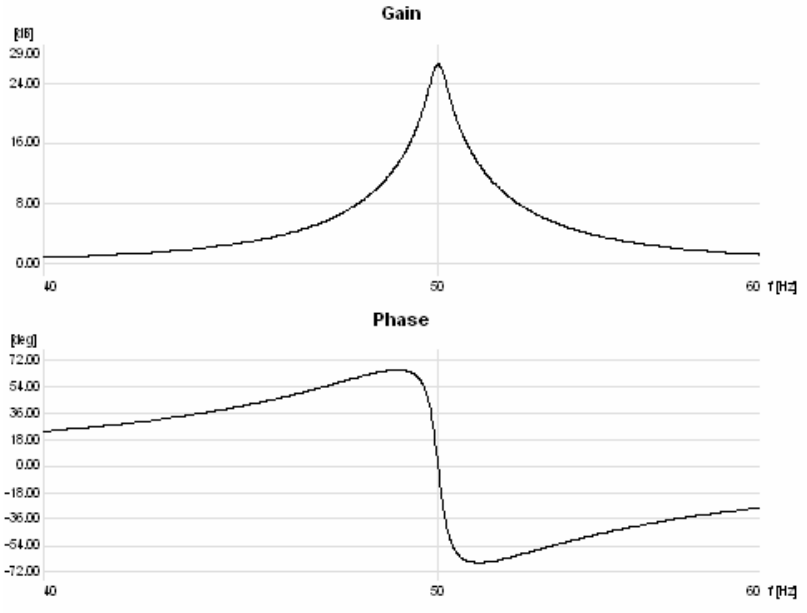

Figure 2.11: The gain and phase characteristics of the damped P+Resonant filter controller for K_p=1, m=1, K_{im}=20, ω_e=2π·50 rad/s, $\tau_1 = 5 \cdot 10^{-3}$

The modified controller gain and phase characteristics of the P+resonant filter bank can be seen in Figure 2.12. The gain characteristics improve slightly at higher frequencies. On the other hand the phase characteristic of the new structure changes significantly. The phase characteristic of the former figures vary between -180^o and 180^o while those of the latter vary between -90^o and 90^o.

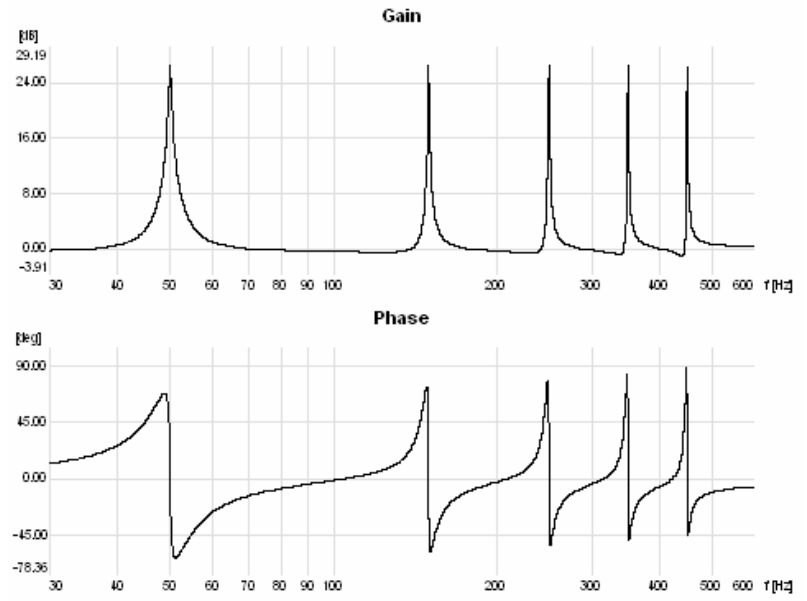

Figure 2.12: The gain and phase characteristics of the constant damped and phase compensated P+resonant filter bank for m= {1, 3, 5, 7, 9}, K_{im}=20, K_p=1, ω_e=2π·50 rad/sec, $\tau_m = 5 \cdot 10^{-3}$, $\phi_m = 2 \cdot T_s \cdot m\omega_e$

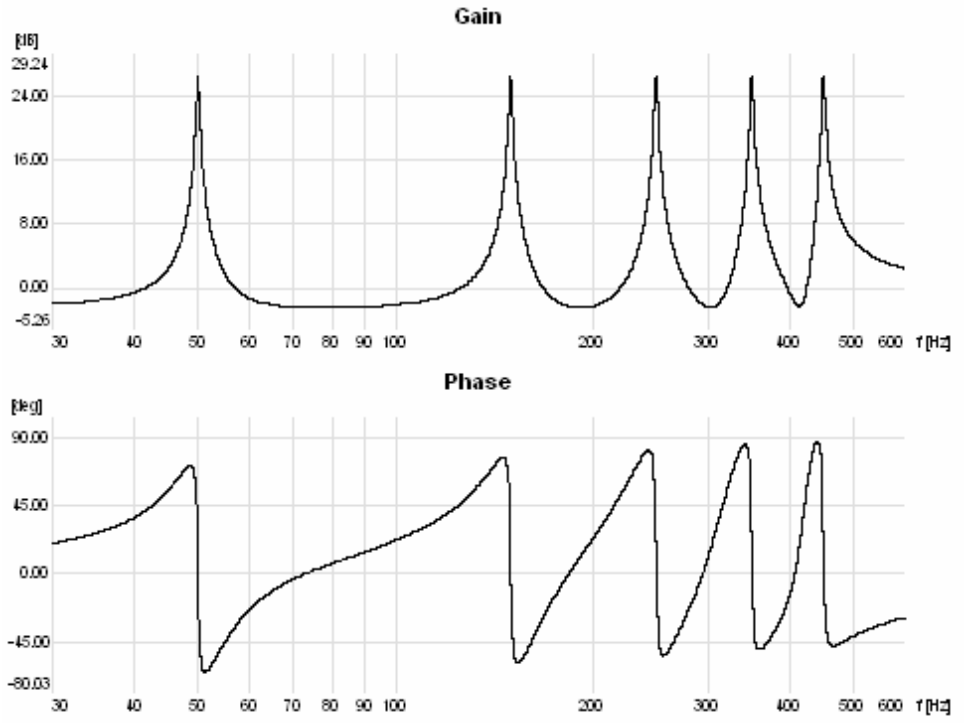

Figure 2.13: The gain and phase characteristics of the variable damped and phase compensated P+resonant filter bank for m= {1, 3, 5, 7, 9}, K_{im}=20, K_p=1, ω_e=2π·50 rad/sec, $\tau_m = m \cdot 5 \cdot 10^{-3}$, $\phi_m = 2 \cdot T_s \cdot m\omega_e$

2.6. The Full Control Structure of the Four Wire PWM Rectifier

In this thesis the three-phase four-wire voltage-source PWM rectifier is controlled by employing cascade controller structure. The outer loop is the voltage loop controller. The voltage controller is chosen as a PI type controller. Since the input variables of the voltage controller are DC signals, a PI type controller achieves high performance. The inner control loop is the current controller. P+resonant filter banks are used in the current controller. Also an input voltage feedforward signal is added for improved tracking performance. The control system block diagram is shown in Figure 2.14 in detail. In the diagram the control structure is primarily shown for one phase and the other phases also have identical controller structure.

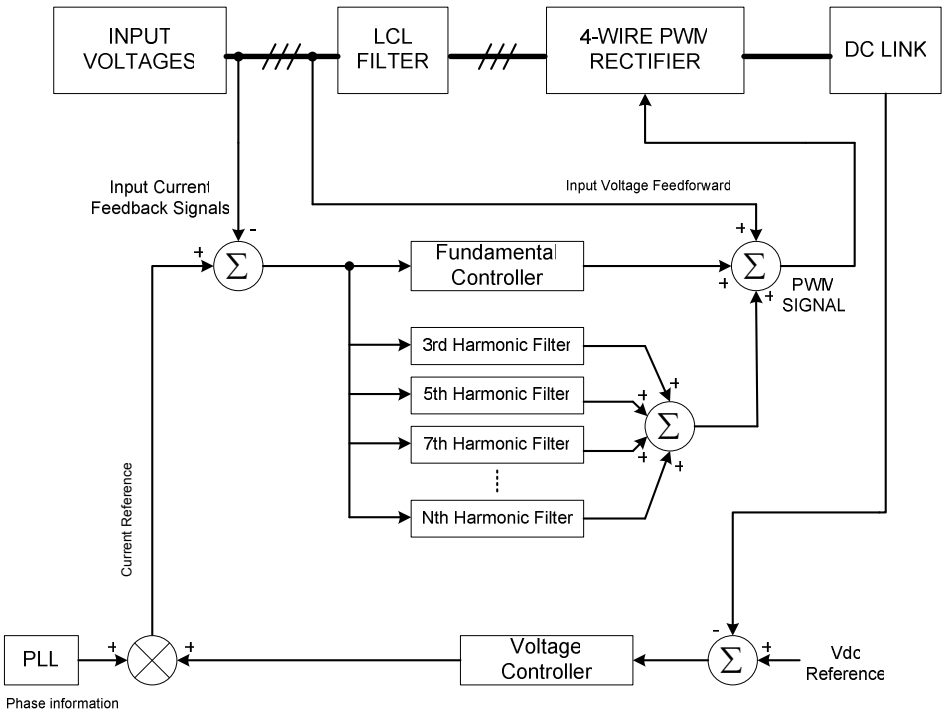

Figure 2.14: The control system block diagram of the four-wire voltage-source PWM rectifier

3. SIMULATION RESULTS

3.1. Introduction

In this chapter, the three-phase four-wire voltage-source pwm rectifier with the control method proposed in Chapter 2 is investigated by means of computer simulation. A three-phase four-wire rectifier system with the power rating of 15 kVA is modeled in the simulation software. The supply voltage of the three-phase rectifier is 220V and 50Hz. The DC bus voltage produced by the rectifier is chosen as 750 Vdc.

Firstly the power stage of the rectifier is modeled in the simulation, and then the proposed control algorithms are implemented. The parameters of the resonant filter bank and the PI type voltage controller are tuned by trial and error. Using this model, steady state and dynamic performance of the three-phase rectifier is investigated under different operating conditions.

3.2. Modeling of the Three Phase Four Wire Voltage Source PWM Rectifier System

The system is modeled by using the Ansoft-Simplorer computer simulation package program [25]. Because of its flexibility in connecting power elements with the digital control blocks, Ansoft-Simplorer is chosen as the simulation program. In this program, the power stage is formed by picking and placing the required components on a graphic window, which is called schematic diagram. Then, PWM signals are produced by using control blocks. These PWM signals are used for switching the power switches, IGBT's. In the simulation, the switching devices are modeled by system level models of these elements. The simulation results are displayed on a new graphic window. Beside of displaying output waveforms in a graphic window, Day Post Processor module of the Simplorer can be used for analysing these waveforms in detail. The input power factor and the input current THD value can be calculated by using Day Post Processor.

The simulation model circuit diagram of the power stage of the three-phase four-wire PWM rectifier is given in Figure 3.1. The utility grid is modeled as a three-phase Y-connected AC voltage-source with 220Vrms/phase (380Vrms line-to-line) and 50Hz ratings. 5^{th}, 7^{th}, 11^{th}, and 13^{th} harmonic voltage-sources with different magnitudes are connected serially to the utility grid for obtaining a distorted utility model. An LCL filter is used for the input filter of the three-phase rectifier. In the LCL filter, a damping resistor is connected serially to the input filter capacitance for passive damping of the resonance at the filter resonance frequency. The additional parameters used in the system are listed in Table 3.1.

Table 3.1: System parameters utilized in the simulation model

LCL Filter	Grid side Inductor (L1,L2,L3)	40 µH
	Rectifier side Inductor (L4,L5,L6)	800 µH
	Filter Capacitor (C1,C2,C3)	10 µF
	Damping Resistor (R4,R5,R6)	5 Ω
	Inductance Resistor (R1,R2,R3)	10 mΩ
DC bus	DC Voltage	750 V
	DC bus Capacitors (C4,C5)	4 mF
Load	Load Resistance	37.5 Ω

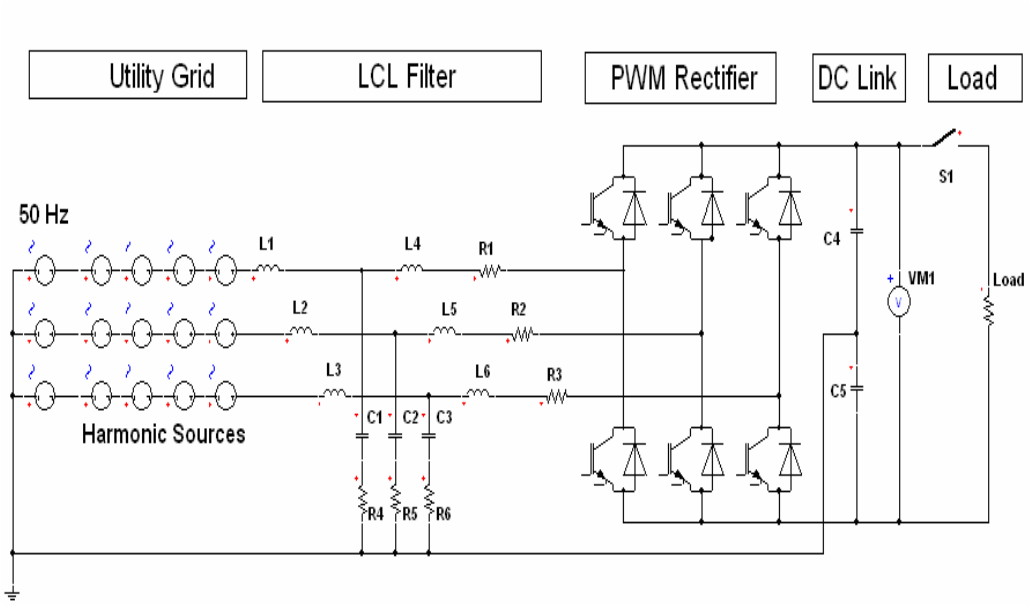

Figure 3.1: Power stage of the Three-Phase Four-Wire PWM rectifier make figure large

The computer simulations of the system shown in Figure 3.1 are simulated for various operating conditions for the purpose of performance investigation. The simulations are carried out by utilizing sufficiently small integration step size in

order to minimize the computational errors. The parameters of the system level switching device models utilized in the simulations are given in Table 3.2. The minimum integration step size is selected as 100 ns so that the simulation results are accurate.

Table 3.2: System level semiconductor device model parameters

Device	Forward Voltage (V)	Bulk Resistance (mΩ)	Blocking Resistance (kΩ)
Diode	1.5	1	100
IGBT	2.5	1	100

In the simulation model, control algorithms are implemented by using the control blocks of Simplorer. The control blocks of Simplorer are executed at a preset rate which could be different than the integration step size. In the three-phase rectifier system, current control loop operates in every PWM cycle and the voltage control loop operates once in eight PWM cycle.

3.3. Simulation Results

In this section, the performance of the three-phase four-wire voltage-source PWM rectifier system is evaluated by means of the computer simulations. Firstly, the gains of the voltage loop PI controller are found by the trial and error method. Then the resonant filter bank based controllers are designed and their control parameters are found by the trial and error method. Once all the controllers are tuned, the design procedure is finished. Following the completion of the controller design stage, the steady state performance of the rectifier system is evaluated under various utility grid conditions.

3.3.1. Trial and Error Based Voltage Controller Tuning Procedure

For adjusting the voltage loop controller gains, the schematic diagram of Figure 3.2 is used. In this schematic diagram the utility grid is pure sine wave with low harmonic content, and the current controller is chosen as a damped P+Resonant controller with only the fundamental frequency component. In the simulation, the switching frequency is set as 12.8 kHz. The sampling rate of the DC bus voltage is chosen as 1.6 kHz. If the voltage controller has a low bandwith, the voltage and current controller loops can be decoupled from each other. This is the reason for choosing the voltage sampling rate very low.

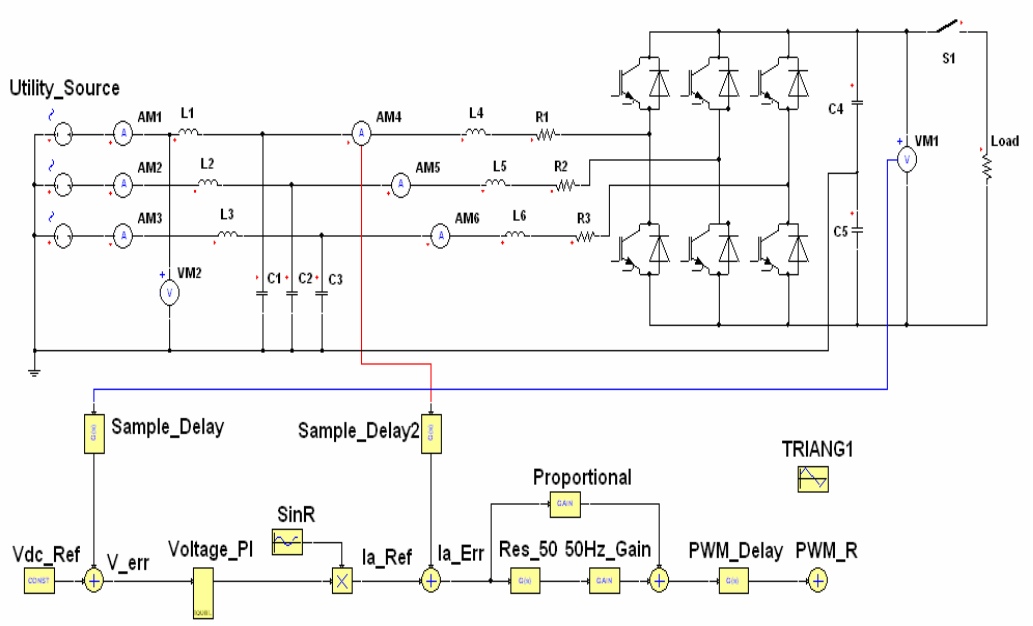

Figure 3.2: Schematic diagram of the Three-Phase Four-Wire PWM Rectifier for adjusting voltage controller gains

Since the voltage controller has a low bandwith, adjusting the controller gains are very easy. After a few simulations, taking care of the overshoot in the DC bus voltage and the settling time, the proportional and integral gains can be adjusted.

3.3.2. Trial and Error Based Current Controller Tuning Procedure

After adjusting the voltage controller gains, for adjusting the current loop controller gains, the schematic diagram of Figure 3.3 is used. The sampling rate of the input currents is chosen as 12.8 kHz, which is equal to the switching frequency.

Resonant filter blocks that can be seen in Figure 3.3 (Res_50, Res_250 etc) are designed using the following equation;

$$G_C(s) = \frac{2K_{im} \cdot \tau_m \cdot m\omega_e \cdot \left(s \cdot \cos(\phi_m) - m\omega_e \cdot \sin(\phi_m)\right)}{s^2 + 2 \cdot \tau_m \cdot m\omega_e \cdot s + (m\omega_e)^2} \qquad \textbf{(3.1)}$$

The parameters of the resonant filters are listed in Table 3.3

Table 3.3: Resonant Filter Parameters

K_{im}	Integral Gain	20
τ_m	Damping Coeffient	0.005
ω_e	Fundamental Frequency	100·π (rad/s)
ϕ_m	Phase Delay Angle	m·2.8125 (degrees)

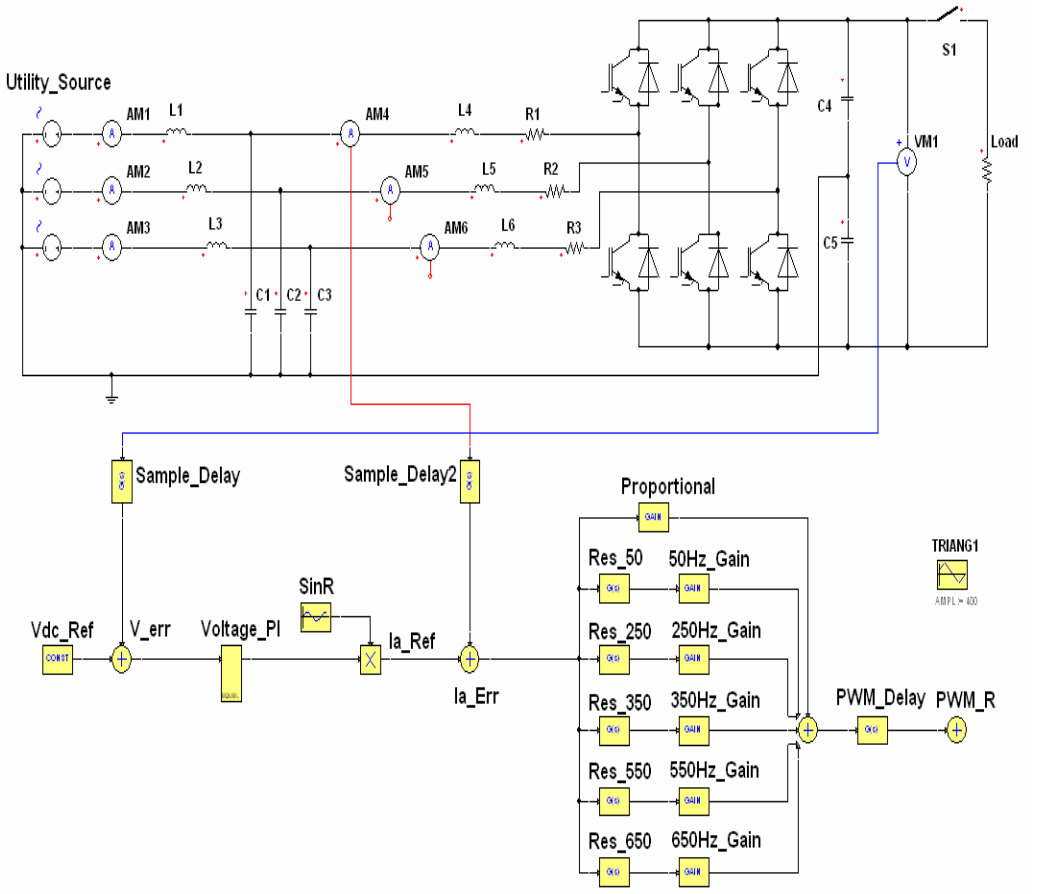

Figure 3.3: Schematic diagram of the Three-Phase Four-Wire PWM Rectifier for adjusting current controller gains

The resonant filters in the current controller of each phase are designed with the same integral gain and parameters at the beginning. The outputs of these filters are multiplied by different gains. For the purpose of adjusting these gains, a highly distorted utility grid is used in Figure 3.3. In the first simulation only the proportional gain of the fundamental component resonant filter is nonzero. In this simulation, the gain of the fundamental component and the proportional gain of the controller are tuned. Then checking the harmonic spectrum of the input current, the proportional gain of the next resonant filter is added. Since each resonant filter is decoupled from each other, the resonant filter gains are tuned in a sequence. Once the resonant filter for this harmonic is built and tuned, this harmonic is suppressed and the next dominant harmonic is taken into consideration. This procedure continues until the highest intended harmonic is suppressed to a sufficient degree. The method of tuning each filter component is based on the degree of improvement. Every filter parameter is increased to a point where it is no more beneficial to further increase the

parameter. The final parameters of the voltage and the current controller are listed in Table 3.4.

Table 3.4: Voltage and Current Controller Parameters of the Three-Phase Four-Wire Voltage-source PWM Rectifier

Voltage Controller	Proportional Gain	0.4
	Integral Gain	100
	Sampling Time	625 us
Current Controller	Proportional Gain	0.6
	50Hz_Gain	1.25
	250Hz_Gain	0.75
	350Hz_Gain	0.75
	550Hz_Gain	0.75
	650Hz_Gain	0.75
	Sampling Time	78.125 us

After adjusting the gains of the all resonant filters, the performance of the three-phase four-wire voltage-source PWM rectifier is tested by simulating the schematic in Figure 3.3 under highly distorted, distorted, and undistorted utility operation. The rms values of the added voltage sources with different frequencies, for simulating the highly distorted, distorted and undistorted utility is given in Table 3.5. In all these simulations, damped and phase compensated type of the resonant filters, Eq. 3.1, are used in the current controllers at the beginning. Also, in order to see the performance differences between different types of resonant filter forms, the schematic in Figure 3.3 is simulated again using the resonant filter forms in Eq. 3.2 and Eq. 3.3.

Table 3.5: Harmonic contents of the voltage-sources used in the simulations

Highly Distorted Utility	Fundamental Frequency, 50 Hz	220 V_{rms} (100 %)
	5^{th} harmonic component	3.64 %
	7^{th} harmonic component	3.64 %
	11^{th} harmonic component	5.45 %
	13^{th} harmonic component	5.45 %
Distorted Utility	Fundamental Frequency, 50 Hz	220 V_{rms} (100 %)
	5^{th} harmonic component	1.82 %
	7^{th} harmonic component	3.18 %
	11^{th} harmonic component	-
	13^{th} harmonic component	1.82 %
Undistorted Utility	Fundamental Frequency, 50 Hz	220 V_{rms} (100 %)
	5^{th} harmonic component	-
	7^{th} harmonic component	-
	11^{th} harmonic component	-
	13^{th} harmonic component	-

$$G_C(s) = \frac{2K_{im} \cdot \tau_m \cdot \omega_e \cdot \left(s \cdot \cos(\phi_m) - m\omega_e \cdot \sin(\phi_m)\right)}{s^2 + 2 \cdot \tau_m \cdot \omega_e \cdot s + (m\omega_e)^2} \quad \textbf{(3.2)}$$

$$G_C(s) = \frac{2K_{im} \cdot \tau_m \cdot m\omega_e \cdot s}{s^2 + 2 \cdot \tau_m \cdot m\omega_e \cdot s + (m\omega_e)^2} \quad \textbf{(3.3)}$$

3.3.2.1. Simulation Results of the Four Wire Rectifier under Higly Distorted Utility

The simulation model of the Three-Phase Four-Wire Voltage-source PWM Rectifier, Figure 3.3, is simulated using the parameters in Table 3.3 and Table 3.4. The results of the simulations for the highly distorted utility are given in Figure 3.5 through Figure 3.11.

Highly distorted three-phase input voltage waveforms can be seen in Figure 3.4. With these fundamental and harmonic components listed in Table 3.5, input voltage total harmonic distortion, V_{THD}, equals to 9.27 %.

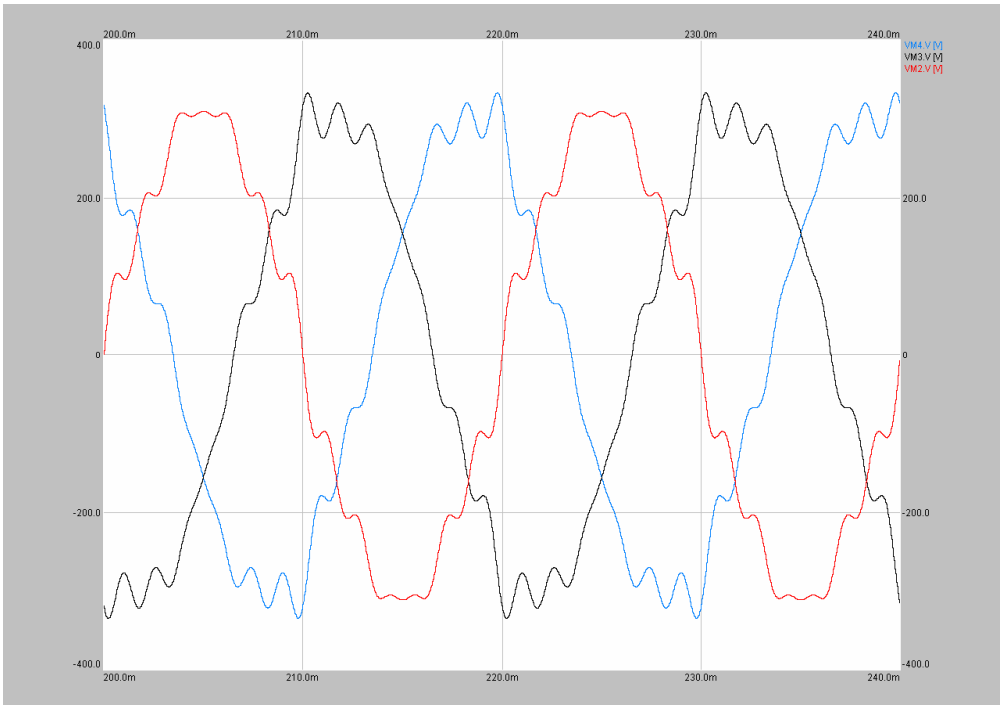

Figure 3.4: Steady state highly distorted input phase voltages

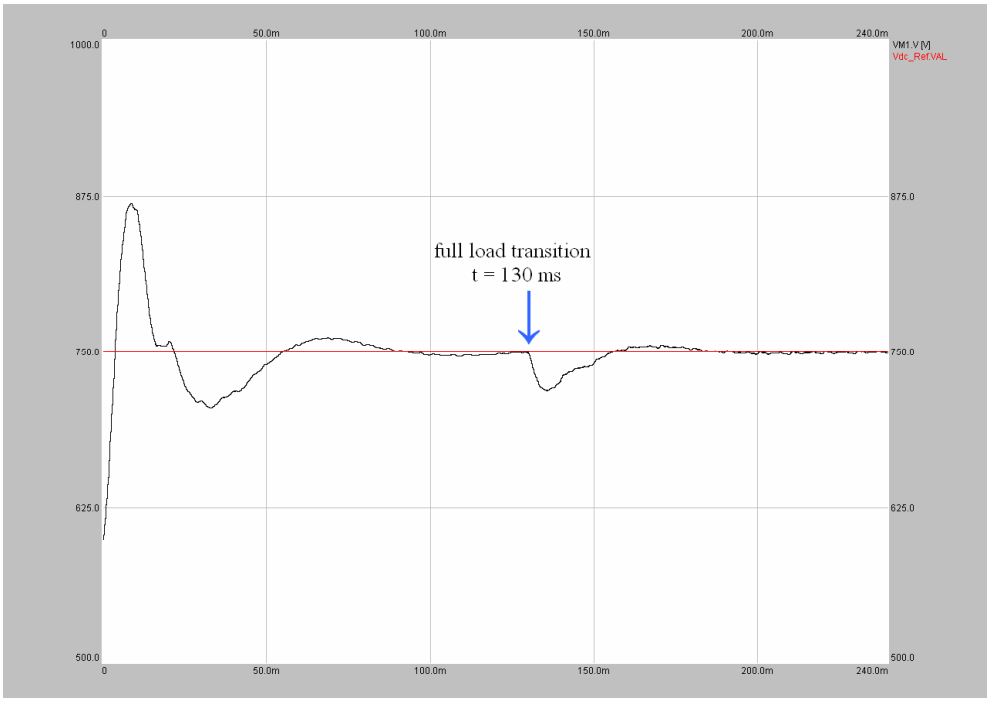

Figure 3.5: DC bus voltage and reference value for the variable damped and phase compensated resonant filter form under highly distorted utility

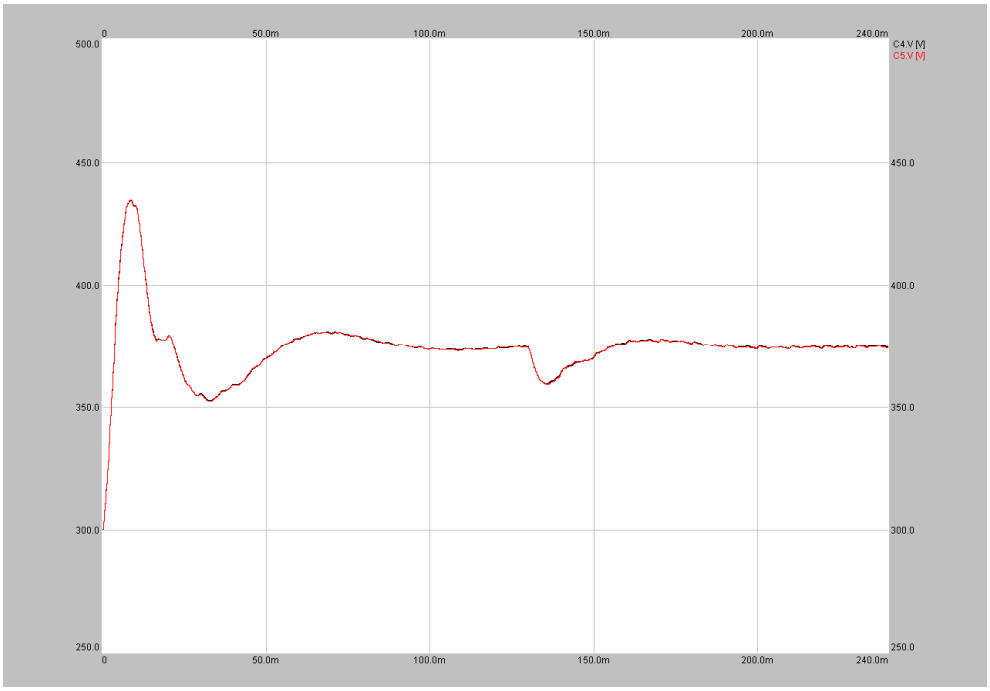

Figure 3.6: Positive and negative half DC bus voltage for the variable damped and phase compensated resonant filter form under highly distorted utility

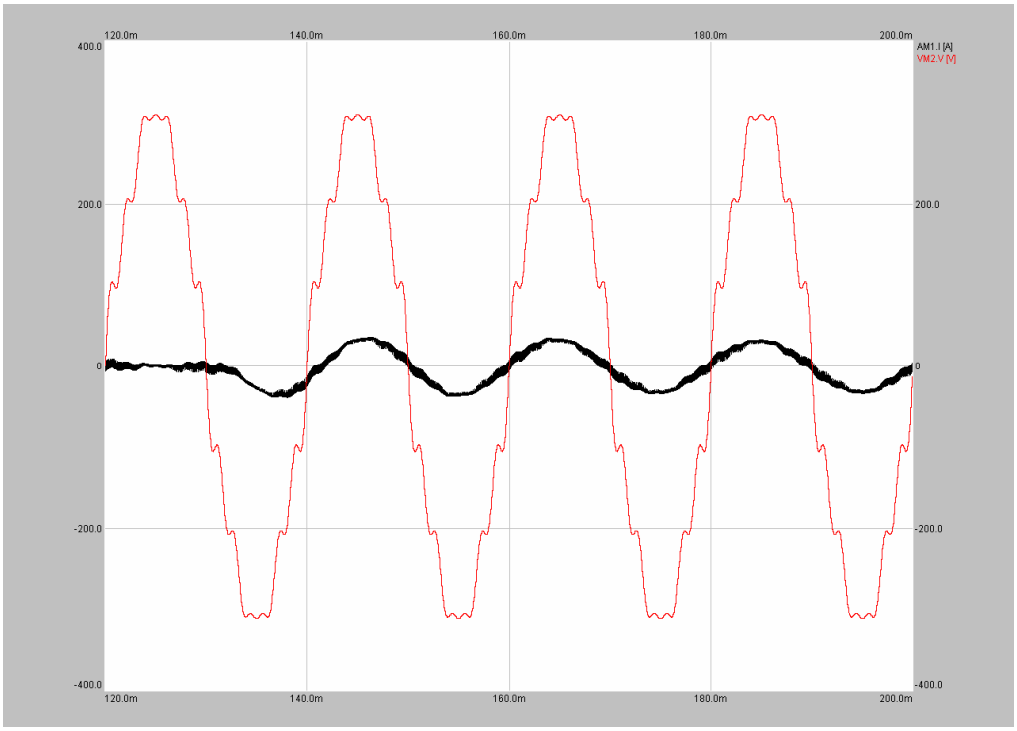

Figure 3.7: Input phase voltage and current at the instant of loading for the variable damped and phase compensated resonant filter form under highly distorted utility

In Figure 3.5 to 3.7, the simulation results of the four-wire PWM rectifier employing variable damped, phase compensated resonant filter form in the current controller under highly distorted utility can be seen. In Figure 3.5, the DC bus voltage reference and the measured value can be seen. As it can be seen from Figure 3.5, when the system is fully loaded at t = 130 ms, the rectifier DC bus voltage decreases only 30 volts, and the proposed control algorithm compensates this voltage decrease in less than two fundamental cycles. In Figure 3.6, the DC voltage waveforms of the two split capacitors that form the DC bus can be seen. The DC voltage levels of the two capacitors are equal to each other. In the transformerless UPS application, if the voltage levels of the two split capacitors are not equal to each other, DC offset occurs on the inverter output voltage waveforms. Thus, it is very important to assure the equality of the DC voltage levels of the two split capacitors in the four-wire PWM rectifier. In Figure 3.7, the rectifier input voltage and current waveforms at the instant of load transition can be seen. The rectifier input voltage and current is measured by voltmeter VM2 and ammeter AM1 in Figure 3.2. The controller reacts to the load change very rapidly and the input current stabilizes in a few miliseconds.

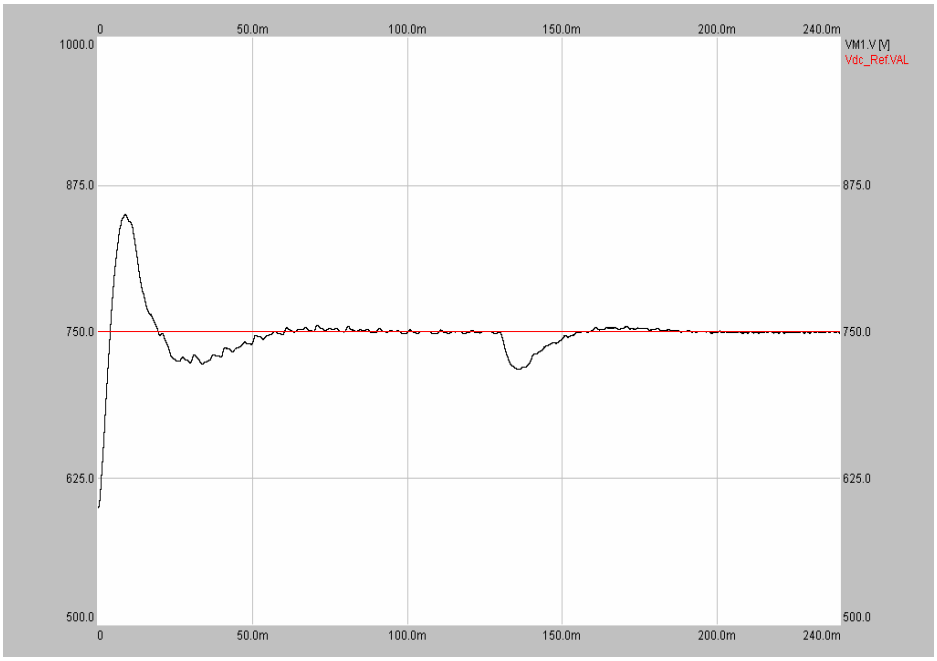

Figure 3.8: DC bus voltage and reference value for the constant damped and phase compensated resonant filter form under highly distorted utility

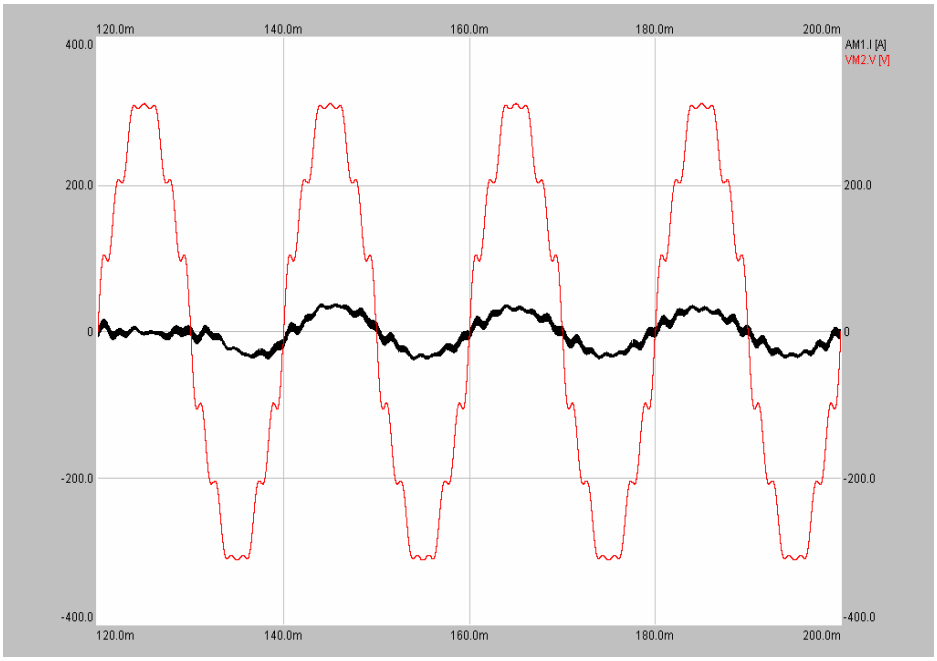

Figure 3.9: Input phase voltage and current at the instant of loading for the constant damped and phase compensated resonant filter form under highly distorted utility

In Figure 3.8 and 3.9, the simulation results of the four-wire PWM rectifier employing constant damped, phase compensated resonant filter form in the current controller can be seen. In this case, the damping coefficient of each resonant filter for

different frequencies is chosen as equal to each other. As a result of this, the performances of the resonant filters with higher resonance frequencies become unsatisfactory. As it can be seen in Figure 3.9, the most dominant harmonic frequencies of the input currents are the 11^{th} and the 13^{th} harmonic components.

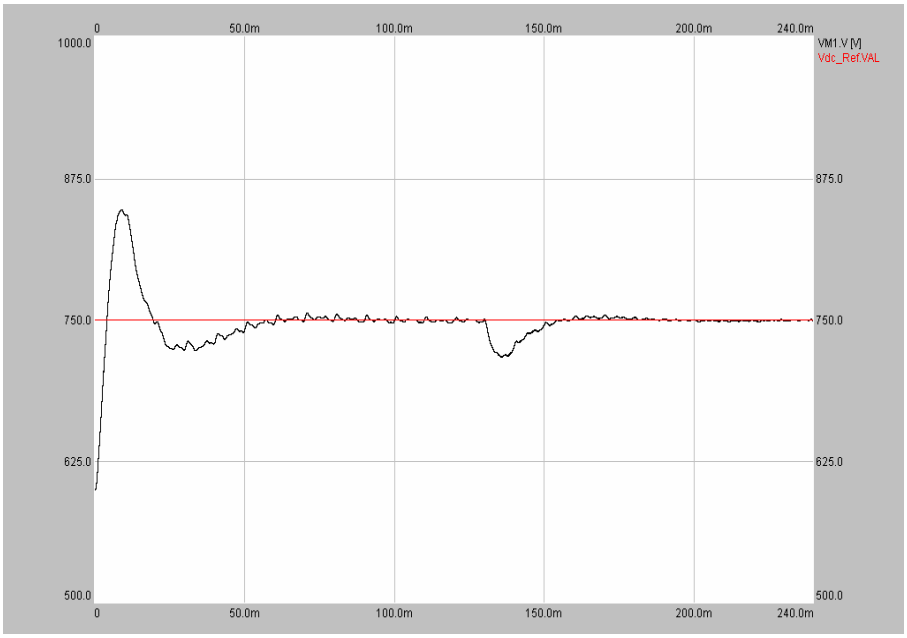

Figure 3.10: DC bus voltage and reference value for the constant damped resonant filter form under highly distorted utility

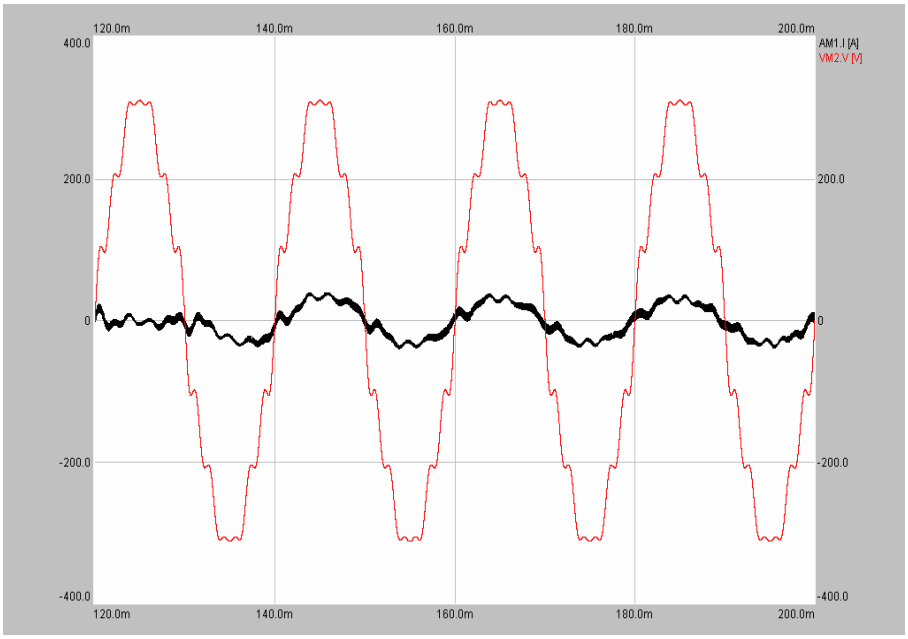

Figure 3.11: Input phase voltage and current at the instant of loading for the constant damped resonant filter form under highly distorted utility

In Figure 3.10 and 3.11, the simulation results of the four-wire PWM rectifier employing only the constant damped resonant filter form in the current controller can be seen. Since the resonant filters used in the current controller of the rectifier are not phase compensated, phase delay of the system results in a poor steady state performance of the four-wire PWM rectifier. As it can be seen in Figure 3.11, all the harmonic components are dominant in the three-phase input current waveforms. Although the input current waveform is highly distorted, the dc bus voltage regulation is sufficient due to the high dc gain of the PI voltage controller.

Table 3.6: Performance comparison of three resonant filter forms under highly distorted utility

	Power Factor, PF	Input Current Total Harmonic Distortion, I_{THD}	Input Voltage Total Harmonic Distortion, V_{THD}
Variable damped phase compensated	**0.989**	**7.38 %**	**9.27 %**
Constant damped phase compensated	**0.973**	**16.07 %**	**9.27 %**
Constant damped	**0.96**	**18.9 %**	**9.27 %**

In Table 3.6, the performance comparison of the simulations with the three different resonant filter forms can be seen. The power factor values of the all three forms are in acceptable limits. However, the input current THD values of the constant damped, phase compensated form and the only constant damped form are very high. For the variable damped, phase compensated resonant filter case; the input current THD value is smaller than the input voltage THD value. The input voltage harmonic components and the current harmonic components for different resonant filter forms can be seen in Table 3.7 through Table 3.10.

Table 3.7: Highly distorted input voltage harmonic content

Frequency (Hz)	**Percentage (%)**
50	100
250	3.64
350	3.64
550	5.45
650	5.45

Table 3.8: Input current harmonic content for the variable damped and phase compensated resonant filter form under highly distorted utility

Frequency (Hz)	Percentage (%)
50	100
250	2.68
350	2.60
550	3.26
650	3.31

Table 3.9: Input current harmonic content for the constant damped and phase compensated resonant filter form under highly distorted utility

Frequency (Hz)	Percentage (%)
50	100
250	3.20
350	3.24
550	8.61
650	12.74

Table 3.10: Input current harmonic content for the constant damped resonant filter form under highly distorted utility

Frequency (Hz)	Percentage (%)
50	100
250	5.36
350	9.27
550	5.37
650	13.77

3.3.2.2. Simulation Results of the Four Wire Rectifier under Distorted Utility

In Figure 3.13 and 3.14, the simulation results of the four-wire PWM rectifier employing variable damped, phase compensated resonant filter form in the current controller under distorted utility can be seen. In Figure 3.13, the DC bus voltage reference and the measured value can be seen. In Figure 3.14, the rectifier input voltage and current waveforms under full load can be seen.

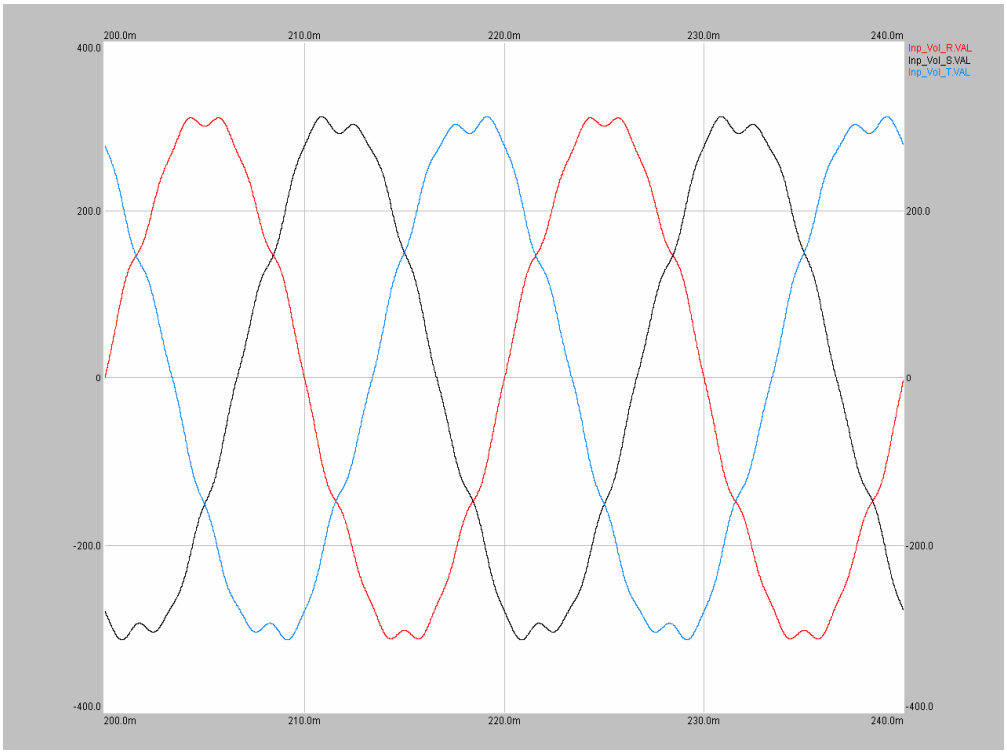

Figure 3.12: Steady state distorted input phase voltages

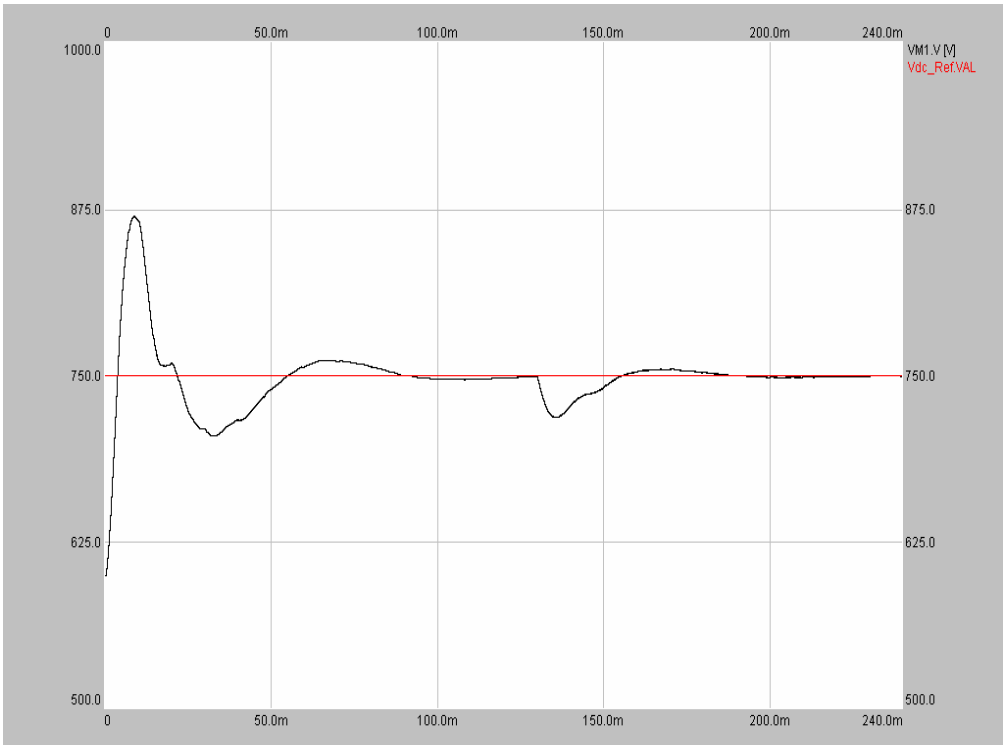

Figure 3.13: DC bus voltage and reference value for the variable damped and phase compensated resonant filter form under distorted utility

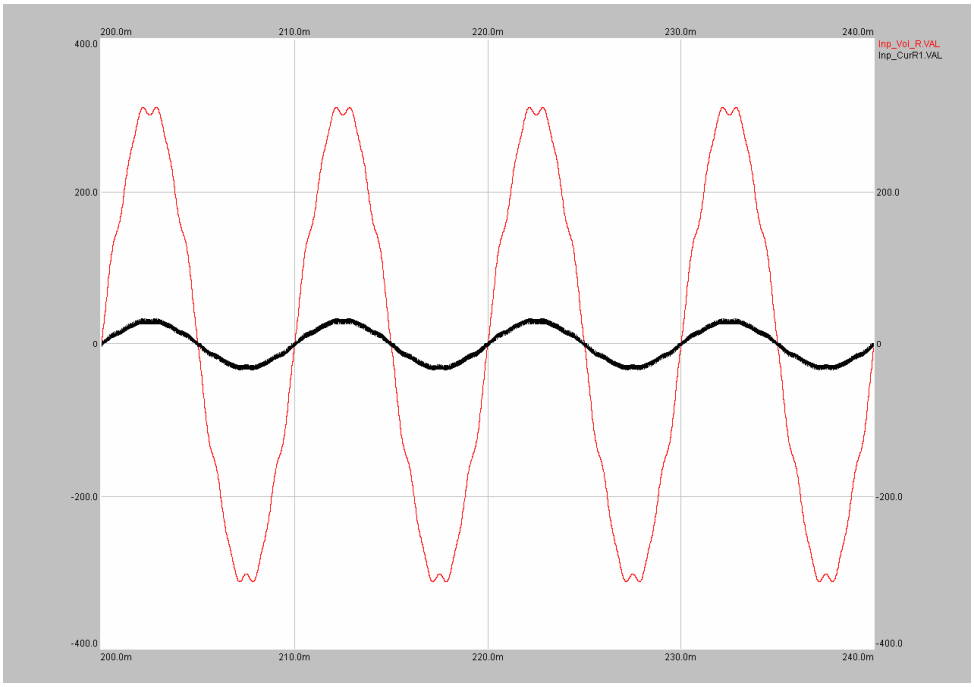

Figure 3.14: Input phase voltage and current under full load for the variable damped and phase compensated resonant filter form under distorted utility

In Figure 3.15 and 3.16, the simulation results of the four-wire PWM rectifier employing constant damped, phase compensated resonant filter form in the current controller under distorted utility can be seen.

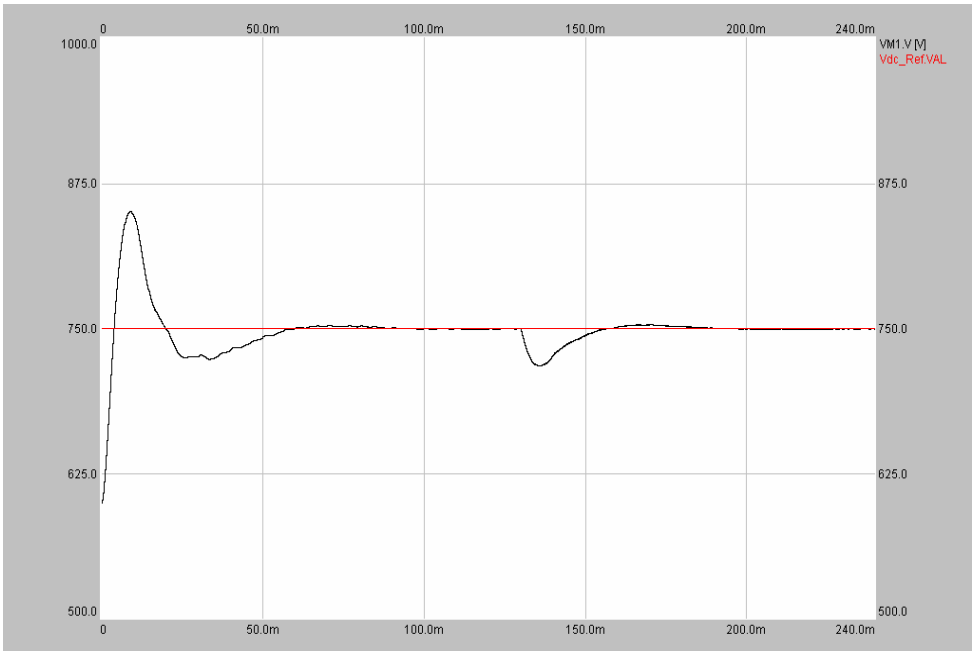

Figure 3.15: DC bus voltage and reference value for the constant damped and phase compensated resonant filter form under distorted utility

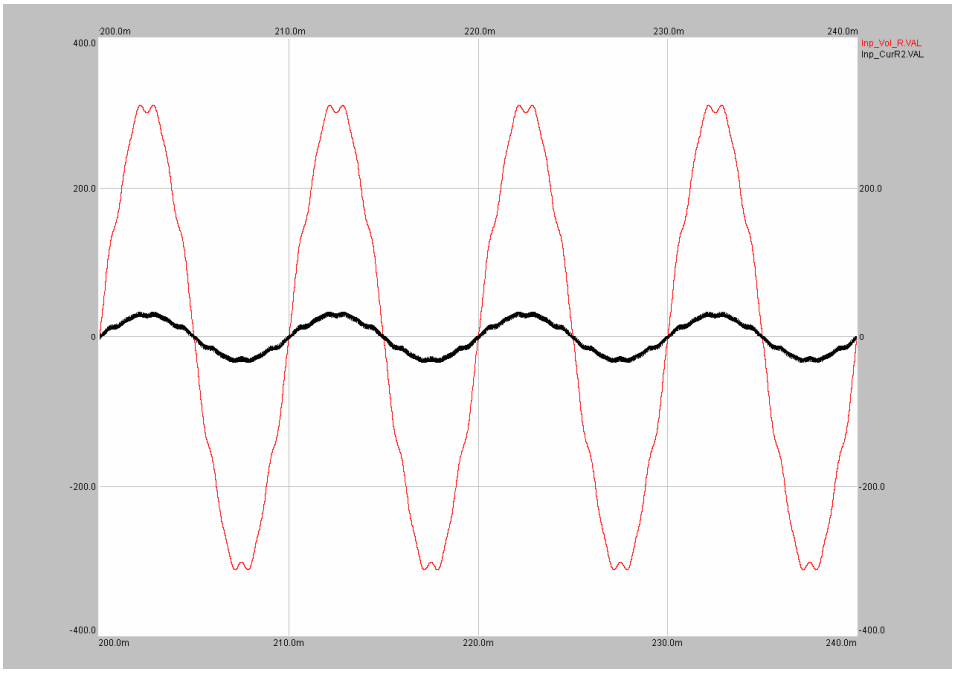

Figure 3.16: Input phase voltage and current under full load for the constant damped and phase compensated resonant filter form under distorted utility

In Figure 3.17 and 3.18, the simulation results of the four-wire PWM rectifier employing only the constant damped resonant filter form in the current controller under distorted utility can be seen.

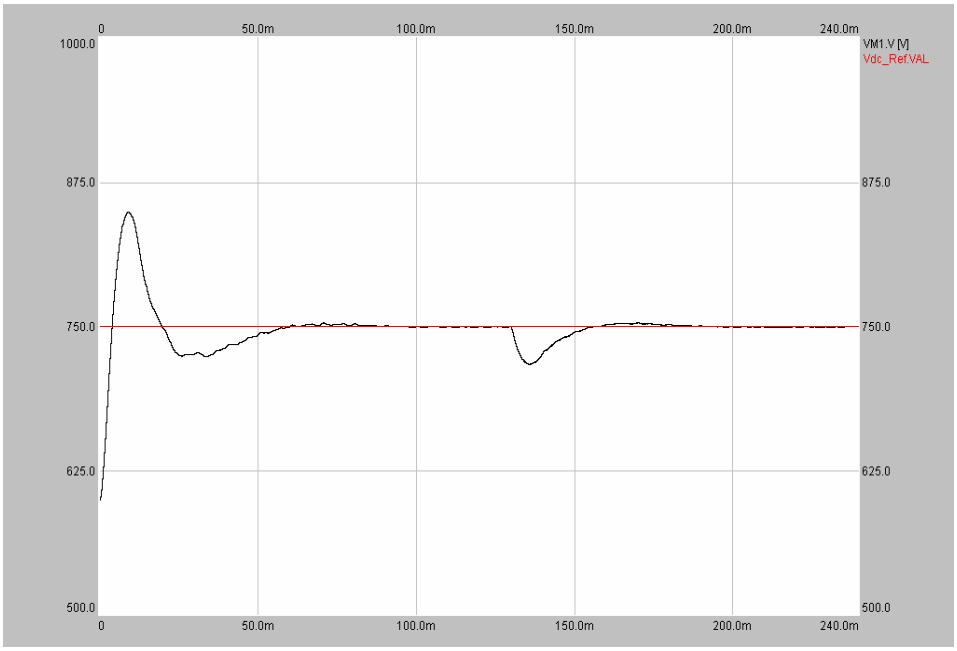

Figure 3.17: DC bus voltage and reference value for the constant damped resonant filter form under distorted utility

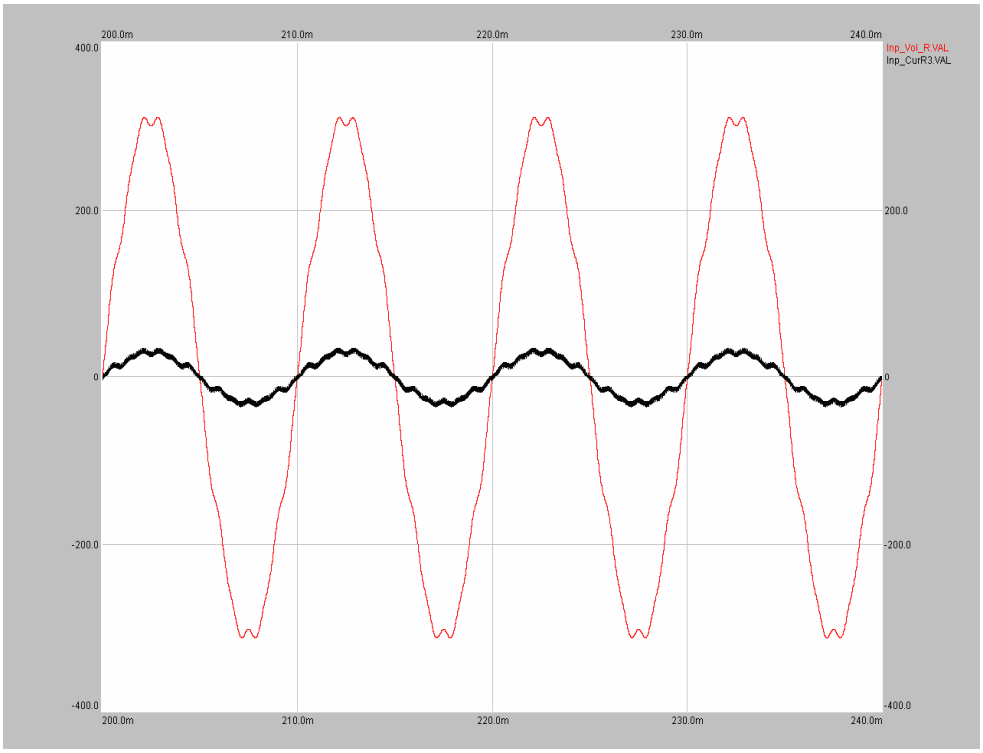

Figure 3.18: Input phase voltage and current under full load for the constant damped resonant filter form under distorted utility

In Table 3.11, the performance comparison of the simulations with the three different resonant filter forms can be seen. As in the highly distorted utility case, the power factor values of the all three forms are in acceptable limits again. However, the input current THD values of the constant damped, phase compensated form and the only constant damped form are very high. For the variable damped, phase compensated resonant filter case; the input current THD value is smaller than 4 %.

Table 3.11: Performance comparison of three resonant filter forms under distorted utility

	Power Factor, PF	Input Current Total Harmonic Distortion, I_{THD}	Input Voltage Total Harmonic Distortion, V_{THD}
Variable damped phase compensated	**0.99**	**3.5 %**	**4.1 %**
Constant damped phase compensated	**0.986**	**6.65 %**	**4.1 %**
Constant damped	**0.98**	**10.11 %**	**4.1%**

Table 3.12: Distorted input voltage harmonic content

Frequency (Hz)	Percentage (%)
50	100
250	1.82
350	3.18
650	1.82

Table 3.13: Input current harmonic content for the variable damped and phase compensated resonant filter form under distorted utility

Frequency (Hz)	Percentage (%)
50	100
250	1.89
350	2.73
650	1.43

Table 3.14: Input current harmonic content for the constant damped and phase compensated resonant filter form under distorted utility

Frequency (Hz)	Percentage (%)
50	100
250	3.07
350	5.23
650	2.77

Table 3.15: Input current harmonic content for the constant damped resonant filter form under distorted utility

Frequency (Hz)	Percentage (%)
50	100
250	3.37
350	6.85
650	7.82

3.3.2.3. Simulation Results of the Four Wire Rectifier under Undistorted Utility

In Figure 3.20 and 3.21, the simulation results of the four-wire PWM rectifier employing variable damped, phase compensated resonant filter form in the current controller under undistorted utility can be seen. In Figure 3.20, the DC bus voltage reference and the measured value can be seen. In Figure 3.21, the rectifier input voltage and current waveforms at the instant of load transition can be seen.

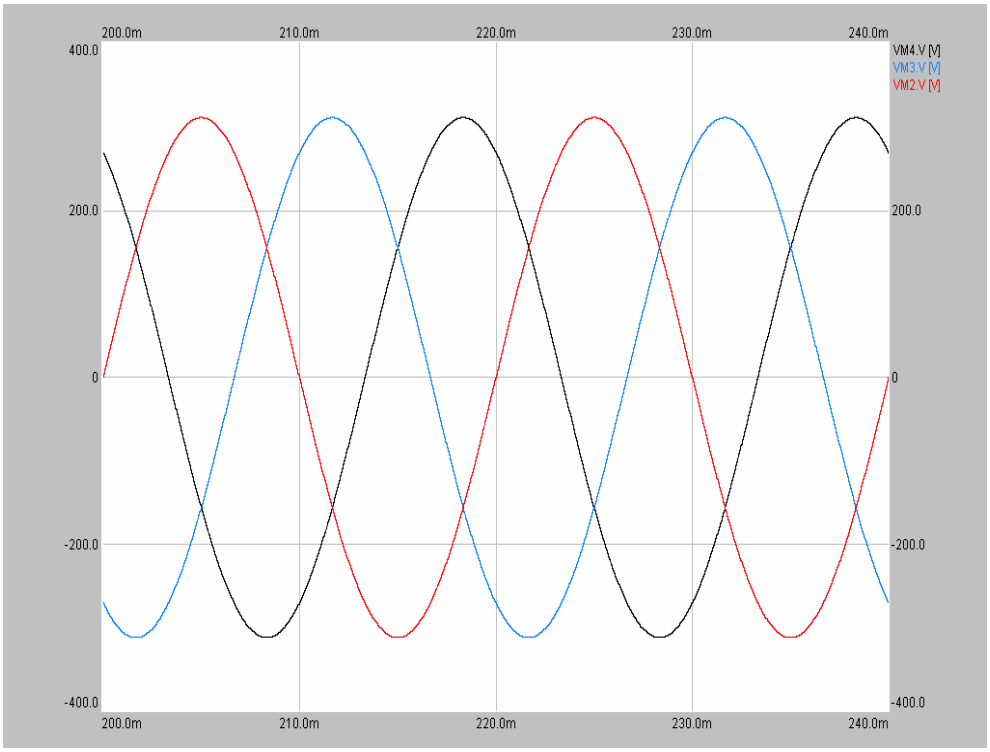

Figure 3.19: Steady state undistorted input phase voltages

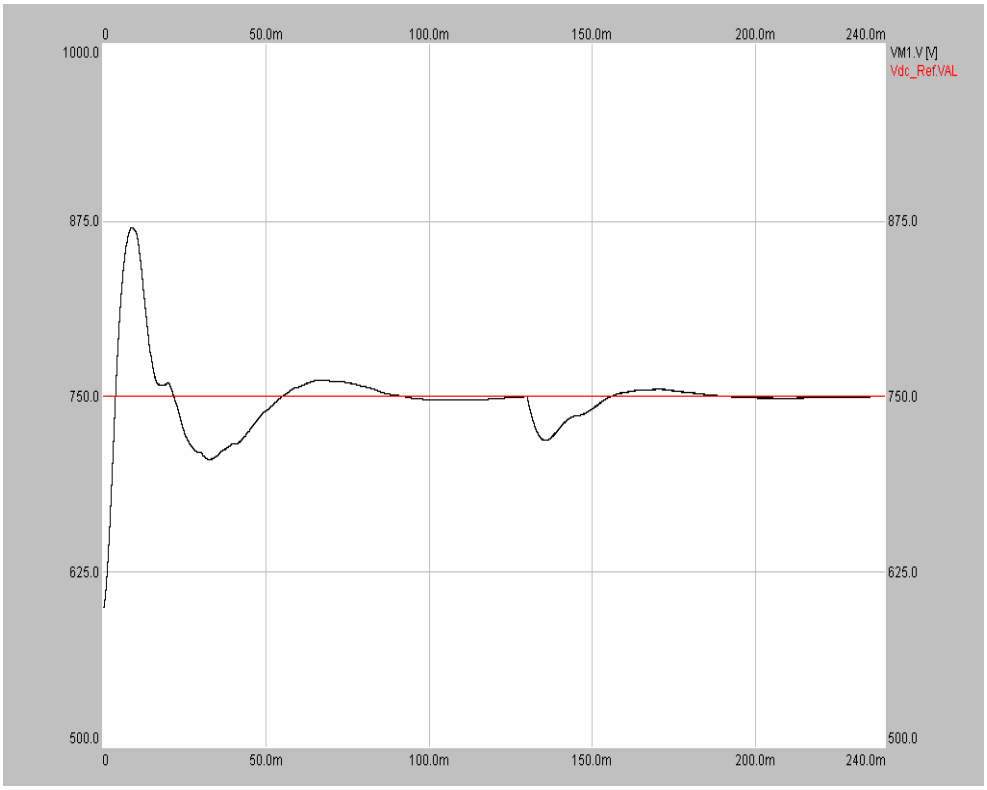

Figure 3.20: DC bus voltage and reference value for the variable damped and phase compensated resonant filter form under undistorted utility

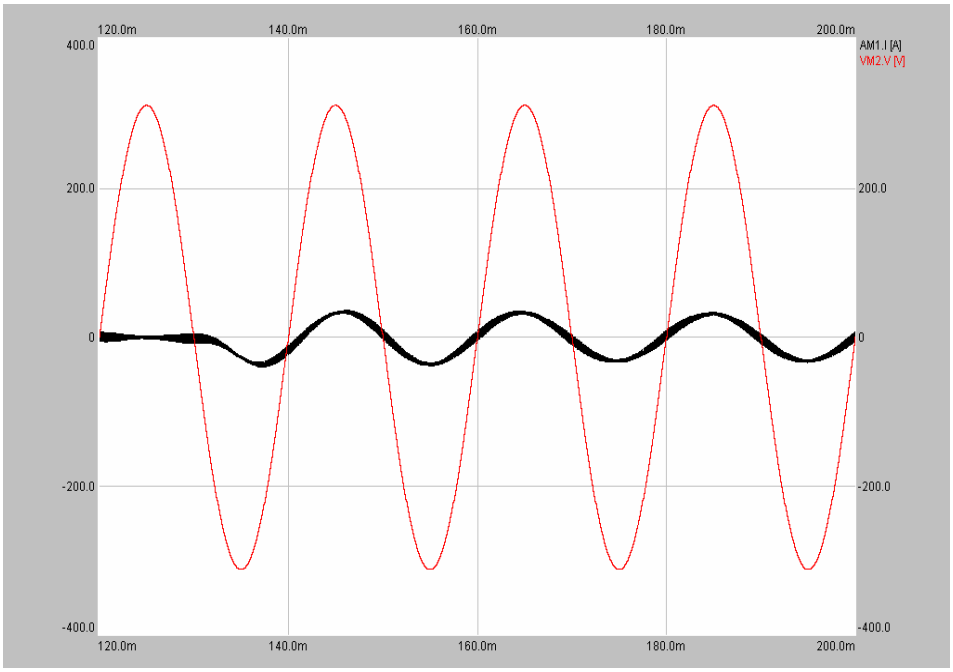

Figure 3.21: Input phase voltage and current at the instant of loading for the variable damped and phase compensated resonant filter form under undistorted utility

In Figure 3.22 and 3.23, the simulation results of the four-wire PWM rectifier employing constant damped, phase compensated resonant filter form in the current controller under undistorted utility can be seen.

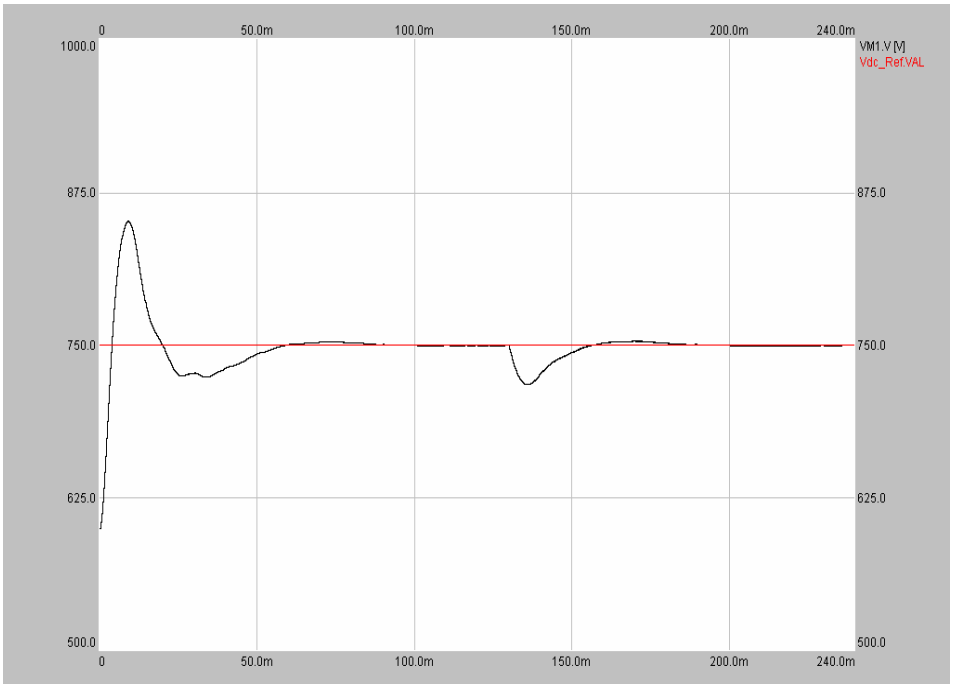

Figure 3.22: DC bus voltage and reference value for the constant damped and phase compensated resonant filter form under undistorted utility

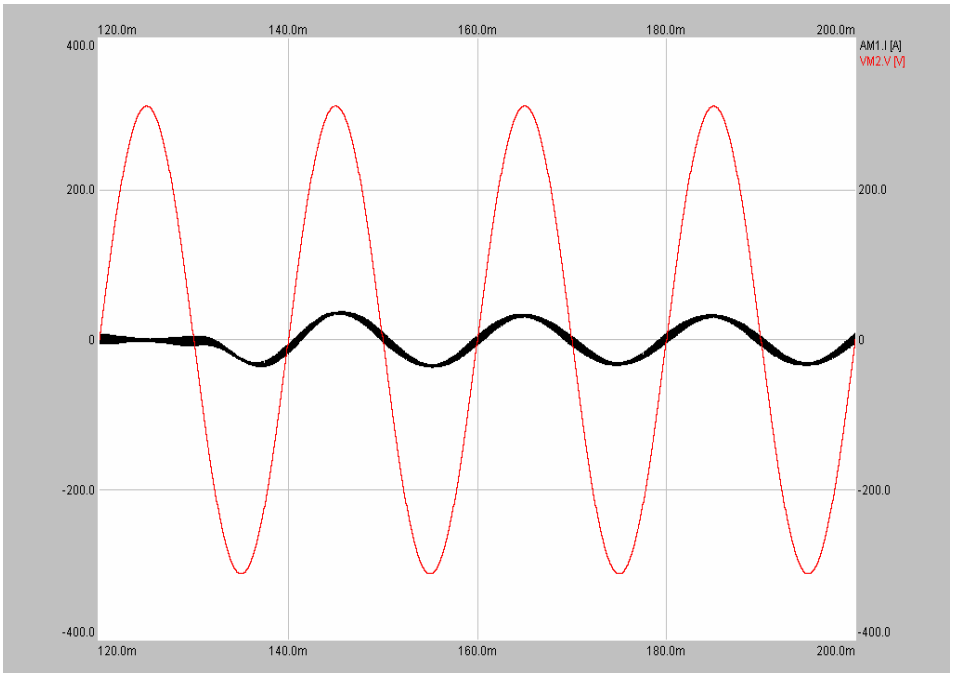

Figure 3.23: Input phase voltage and current at the instant of loading for the constant damped and phase compensated resonant filter form under undistorted utility

In Figure 3.24 and 3.25, the simulation results of the four-wire PWM rectifier employing only the constant damped resonant filter form in the current controller under undistorted utility can be seen.

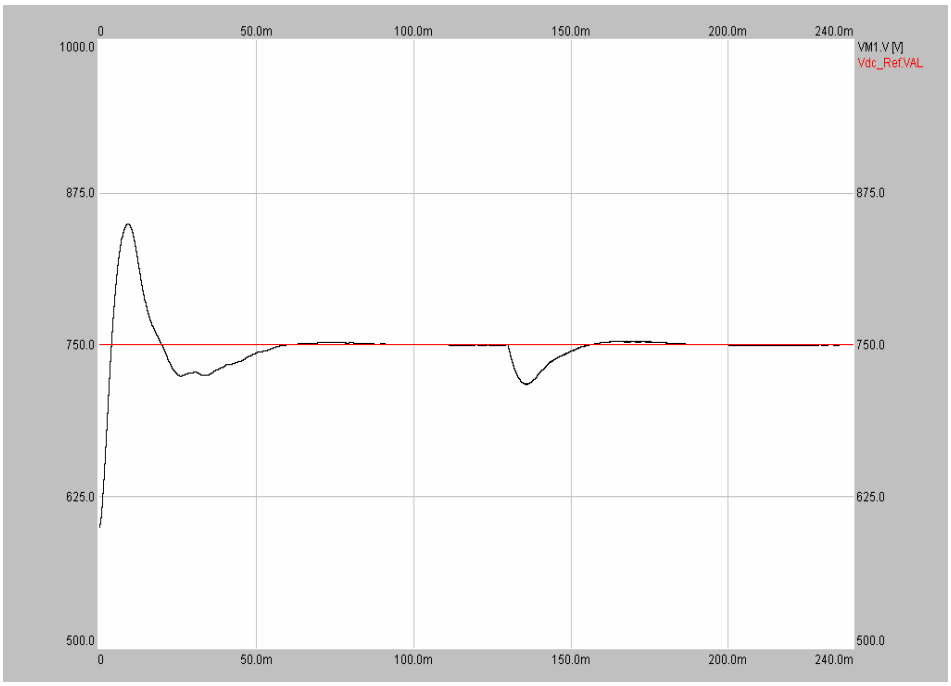

Figure 3.24: DC bus voltage and reference value for the constant damped resonant filter form under undistorted utility

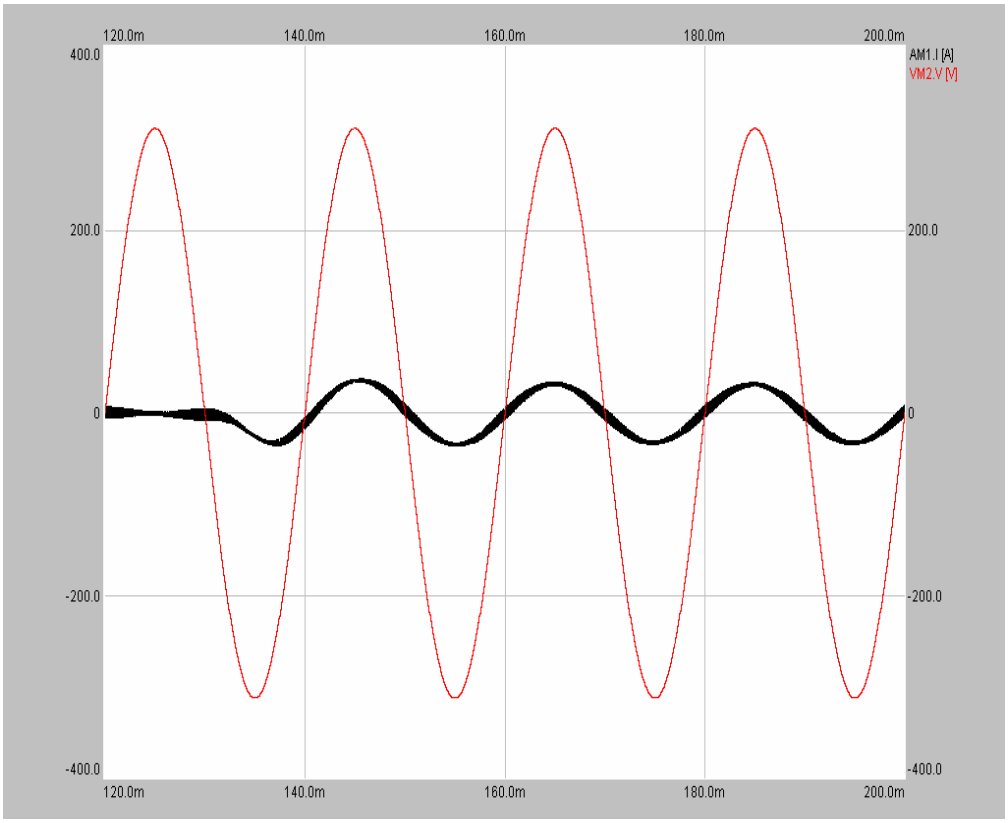

Figure 3.25: Input phase voltage and current at the instant of loading for the constant damped resonant filter form under undistorted utility

In Table 3.16, the performance comparison of the simulations with the three different resonant filter forms can be seen. As in the distorted utility case, the power factor values of the all three forms are in acceptable limits again. By using the variable damped, phase compensated resonant filter forms in the current controller, the four-wire voltage-source PWM rectifier exhibits superior performance. The input current THD value is smaller than 3.5 %.

Table 3.16: Performance comparison of three resonant filter forms under undistorted utility

	Power Factor, PF	Input Current Total Harmonic Distortion, I_{THD}	Input Voltage Total Harmonic Distortion, V_{THD}
Variable damped phase compensated	**0.99**	**3.3 %**	**1.3 %**
Constant damped phase compensated	**0.99**	**4.34 %**	**1.3 %**
Constant damped	**0.99**	**4.39 %**	**1.3 %**

Table 3.17: Undistorted input voltage harmonic content

Frequency (Hz)	Percentage (%)
50	100

Table 3.18: Input current harmonic content for the variable damped and phase compensated resonant filter form under undistorted utility

Frequency (Hz)	Percentage (%)
50	100
250	1.81
350	1.24
550	0.52
650	0.23

Table 3.19: Input current harmonic content for the constant damped and phase compensated resonant filter form under undistorted utility

Frequency (Hz)	Percentage (%)
50	100
250	2.32
350	1.04
550	0.95
650	0.81

Table 3.20: Input current harmonic content for the constant damped resonant filter form under undistorted utility

Frequency (Hz)	Percentage (%)
50	100
250	2.98
350	1.99
550	1.71
650	2.07

3.3.2.4. Simulation Results of the Four Wire Rectifier under Highly Distorted Utility with the Fundamental Frequency of 49.8 Hz

In a three-phase rectifier application, usually the input voltage frequency is constant. However for some unusual cases, the input voltage frequency can change slightly. For instance, in a three-phase UPS, usually the input voltage frequency tolerance is set as 50±2.5 Hz. In this frequency range, the rectifier unit of the UPS must operate without any problem.

The resonant filters in the current controller of the three-phase four-wire rectifier are designed for specific frequency components. The gain of the filters at the resonant

frequency is very high, and for the other frequencies it is negligible. And if the input voltage frequency changes slightly, the gain of the each resonant filter decreases, as a result the performance of the resonant filter bank degrades. This is the main reason for using damped resonant filter forms in the resonant filter bank. In order to see the performance difference between the different forms of the resonant filters, the schematic in Figure 3.3 is simulated with the input voltage fundamental frequency is set as 49.8 Hz. Each harmonic component frequency is set as (m·49.8) Hz. Simulation results are given in Figure 3.27 to 3.32.

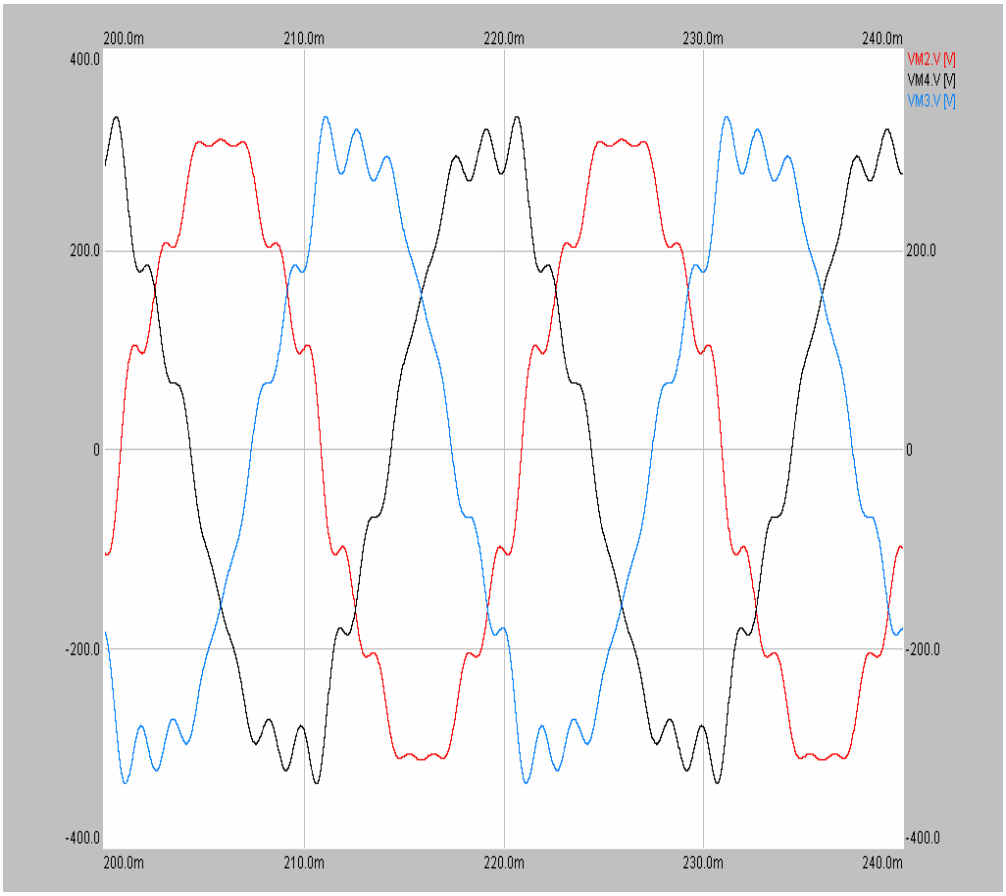

Figure 3.26: Steady state highly distorted 49.8 Hz input phase voltages

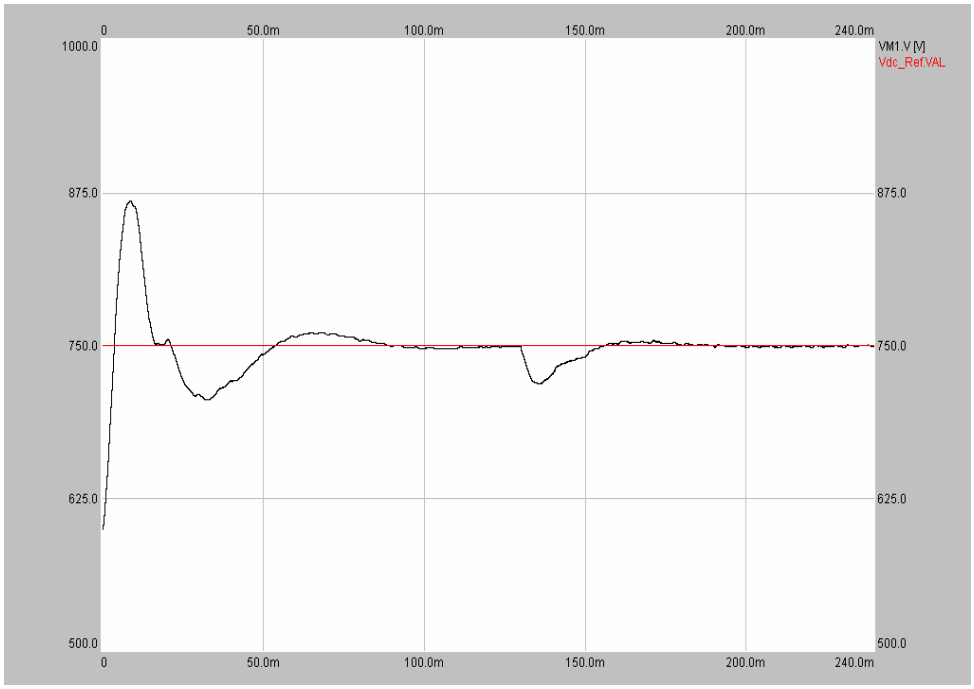

Figure 3.27: DC bus voltage and reference value for the variable damped and phase compensated resonant filter form under highly distorted 49.8 Hz utility

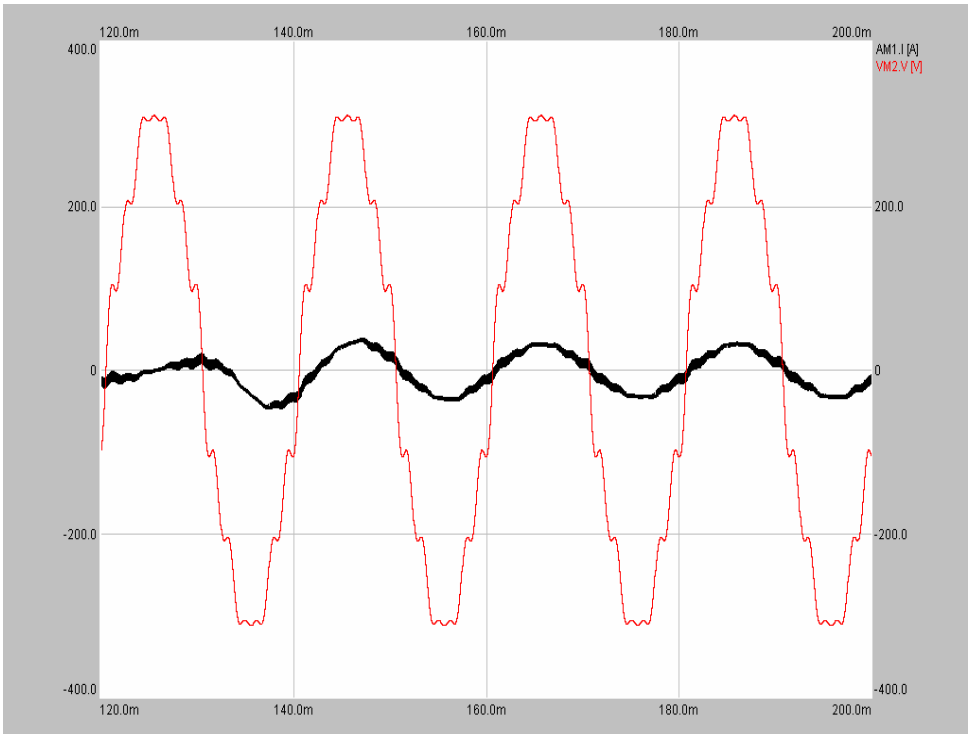

Figure 3.28: Input phase voltage and current at the instant of loading for the variable damped and phase compensated resonant filter form under highly distorted 49.8 Hz utility

As it can be seen in Figure 3.28, the performance of the variable damped and phase compensated resonant filter is sufficient. The input current THD value is smaller than the input voltage THD value again.

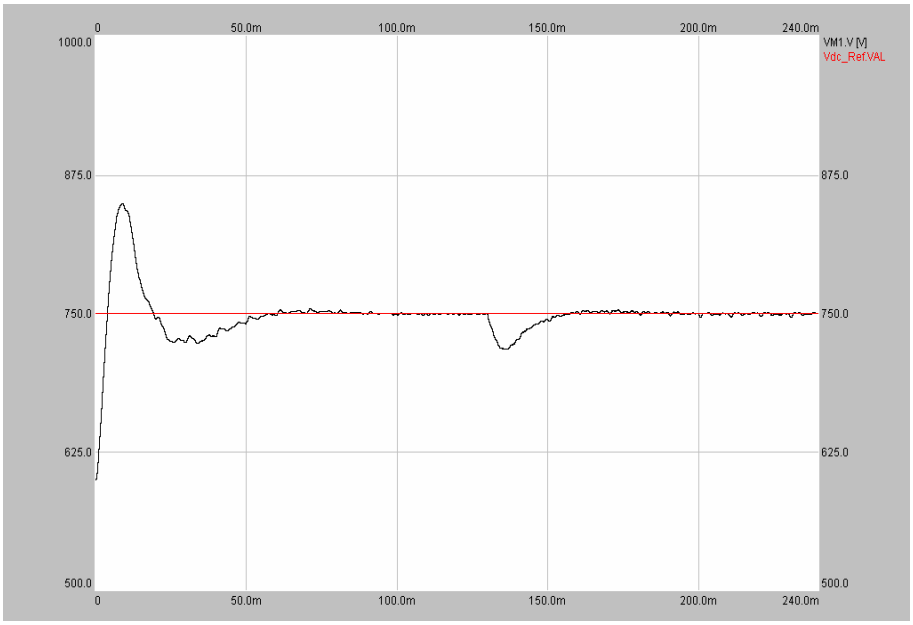

Figure 3.29: DC bus voltage and reference value for the constant damped and phase compensated resonant filter form under highly distorted 49.8 Hz utility

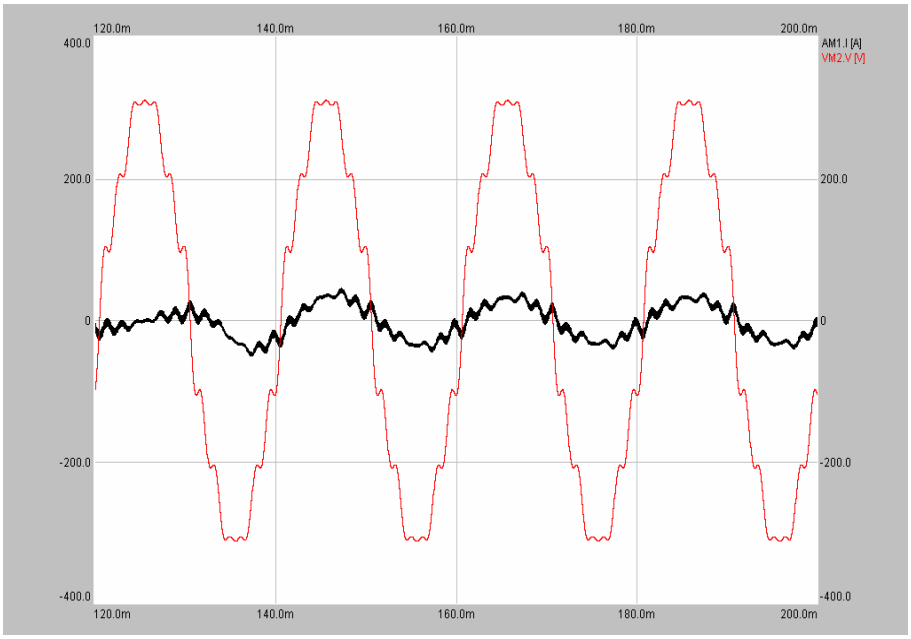

Figure 3.30: Input phase voltage and current at the instant of loading for the constant damped and phase compensated resonant filter form under highly distorted 49.8 Hz utility

For the consant damped and phase compensated filter form, since the selectivity of the resonant filters for the 11^{th} and 13^{th} harmonics increases, the performance of these filters are insufficient. As it can be seen in Figure 3.30, the 11^{th} and 13^{th} harmonics are the most dominant components in the input current waveform.

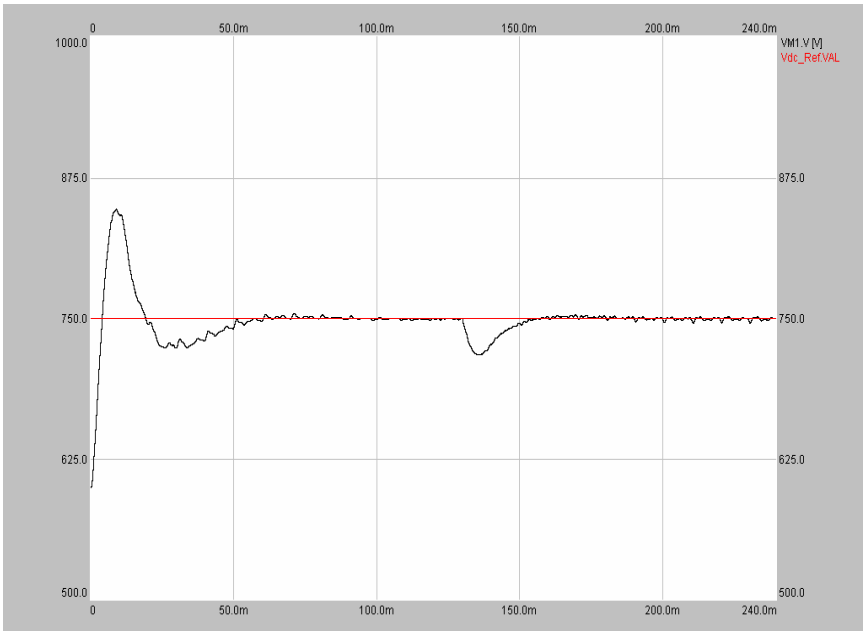

Figure 3.31: DC bus voltage and reference value for the constant damped resonant filter form under highly distorted 49.8 Hz utility

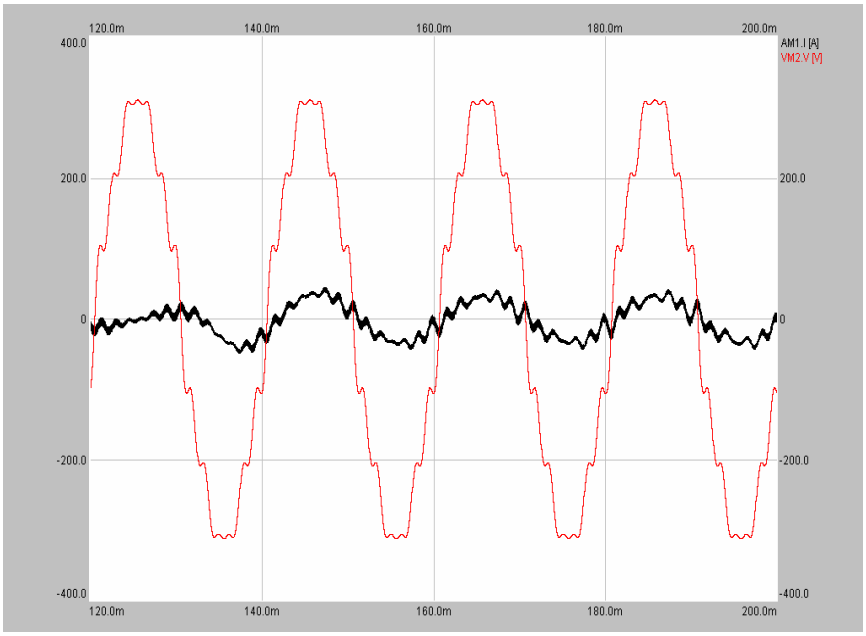

Figure 3.32: Input phase voltage and current at the instant of loading for the constant damped resonant filter form under highly distorted 49.8 Hz utility

For the constant damped resonant filter case, all harmonic components are dominant. As it can be seen in Figure 3.32, the input current waveform is much distorted.

Table 3.21: Performance comparison of three resonant filter forms

	Power Factor, PF	Input Current Total Harmonic Distortion, I_{THD}	Input Voltage Total Harmonic Distortion, V_{THD}
Variable damped phase compensated	**0.99**	**8.38 %**	**9.27 %**
Constant damped phase compensated	**0.954**	**24.74 %**	**9.27 %**
Constant damped	**0.943**	**28.98 %**	**9.27 %**

Table 3.22: Highly distorted 49.8 Hz input voltage harmonic content

Frequency (Hz)	**Percentage (%)**
49.8	100
249	3.64
348.6	3.64
547.8	5.45
647.4	5.45

Table 3.23: Input current harmonic content for the variable damped and phase compensated resonant filter form under highly distorted 49.8 Hz utility

Frequency (Hz)	**Percentage (%)**
49.8	100
249	2.97
348.6	2.72
547.8	3.88
647.4	4.29

Table 3.24: Input current harmonic content for the constant damped and phase compensated resonant filter form under highly distorted 49.8 Hz utility

Frequency (Hz)	**Percentage (%)**
49.8	100
249	7.32
348.6	9.43
547.8	16.35
647.4	13.47

Table 3.25: Input current harmonic content for the constant damped resonant filter form under highly distorted 49.8 Hz utility

Frequency (Hz)	**Percentage (%)**
49.8	100
249	8.43
348.6	10.35
547.8	18.73
647.4	16.91

4. EXPERIMENTAL PERFORMANCE INVESTIGATION OF THE THREE PHASE FOUR WIRE VOLTAGE SOURCE PWM RECTIFIER

4.1. Introduction

In this chapter, the experimental performance investigation of the three-phase four-wire voltage-source PWM rectifier is conducted. The four-wire PWM rectifier, with the proposed control method, performance is experimentally investigated under steady-state and dynamic operating conditions. Thus, the theoretical study results of Chapter 3, and the computer simulation studies of Chapter 4 are verified by the experimental work in this chapter. First the experimental system hardware and software are described, and then the performance investigations are given in detail.

4.2. Hardware and Software set up of the Three Phase Four Wire Voltage Source PWM Rectifier

The four-wire PWM rectifier is designed and manufactured at ENEL Enerji Elektronik San. Tic. A.S. laboratory. The block diagram of the experimental setup is given in Figure 4.1. The electrical power circuitry of the overall system is shown in Figure 4.2. The parameters, which are utilized in the experimental setup and experiments, are given in Table 4.1. Figure 4.3 through Figure 4.5 shows the laboratory prototype of the three-phase four-wire voltage-source PWM rectifier.

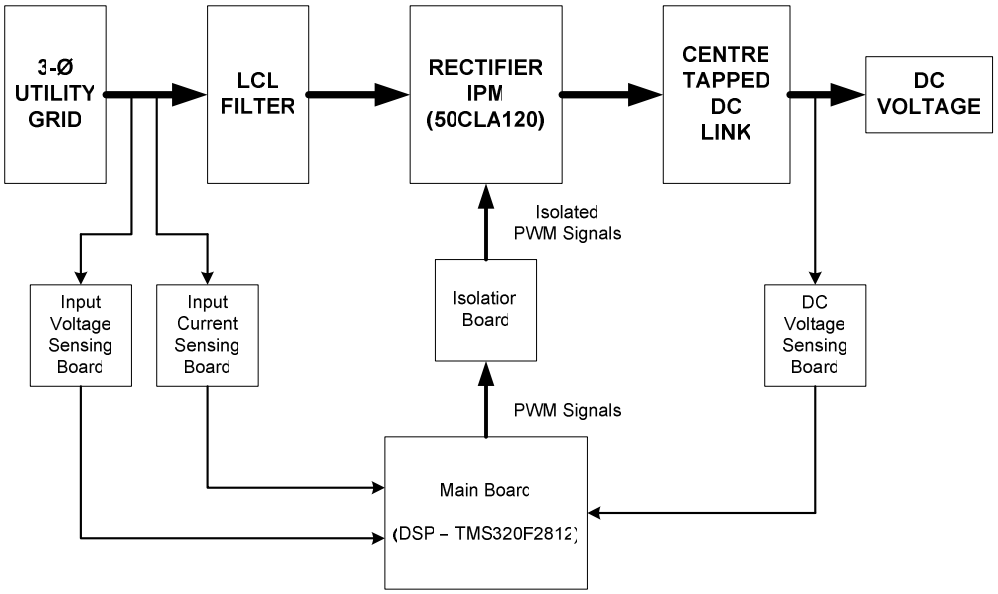

Figure 4.1: The system block diagram of the experimental setup.

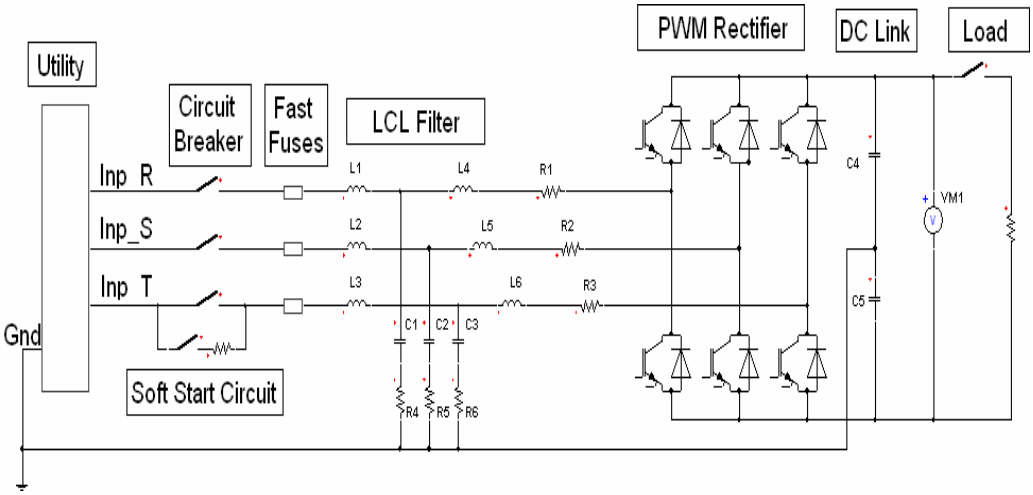

Figure 4.2: The electrical power circuitry of the overall system.

Table 4.1: Experimental system parameters

Rectifier	Rated Power	15 kVA
	Input Frequency	50 Hz
DC bus	Voltage	750 Vdc
	Capacitors	4 mF, 500 Vdc (Center-tapped)
LCL Filter	Grid Side Inductance	40 µH
	Converter Side Inductance	800 µH
	Filter Capacitor	10 µF
	Damping Resistor	5 Ω - 10 W
Loading Circuit	Three-Phase inverter load	10 Ω (each phase)

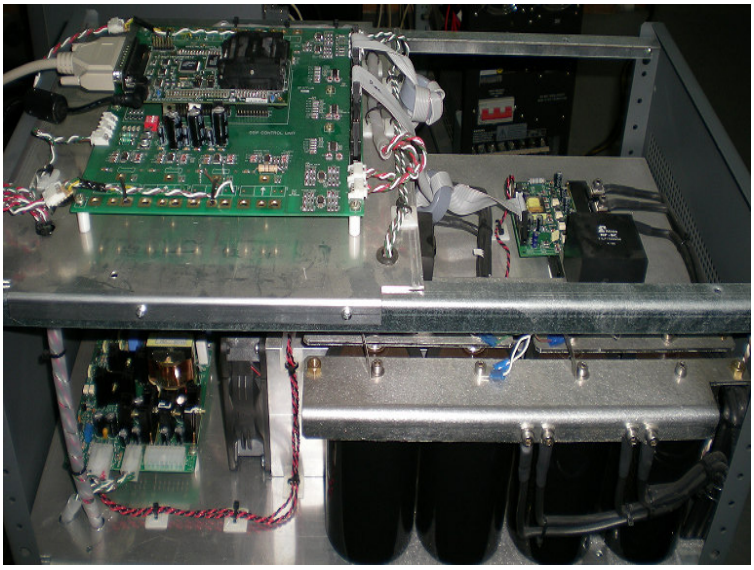

Figure 4.3: Main parts of the experimental set up.

In Figure 4.3, the main board, isolation board, PM50CLA120 module, DC bus capacitors, busbar design and the switch mode power supply, SMPS, of the experimental set up can be seen. In Figure 4.4, input LCL filter, output LC filter, and the input current sensor board of the experimental set up can be seen. In Figure 4.5, the main board and the eZdsp F2812 board can be seen. The main board supplies the scaled and filtered feedback signals to the eZdsp F2812 board.

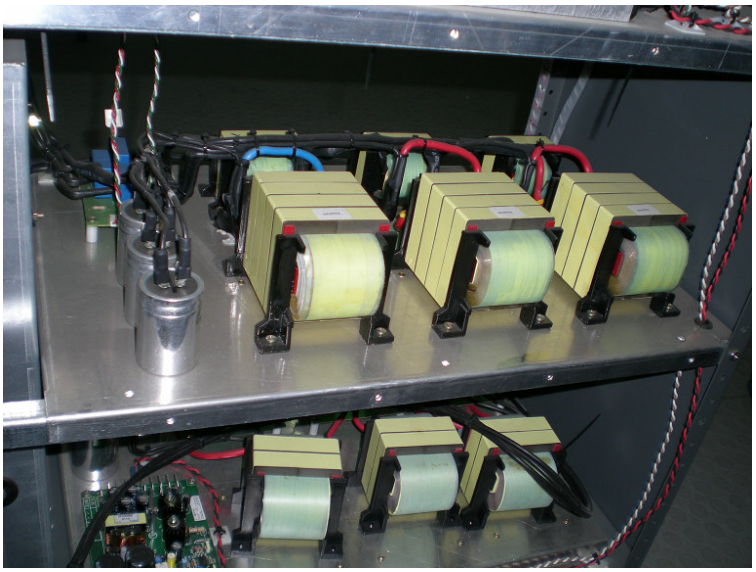

Figure 4.4: The filtering elements of the experimental set up.

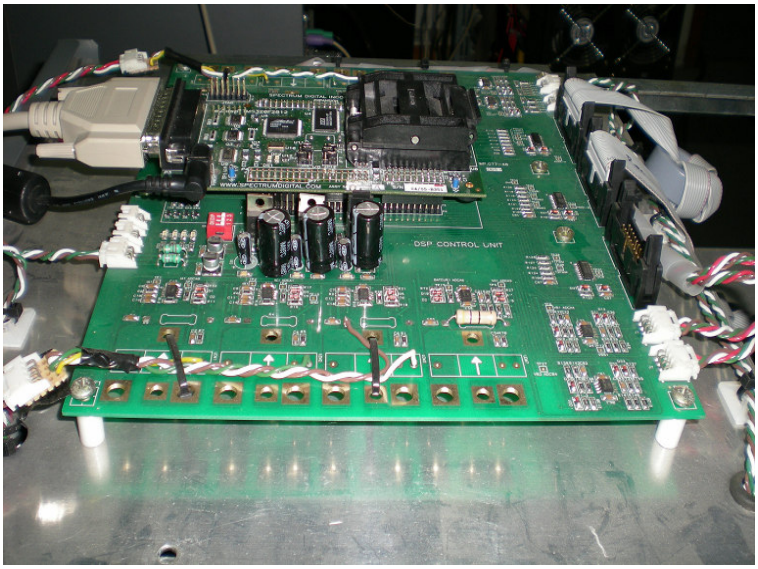

Figure 4.5: Main board of the experimental system.

In the experimental system, in order to protect the power switches a three-phase 30 A automatic fuse and a three-phase 35 A circuit breaker are used at the utility grid connection point. A soft start circuit is used in the experimental system for precharging the DC bus capacitors. Since the capacitance values of the DC bus capacitors are very high, they may result in a high inrush current when the utility grid is connected to the system by turning on the circuit breakers. In order to protect the diodes of the IPM from this inrush current, the DC bus capacitors are precharged by using the soft start circuit. Before turning on the circuit breaker of the system, the soft start switch must be turned on. Then, after a few seconds, the soft start switch is turned off and the circuit breaker is turned on.

The four-wire PWM rectifier is built by using Intelligent Power Modules, IPM's. Mitsubishi brand IPM modules, PM50CLA120 are utilized in the experimental system. Intelligent Power Modules are advanced hybrid power devices that combine high speed, low loss IGBTs with optimized gate drive and protection circuitry. Highly effective over-current and short-circuit protection is realized through the use of advanced current sense IGBT chips that allow continuous monitoring of power device current. System reliability is further enhanced by the IPM's integrated over temperature and under voltage lock out protection. The basic specifications of the intelligent power module, PM50CLA120 are summarized in Appendix A.

The DC bus of the four-wire rectifier is constructed by utilizing a planar bus structure to obtain low parasitic inductance on the DC bus. Three aluminum plates are mounted on the DC bus capacitors for positive, negative, and the neutral DC bus rails. Between the positive and the negative busbar an insulation material having an insulation level of 3.3 kV is inserted. A snubber capacitor is installed between the positive and negative voltage terminal of the each IPM, so that the switching stress on the IGBTs due to the parasitic inductances is reduced. The utilized snubber capacitors in the system have a 2.2 μF capacitance and 1000 V voltage rating.

The isolation board is used for isolating the PWM signals produced by the main board. The isolated PWM signals are directly applied to the PWM inputs of the IPM module. Beside of isolating the PWM signals, the isolation board converts the PWM signals with +5/0 voltage levels produced by the main board to an amplified +15/0 voltage levels, which is required for the IGBT turn-on and turn-off operations of the IPM.

In the performance tests, the four-wire PWM rectifier is loaded by the three-phase inverter which can be seen in Figure 4.2. Since 750 Vdc and 20 A rated resistive load does not exist in the laboratory set up, a three-phase inverter load is used in the experimental system. Each phase of the inverter is loaded by a 5 kW rated load bank, and each load bank consists of 5 parallel connected resistances which can be turned on and off via manual switches.

The three-phase input voltages, input currents, and the DC bus voltage are measured for controlling the four-wire PWM rectifier experimental system. The rectifier input currents are measured by utilizing the Hall Effect based current sensor, LA 55-P/SP1 model manufactured by LEM. All the measured signals are scaled and filtered by utilizing basic operational amplifier circuits and passive noise filters in the main board.

A digital signal processor, TMS320F2812, is used for controlling the four-wire PWM rectifier in the main board. In the DSP unit, analog to digital conversions, control block calculations, and PWM output signal generation are carried out. In the experimental set up, the eZdsp F2812 board manufactured by Spectrum Digital Inc., is employed. The features of the eZdsp F2812 board and TMS320F2812 are given in Appendix B.

The digital signal processor executes the control loops using the ADC feedback signals, and then it generates the necessary PWM signals. The control and PWM cycles are synchronized and they are executed at the same rate. These goals are achieved by using the two event managers, EVA and EVB, of the DSP. The TMS320F2812 DSP chip utilized in controlling the UPS system has event managers which have timers that can be used for generating the PWM signals. With each one of them, by utilizing a timer, three comparators and dead-time generators, three-phase modulation signals can be converted to six PWM logic signals. The control algorithms are executed within the event manager timer interrupt period. When the interrupt occurs, the DSP processes the "interrupt service routine" function to generate the PWM output signals for the IGBT switches. The flow chart of the interrupt service routine is shown in Figure 4.6. As seen from the figure, the interrupt service routine starts with the A/D conversion of the feedback signals. Then, picking up the stored A/D signals from the allocated memory locations, the signals are scaled and normalized to appropriate values. The voltage error signal, which is the difference between the reference DC bus voltage and the measured DC bus voltage, is fed to the PI type voltage controller. The current references are obtained by multiplying the output of the PI controller with the sinusoidal signals, which are synchronized with the three input phases. These synchronized signals are produced by the phase lock loop, PLL. Using the synchronized signals guarantees the high input power factor of the four-wire PWM rectifier. The current error signals, which are the difference between the current references and the measured input currents, are fed to the discrete time implemented resonant filter bank of each phase. The outputs of the resonant filter banks form the reference PWM signals for each phase. After selecting the modulation method, the PWM unit of the DSP generates the rectifier gate logic signals. In the experiments, the switching frequency is chosen as 12.8 kHz, and the dead-time is set to 2 μs for the complementary PWM logic signals, which is equal to the miminum dead time requirement of the IPM module.

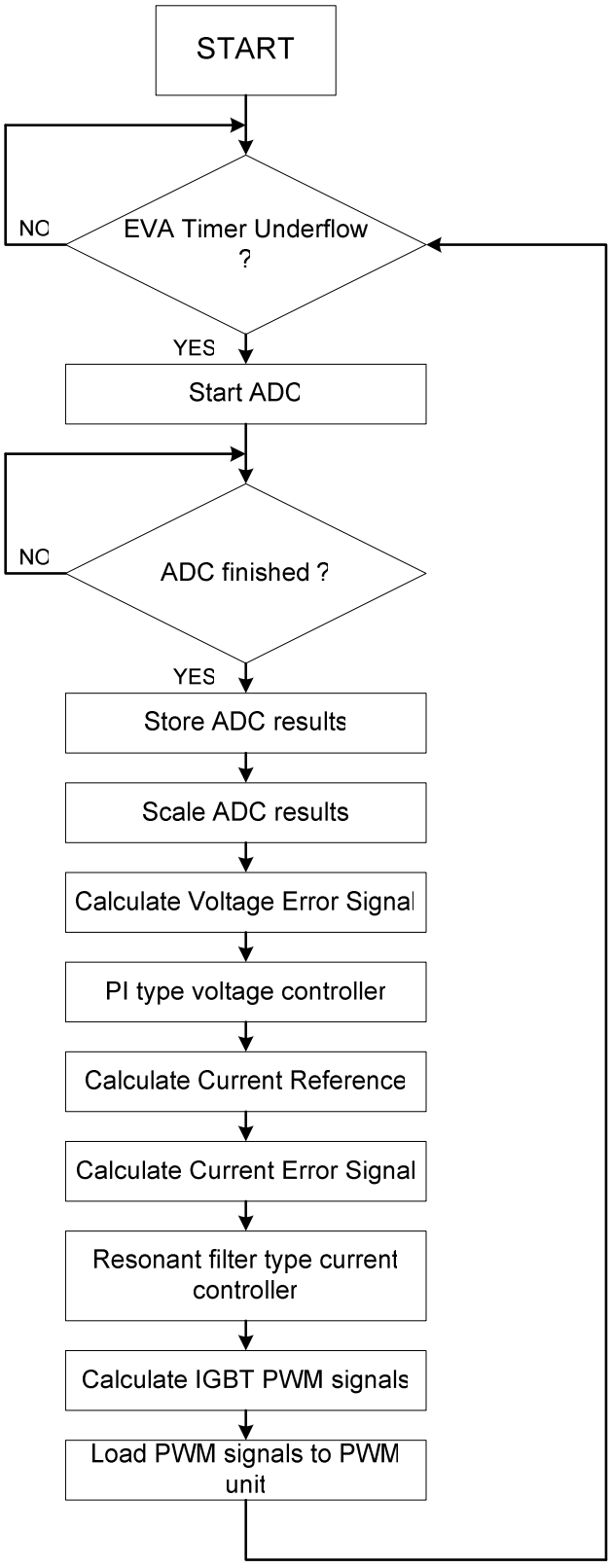

Figure 4.6: The flowchart of the DSP program

4.3. Experimental Results

In this section, the performance of the three-phase four-wire voltage-source PWM rectifier is evaluated experimentally. Firstly, the voltage controller and the current controllers are programmed using the parameters that are obtained in the previous chapter. Following the completion of the controller design stage, the steady-state and the dynamic performance of the four-wire rectifier is evaluated under 220 V_{rms}, 50 Hz distorted utility. The harmonic content of the distorted utility is given in Table 4.2.

Table 4.2: Harmonic content of the distorted utility

5^{th} harmonic component	2.1 %
7^{th} harmonic component	3.2 %
11^{th} harmonic component	1.1 %
13^{th} harmonic component	1.8 %

The control system parameters which were tuned by means of computer simulations in the previous chapter are utilized in the experimental stage. The performance of the controller for these parameters are experimentally evaluated and compared to the performance obtained by simulations.

Throughout the experimental studies the waveform and power quality measurements are conducted with a LeCroy Waverunner 6100A four channel 1 GHz oscilloscope, and a Fluke 43B power analyzer. Current and voltage waveform measurements are conducted with the LeCroy Waverunner 6100A, and the Fluke 43B is used for obtaining the harmonic spectrum, voltage-current THD, and the power factor values of the four-wire PWM rectifier. For the three-phase current measurement with Lecroy Waverunner 6100A, three Lecroy CP500 current transducers are used. For the isolated DC bus measurement, Lecroy ADP 305 voltage sensor is used. The experimental results of the three-phase four-wire voltage-source PWM rectifier are shown in Figure 4.7 through Figure 4.18. In Figure 4.7, Figure 4.8, Figure 4.10, and Figure 4.11 CH1 is the total DC bus voltage waveform, CH2 is the input phase-R current waveform, CH3 is the input phase-S current waveform , and finally CH4 is the input phase-T current waveform. In Figure 4.9, and Figure 4.12 CH1 is the input phase-R voltage waveform, and CH2 is the input phase-R current waveform.

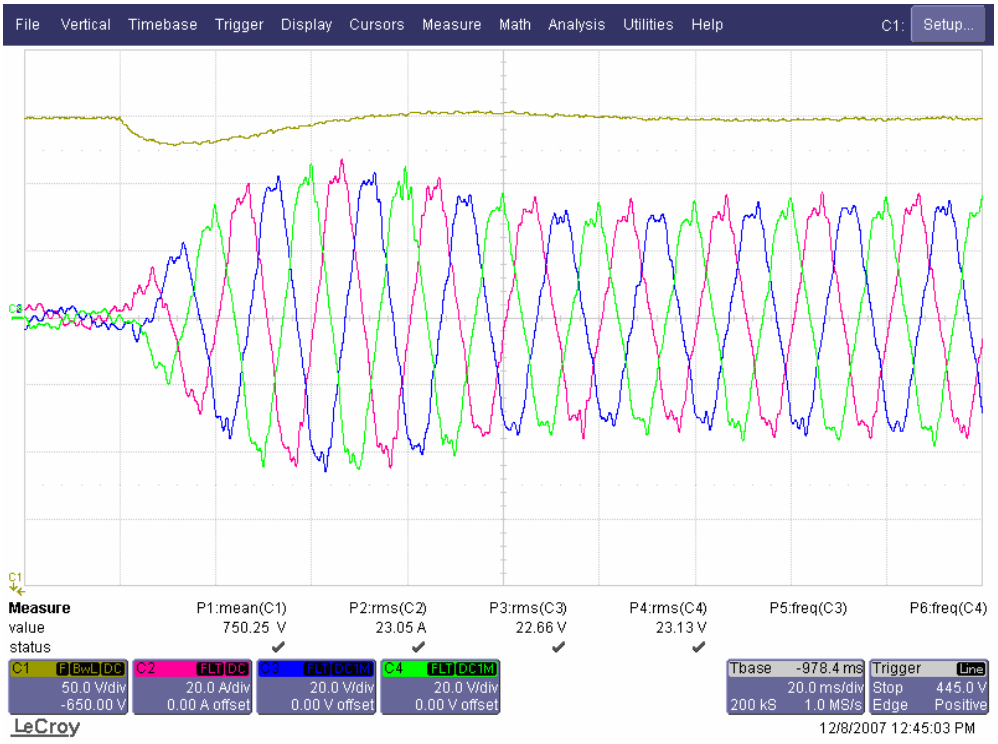

Figure 4.7: Input currents and DC bus voltage waveforms for the constant damped resonant filter bank case at the instant of full loading

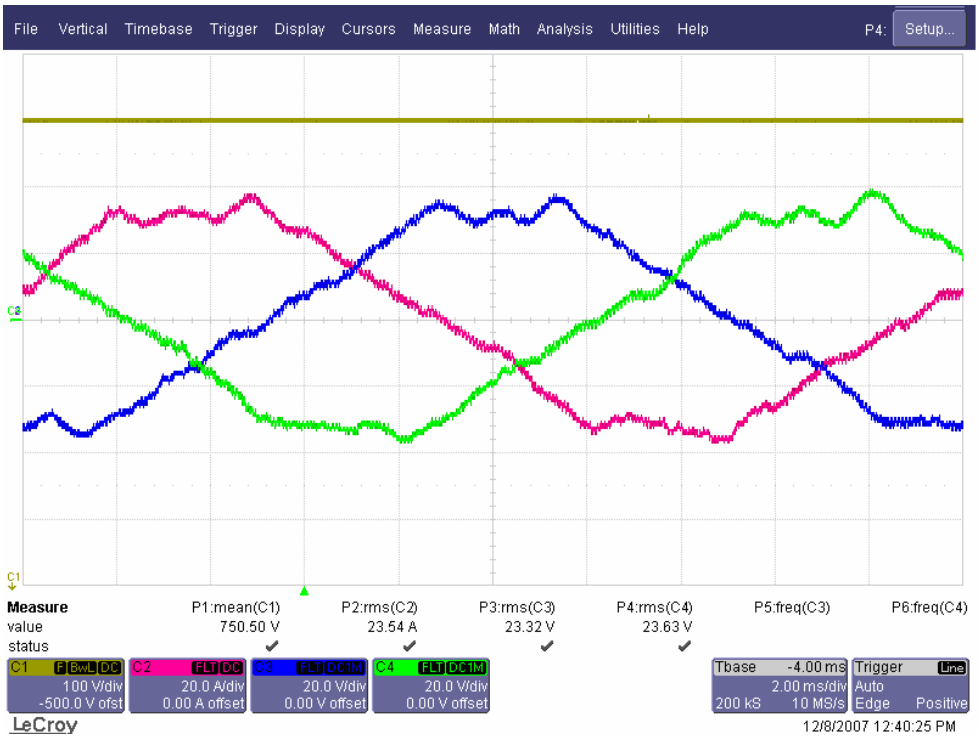

Figure 4.8: Steady state input currents and DC bus voltage waveforms for the constant damped resonant filter bank case under full load

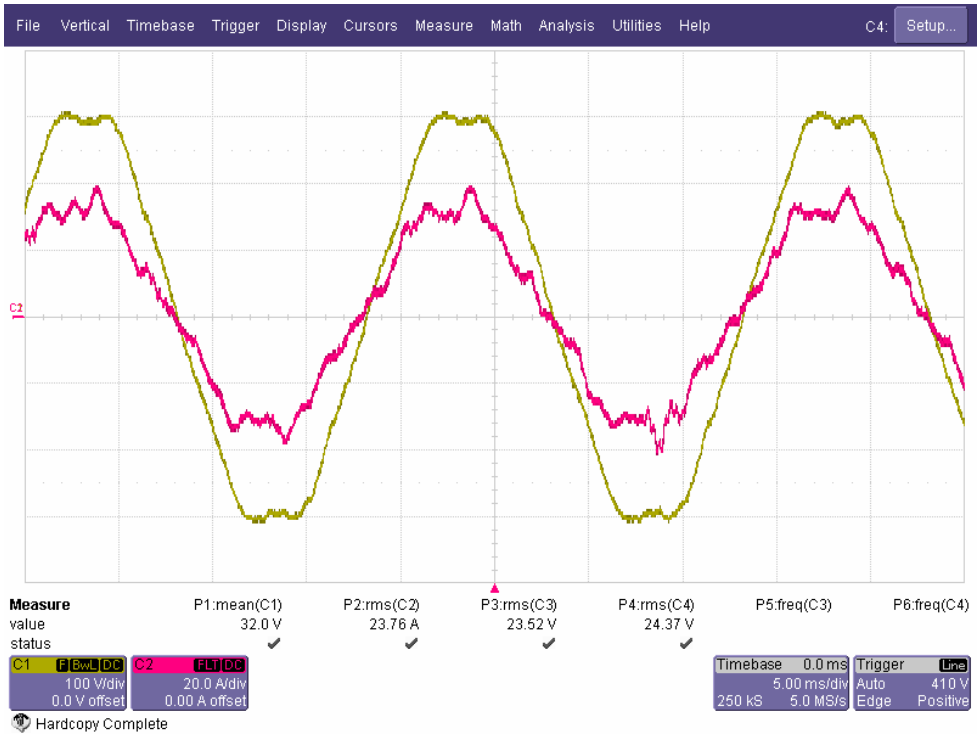

Figure 4.9: Steady state input current and voltage waveform for the constant damped resonant filter bank case under full load

In the performance tests of the experimental set up, firstly the constant damped resonant filter form is used in the current controller of the four-wire PWM rectifier. In this form of resonant filter, the phase delays on the feedback signals are not compensated. Beside of this, the selectivity of the resonant filter increases with the increasing frequency. As a result, the performance of the resonant filters in each frequeny component of the current controller becomes poor. The poor performance of the four-wire PWM rectifier can be seen in Figure 4.7, 4.8, 4.9. In Figure 4.7, three-phase input currents and the DC bus voltage waveforms at the instant of full load transition can be seen. Since the DC voltage is regulated by the PI type controller with the parameters obtained in the simulation results, the regulation performance is perfect. In Figure 4.8, the steady-state three-phase input currents and the DC bus voltage waveforms under full load operation can be seen. Again in this figure, the DC voltage regulation is perfect; however, the phase currents contain high harmonic content. This is the result of the poor resonant filter performance. In Figure 4.9, the steady state input voltage and current waveforms can be seen.

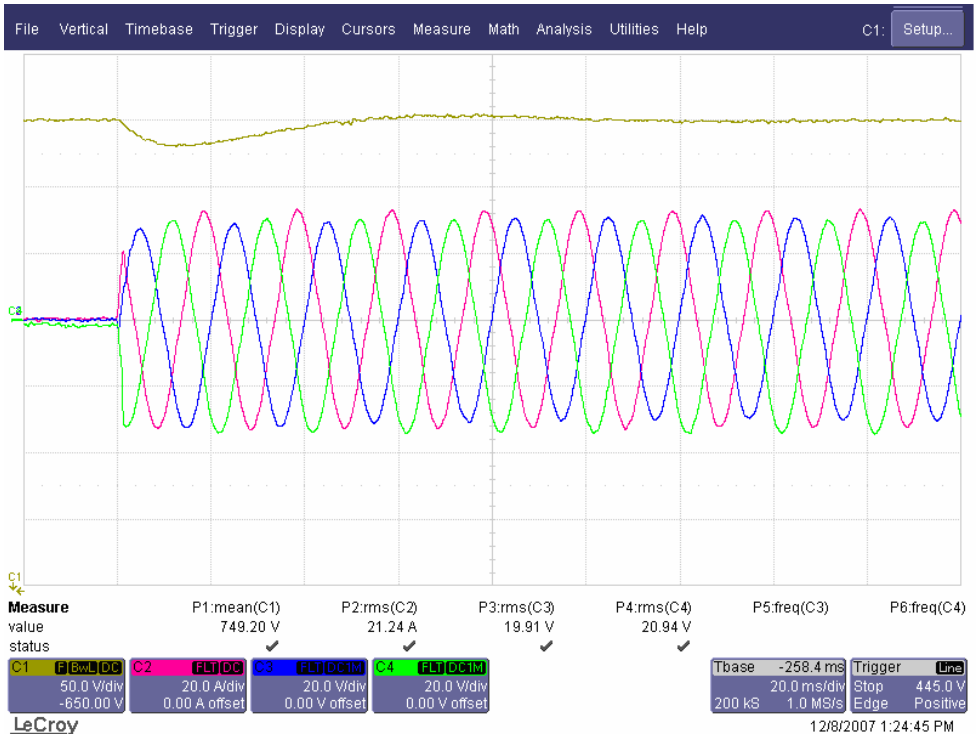

Figure 4.10: Input currents and DC bus voltage waveforms for the variable damped and phase compensated resonant filter bank case at the instant of full loading

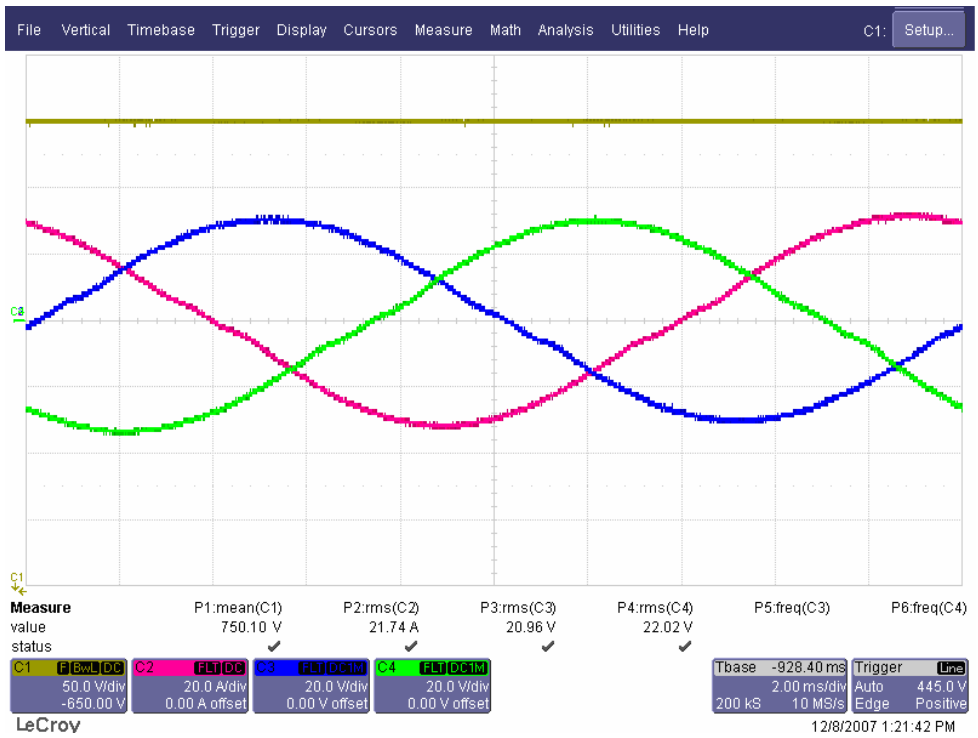

Figure 4.11: Steady state input currents and DC bus voltage waveforms for the variable damped and phase compensated resonant filter bank case under full load

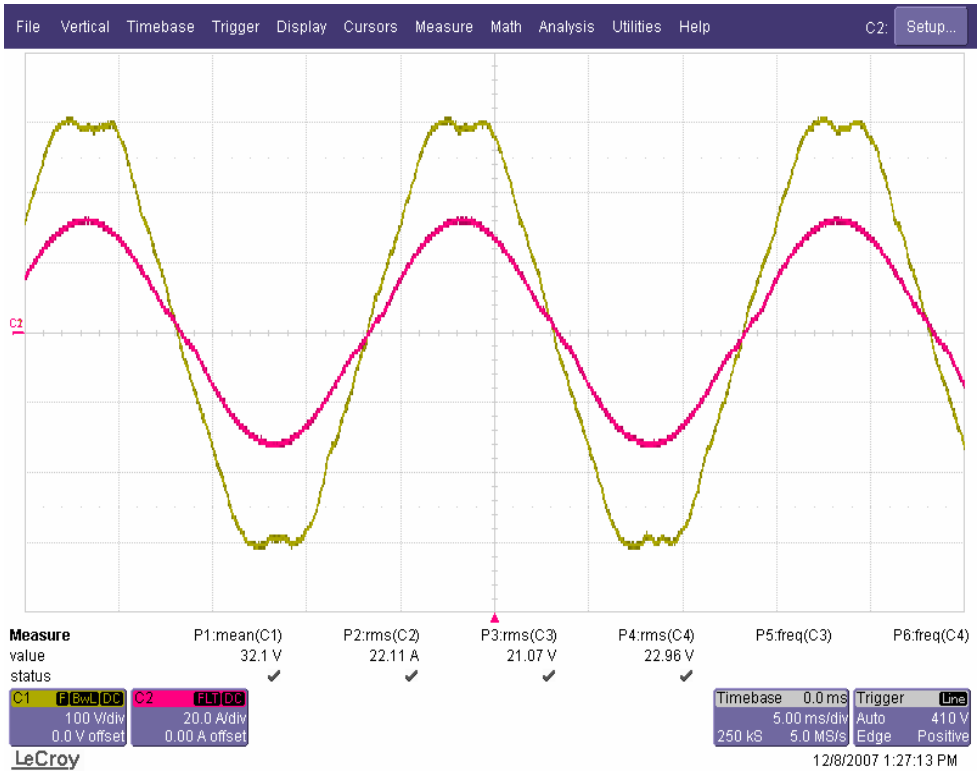

Figure 4.12: Steady state input current and voltage waveform for the variable damped and phase compensated resonant filter bank case under full load operation

In the second part of the performance tests, the variable damped and phase compensated resonant filter form is used in the current controller of the four-wire PWM rectifier. As a result, the performance of the resonant filters in each frequeny component of the current controller becomes perfect. In Figure 4.10, three-phase input currents and the DC bus voltage waveforms at the instant of full load transition can be seen. In Figure 4.11, the steady state three-phase input currents and the DC bus voltage waveforms under full load operation can be seen. Both the DC voltage regulation and the input current regulation of the four-wire PWM rectifier are perfect with this type of resonant filter form. In Figure 4.9, the steady state input voltage and current waveforms can be seen.

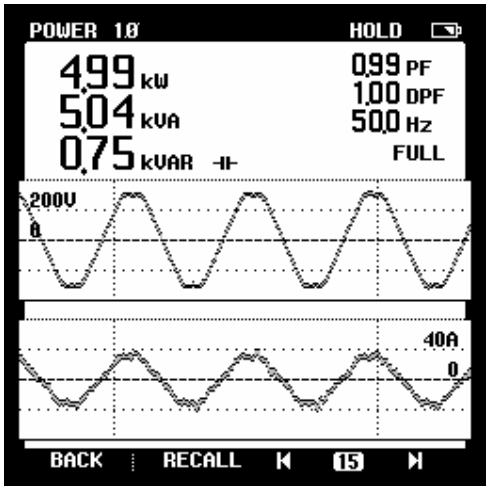

Figure 4.13: Input power and the power factor for the constant damped resonant filter bank case under full load operation

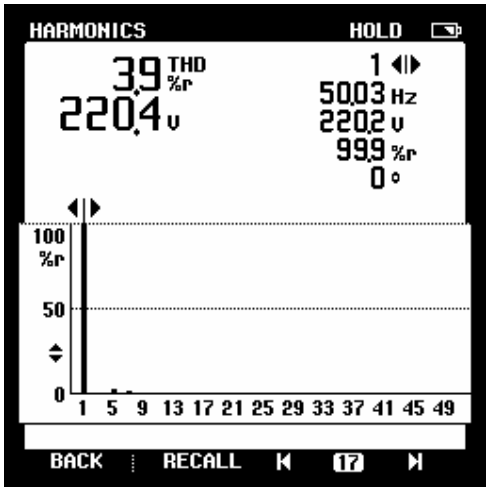

Figure 4.14: Input voltage harmonic content for the constant damped resonant filter bank case under full load operation

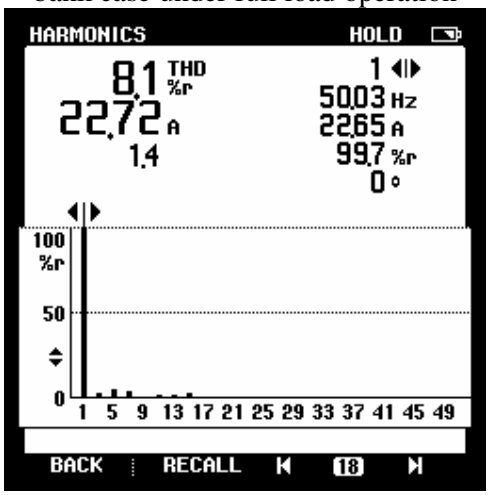

Figure 4.15: Input current harmonic content for the constant damped resonant filter bank case under full load operation

In Figure 4.13, 4.14, and 4.15, power analyzer results of the four-wire PWM rectifier, which employs the constant damped resonant filter form in the current controller, can be seen. The input power factor of the four-wire PWM rectifier is 0.99, which satisfies the IEC, IEEE standards. However, the input current THD of the four-wire rectifier is 8.1%. As it can be seen from the current harmonic spectrum, the 5^{th}, and the 7^{th} harmonic is the most dominant harmonic component. The 5^{th} and 7^{th} harmonics in the input voltage waveform is the main reason of this. Since the resonant filters in the current controller does not work properly, the 5^{th}, 7^{th} harmonic voltage components can not be compensated in the current waveform.

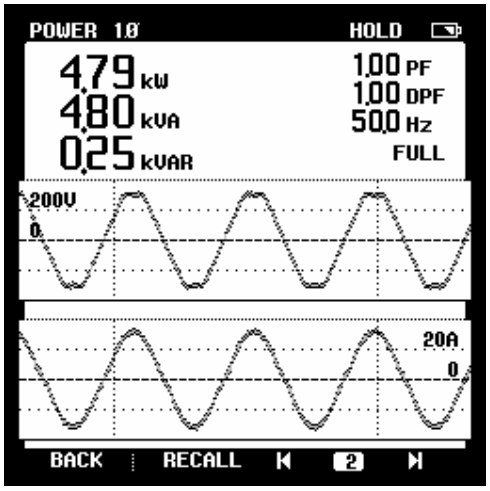

Figure 4.16: Input power and the power factor for the variable damped and phase compesated resonant filter bank case under full load operation

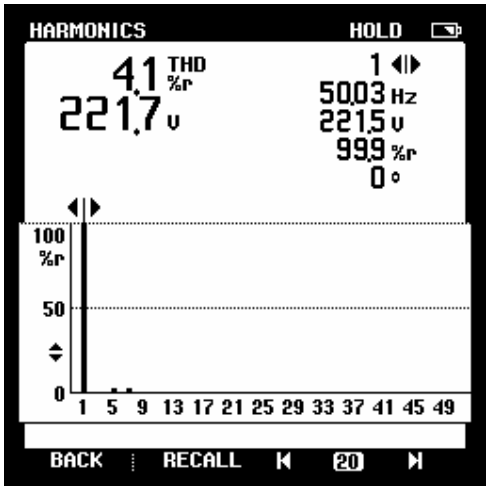

Figure 4.17: Input voltage harmonic content for the variable damped and phase compensated resonant filter bank case under full load operation

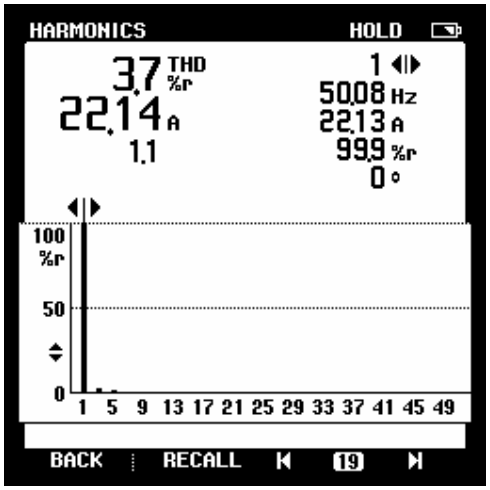

Figure 4.18: Input current harmonic content for the variable damped and phase compensated resonant filter bank case under full load operation

In Figure 4.16, 4.17, and 4.18, power analyzer results of the four-wire PWM rectifier, which employs the variable damped, phase compensated resonant filter form in the current controller can be seen. The input power factor of the four-wire PWM rectifier is 1.00, which satisfies the IEC, IEEE standards. As it can be seen from the harmonic spectrum of the input voltage and current, the THD of the input current is smaller than the input voltage. The variable damped, phase compensated resonant filters compensate all the harmonic components in the input voltage.

Table 4.3: Comparison of experimental and simulation results

		Input voltage total harmonic distortion, V_{THD}	Input current total harmonic distortion, I_{THD}	Input power factor, PF
Variable damped phase compensated filters	Simulation result	4.1 %	3.5 %	0.99
	Experimental result	4.1 %	3.7 %	1.00
Constant damped phase compensated filters	Simulation result	4.1 %	6.65 %	0.986
	Experimental result	3.9 %	8.1 %	0.99

As it can be seen in Table 4.3, experimental results are quite similar to those obtained in the simulations of the four-wire rectifier under distorted utility condition. For the same utility conditions, the input current total harmonic distortion value of the simulation and experimental study which employs variable or constant damped, phase compensated filters is nearly equal to each other. This is due to the design accuracy of the rectifier and design accuracy of the computer simulation model.

5. CONCLUSION

This thesis investigated the control method for the three-phase four-wire voltage-source PWM rectifier. In the literature there exists several control methods for the voltage-source PWM rectifier. These control techniques are mainly based on complex d-q-0 transformations. In these methods all AC quantities are transformed to DC quantities, so that PI type controllers with high DC gains can be used in the control. Beside of this, the positive and negative sequence components of these control quantities must be considered in the controller structure. Thus, the control of the four-wire voltage-source PWM rectifier with the commonly used control techniques is very complex.

This thesis has contributed towards significant simplification of the control methods of the four-wire voltage-source PWM rectifier. In order to simplify the input current control of the rectifier without sacrification from performance, the resonant filter bank is used in the current control loop. With such a control structure, neither a coordinate transformation, nor complex computations and algorithms are necessary. The resonant filter controller design has been carefully discussed and emphasis was placed on the filter damping and phase delay compensation.

Using the resonant filter bank based controller in the current control loop, the rectifier input current can be precisely regulated under steady-state and dynamic loading conditions. Since the controller is implemented per phase and in the stationary frame, the control method is simple and full resolution of the signal processor is utilized as there is no coordinate transformations, no mixture of controllers for positive/negative/zero sequence components. The resonant filter bank approach involves a simple structure and its careful implementation provides precise input current regulation with high bandwidth. In the thesis, the design of the controller involving practical implementations and operating conditions has been carefully investigated. For this purpose a detailed study on the damping and phase delay compensation of the resonant filters is conducted. Based on the study it

has been found that the delay compensation plays a major role for controlling the high frequency harmonic distortion.

The theoretical work developed in this thesis has been supported by the simulation studies. Firstly, the simulation model of the four-wire PWM rectifier is formed using simulation software. Then, the model is simulated for various operating and loading conditions. It has been shown that the computer simulation results are in well agreement with the theoretical study and the proposed control method provides high steady state and dynamic performance. For the undistorted utility conditions, the input current THD of the four-wire PWM rectifier is less than 3.5% and the input power factor is nearly equals to one. In the dynamic performance study it has been shown that the instantaneous loading has been compensated for a few fundamental cycles. Thus the computer simulations have thoroughly verified the performance of the proposed methods.

Finally, the feasibility of the proposed control algorithm proven by theory and simulation studies has been verified by the 15-kVA three-phase four-wire voltage-source PWM rectifier prototype laboratory tests. The proposed control algorithms are implemented using a Digital Signal Processor and the inverter employed the intelligent IGBT modules (IPM's). A prototype rectifier was built and tested under various operating conditions to illustrate the feasibility of the methods proposed. Experimental studies have been in good agreement with the theory and simulations.

Overall, this thesis has contributed to the control method development for the four-wire PWM rectifier. The main contribution is towards implementation simplification without performance sacrification. The contributions regarding the control algorithms involve analytical evaluation, design simplification and implementation. With the results of this research, it can be claimed that the three-phase four-wire voltage-source PWM rectifier can be easily used in UPS and drive applications.

Future work relating to the study of this thesis involves several issues. First of all, in spite of using parallel connected resonant filters, a single digital filter form can be designed. If such a filter form is designed, implementation of the control method becomes very simple. Beside of this, since the resonant filters are synchronous frame equivalent verisons of the stationary frame PI regulators, limiting the integrators of these controllers must be considered.

REFERENCES

[1] **Rowan, T.M. and Kerkman, R.J.**, 1986. "A new synchronous current regulator and an analysis of current regulated PWM inverters," *IEEE Transactions on Industry Applications*, Volume IA-22, pp. 678–690, July/Aug.

[2] **Rowan, T.M., Kerkman, R.J. and Lipo T.A.,** 1987. "Operation of naturally sampled current regulators in the transition region," *IEEE Transactions on Industry Applications*, Volume IA-23, pp. 586–596, July/Aug.

[3] **Rim, C.T., Choi, N.S., Cho, G.C. and Cho, G.H.,** 1994. "A complete DC and AC analysis of three-phase controlled-current PWM rectifier using circuit D-Q transformation," *IEEE Transactions on Power Electronics*, Volume 9, pp. 390–396, July

[4] **Kamran, F.,** 1995. "A new UPS topology and deadbeat control techniques for improved utility interface compatibility," Georgia Institute of Technology, October

[5**] Kükrer, O.,** 1996. "Deadbeat control of a three-phase inverter with an output LC filter," *IEEE Transactions on Power Electronics*, Volume 11, pp. 16-23, January

[6] **Kükrer, O. and Kömürcügil, H.,** 1999. "Deadbeat control method for single phase UPS inverters with compensation of computation delay," *IEE Proceeding- Electronics Power Application*, Volume 146, pp. 123-128, January

[7] **Radulovic, Z. and Sabanovic, A.**, 1994. "Active filter control using a sliding mode approach," in *Proc. IEEE PESC'94*, pp. 177–182.

[8] **Kawamura, A. and Hoft, R.G.**, 1984. "Instantaneous feedback controlled PWM inverters with adaptive hysteresis," *IEEE Transactions on Industry Applications*, Volume IA-20, pp. 769–775, July/Aug.

[9] **Chiarelli, C., Malesani, L., Pirondini, S. and Tomasin, P.,** 1993. "Single-phase, three-level, constant frequency current hysteresis control for UPS applications," in *Proc. European Conf. Power Electronics and Applications*, Brighton, U.K., September, pp. 180–185.

[10] **Malesani, L. and Tenti, P.,** 1990. "A novel hysteresis control method for current controlled VSI PWM inverters with constant modulation frequency," *IEEE Transactions on Industry Applications*, Volume 6, pp. 88-92.

[11] **Yao, Q. and Holmes, D.G.,** 1993. "A simple, novel method for variable hysteresis-band current control of a three phase inverter with constant switching frequency," in *Conf. Rec. IEEE-IAS Annu. Meeting*, Toronto, Ont., Canada, October, pp. 1122–1129.

[12] **Malesani, L., Mattavelli, P. and Tomasin, P.**, 1996. "High-performance hysteresis modulation technique for active filters," in *Proc. IEEE APEC'96*, pp. 939–946.

[13] **Zmood, D.N. and Holmes, D.G.**, 1999. "Stationary frame current regulation of PWM inverters with zero steady-state error," Power Electronics Specialists Conference, PESC 99, Volume 2, pp. 1185–1190.

[14] **Zmood, D.N., Holmes, D.G. and Bode, G.H.,** 2001. "Frequency-domain analysis of three-phase linear current regulators," *IEEE Transactions on Industry Applications*, Volume 37, pp. 601–610.

[15] **Mattavelli, P.,** 2001. "Closed-loop selective harmonic compensation for active filters," *IEEE Transactions on Industry Applications*, Volume 37, pp. 81–89.

[16] **Newman, M.J., Zmood, D.N. and Holmes, D.G.,** 2002. "Stationary frame harmonic reference generation for active filter systems," in *Proc. IEEE/APEC Conf.*, Dallas, TX, March.

[17] **Mattavelli, P.,** 2001. "Synchronous-frame harmonic control for high-performance AC power supplies," *IEEE Transactions on Industry Applications*, Volume 37, pp. 864–872.

[18] **Loh, P.C., Newman, M.J., Zmood, D.N., Holmes, D.G.,** 2003. "A comparative analysis of multiloop voltage regulation strategies for single and three-phase UPS systems," *IEEE Transactions on Power Electronics*, Volume 18, pp. 1176-1185, September.

[19] **Sato, Y., Ishizuka, T., Nezu, K. and Katako, T.,** 1998. "A new control strategy for voltage-type PWM rectifiers to realize zero steady-state control error in input current," *IEEE Transactions on Industry Applications*, Volume 34, pp. 480-486, May/June.

[20] **Fraser, M.E., Manning, C.D. and Wells, B.M.**, 1995. " Transformerless four-wire PWM rectifier and its application in AC-DC-AC converters," *IEE Proceedings on Electric Power Applications*, Volume 142, no 6, November.

[21] **Zmood, D.N. and Holmes, D.G.,** 2003. "Stationary frame current regulation of PWM inverters with zero steady-state error," *IEEE Transactions on Power Electronics*, Volume 18, pp. 814-822, May.

[22] **Kazmierkowski, M., Krishnan, R. and Blaabjerg, F.,** 2002. "Control in power electronics," Academic Press.

[23] **Kim, K., Park, N. and Hyun, D.,** 2005. "Advanced synchronous reference frame controller for three-phase UPS powering unbalanced and nonlinear loads," Power Electronics Specialists Conference, PESC 05, pp. 1699-1704.

[24] **Cruz, J.B. and Valkenburg, M.E.V.,** 1974. "Signals in Linear Circuits," Houghton Mifflin Company, Boston.

[25] **Ansoft-Simplorer V7.0**, 2004.

APPENDIX A

Table A.1: Basic specifications of the PM50CLA120

Symbol	Parameter	Condition		Limits			Unit
				Min.	Typ.	Max.	
$V_{CE(sat)}$	Collector-Emitter Saturation Voltage	V_D = 15V, I_C = 50A, V_{CIN} = 0V (Fig. 1)	T_j = 25°C	—	1.8	2.3	V
			T_j = 125°C	—	1.9	2.4	
V_{EC}	FWDi Forward Voltage	$-I_C$ = 50A, V_D = 15V, V_{CIN} = 15V (Fig. 2)		—	2.5	3.5	V
t_{on}	Switching Time	V_D = 15V, V_{CIN} = 0V↔15V, V_{CC} = 600V, I_C = 50A, T_j = 125°C, Inductive Load (Fig. 3,4)		0.5	1.0	2.5	µs
t_{rr}				—	0.5	0.8	
$t_{c(on)}$				—	0.4	1.0	
t_{off}				—	2.0	3.0	
$t_{c(off)}$				—	0.7	1.2	
I_{CES}	Collector-Emitter Cutoff Current	V_{CE} = V_{CES}, V_{CIN} = 15V (Fig. 5)	T_j = 25°C	—	—	1	mA
			T_j = 125°C	—	—	10	

THERMAL RESISTANCES

Symbol	Parameter	Condition	Limits			Unit
			Min.	Typ.	Max.	
$R_{th(j-c)Q}$	Junction to case Thermal Resistances	Inverter IGBT (per 1 element) (Note-1)	—	—	0.26*	°C/W
$R_{th(j-c)F}$		Inverter FWDi (per 1 element) (Note-1)	—	—	0.39*	
$R_{th(c-f)}$	Contact Thermal Resistance	Case to fin, (per 1 module) Thermal grease applied (Note-1)	—	—	0.038	

APPENDIX B

Table B.1: Main features of the eZdsp F2812 board

Digital Signal Processor	TMS320F2812
External Clock Frequency	30 MHz
External memory	64K words SRAM
Expansion connectors	Analog Digital I/O External Interface
Interface	IEEE 1149.1 JTAG* controller IEEE 1149.1 JTAG emulation connector

*: Joint Test Action Group

Table B.2: Main features of the TMS320F2812 DSP

Operating frequency	150 MHz
Clock and system clock	On-chip oscillator
	Watchdog timer
Central processing unit (CPU)	32-bit high performance CPU
On chip memory	128K×16 Flash memory
	18K×16 RAM*
	1K×16 OTP ROM**
Timers	Three 32-Bit CPU Timers
Motor control peripherals	Two event manager (EVA, EVB)
Analog-digital converter (ADC)	12-Bit ADC
	16 Channels
	Fast conversion rate: 80ns/12.5 MSPS
General purpose input/output	Up to 56 pins
External interface	Up to 1M total memory
	Three individual chip selects
Serial port peripherals	Serial peripheral interface
	Two serial communications interfaces
	Enhanced controller area network
	Multi-channel buffered serial port

*: Random Access Memory
**: One-Time Programmable Read Only Memory